Norwegian University
of Life Sciences

Master's Thesis 2021 60 ECTS
Faculty of Environmental Sciences and Natural Resource Management

Organic Matter Decomposition and Mercury Mobilization in Thawing Subarctic Permafrost Peat Plateaus

Nora Nedkvitne
Environment and Natural Resources

Abstract

Mercury (Hg) is a highly potent neurotoxin which is naturally present in the environment. A vast amount of the global Hg is stored in Arctic permafrost soils, immobilized by complexation with organic matter (OM). With an increasingly warmer climate, 37-81% of the near surface permafrost in the Northern Hemisphere is estimated to be lost by the end of the century. Since previously frozen permafrost OM is prone to degradation, the fate of the currently immobilized Hg is of concern. Release of Hg bound to dissolved organic carbon (DOC) into surface waters is one possible fate. Once released to surface waters, Hg may be subject to enhanced rates of methylation with potentially detrimental effects to northern fisheries, human populations, and ecosystems. Another possible fate is reduction and revolatalization back to the atmosphere. To assess pools of Hg in permafrost and their potential for mobilization with permafrost thaw and OM degradation, three permafrost peat plateaus along a coast to inland gradient in the Norwegian Subarctic were sampled. Peat and water samples were analyzed for chemical properties including total Hg content. Selected peat samples were further used in 70–108-day incubation experiments to investigate the potential release of Hg after permafrost thaw and its coupling to OM degradation under defined conditions (availability of O_2, SO_4^{2-}, essential nutrients) at 10ºC.

The vertical and lateral distribution of Hg in peat plateaus varied greatly between sites depending on the geohydrological conditions during formation. Concentrations of Hg were generally highest in the top layers, likely reflecting anthropogenically driven atmospheric deposition since the Industrial Revolution. Anoxically incubated samples from the top of the active layer generally showed the highest rates of Hg mobilization to water, suggesting that collapse of peat plateaus followed by thermokarst formation submerging the AL *in situ* plays an important role for Hg mobilization from Nordic peat plateaus. Additionally, decreasing Hg:C ratios across a transect from active layer to thermokarst sediment suggest loss of Hg, possibly due to volatilization of elemental Hg. Secondary emission of Hg from peat plateaus can possibly counteract recent efforts to minimize Hg concentrations in the environment.

Abstrakt

Kvikksølv (Hg) er et giftig grunnstoff som finnes naturlig i varierende mengder i miljøer. En betydelig andel av verdens Hg er lagret i arktisk permafrost og immobilisert av binding med organisk materiale (OM). I et stadig varmere klima er 37-81% av all permafrost nær overflaten på den nordlige halvkule forventet å forsvinne innen slutten av dette århundre. Siden OM fra tidligere frosset permafrost er tilgjengelig for degradering, kan tining av permafrost føre til mobilisering av bundet Hg. Utslipp av Hg bundet til løst organisk karbon (DOC) i overflatevann er et mulig utfall. Kvikksølv sluppet ut i overflatevann kan deretter bli metylert, med potensielt skadelige virkninger på arktiske fiskerier, populasjoner og økosystem. Et annet mulig utfall er reduksjon til Hg^0 og fordampning tilbake til atmosfæren. For å undersøke lagre av Hg i subarktisk permafrost, og dens potensiale for mobilisering med tining og degradering av OM, ble prøver tatt fra tre subarktiske torvplatå. Torvplatåene var spredt langs en gradient fra kyst til innland i Finnmark, Norge. Kjemiske egenskaper og sammensetning ble analysert i både torv og vannprøver. Utvalgte torvprøver ble brukt i 70-108 dagers inkubasjonseksperimenter for å utforske potensiell frigjøring av Hg etter tining av permafrost og dens sammenheng med degradering av OM under definerte forhold (tilgjengelighet av O_2, SO_4^{2-}, essensielle næringsstoffer) ved 10ºC.

Den vertikale og laterale fordelingen av Hg i torvplatå viste store variasjoner mellom steder, avhengig av geohydrologiske forhold ved formasjon. Konsentrasjoner av Hg var generelt høyest i topplagene, som trolig er en gjenspeiling av økt antropogent utslipp siden den industrielle revolusjonen. Prøver fra topplagene inkubert anoksisk viste generelt de høyeste ratene av Hg mobilisering til vann. Dette tilsier at vannmetning av permafrost torv ved innsynkning og formasjon av termokarsdammer som oversvømmer topplaget kan spille en viktig rolle for mobilisering av Hg i nordiske torvplatå. Videre viste et transekt fra topplaget av torvplatå til termokarstsediment minkende Hg:C forhold som kan tyde på tap av Hg, muligens via reduksjon og fordampning. Sekundærutslipp av Hg fra torvplatå kan være til hinder for nylig inngåtte konvensjoner for å minimere Hg konsentrasjoner i miljøet.

Acknowledgements

First of all, I would like to thank my main-supervisor Peter Dörsch (NMBU) for the extensive help and support throughout the work on this thesis. I truly appreciate the faith you have placed in me by letting me design a topic outside of your area of expertise. You have been an amazing supervisor, going above and beyond to help me succeed. Your support through this work has been invaluable.

I would also like to thank Sebastian Westermann (UiO) for including us in your ongoing work in the studied area, guiding us during the fieldwork, and sharing in your extensive knowledge. This project would not have been possible without your involvement.

My co-supervisors, Heleen de Wit (NIVA) and Alexander Eiler (UiO), also deserves a huge thanks for their guidance during the planning and execution of this project. Heleen has been truly helpful in the planning and interpretation of data related to Hg, and Alex has provided me with good advice regarding molecular work.

I further would like to thank the staff at the environmental chemistry lab and soil biology lab at NMBU, particularly Solfrid Lohne, Mina Marthinsen Langfjord, Pia Frostad, and Trygve Fredriksen. This project called for a lot of unexpected adjustments, and your help and ability to adapt on short notice has been crucial. I also would like to thank Solfrid Lohne and Karl Andreas Jensen (NMBU) for the additional guidance in relation to work with Hg.

Åsa Frostegård and Rannei Tjåland at the microbial ecology and physiology lab at NMBU also deserves a huge thanks for their involvement and guidance related to the molecular work during this project. I would also like to thank you for letting me use your lab unlimited.

Thank you to the lab staff at NIVA, particularly Tina Bryntesen, for the help and flexibility regarding the samples analyzed at the NIVA lab in Oslo.

I would like to thank Sigrid Trier Kjær for the collaboration during this project. You have been my rock through ups and downs, always seeing solutions. I am forever impressed by your unlimited knowledge and having you as my partner through this process has been irreplaceable.

Finally, I would like to thank friends and family for support and help with proofreading throughout the process.

Table of Contents

List of figures

List of tables

List of Appendices

1. Introduction

Mercury (Hg) is a naturally occurring trace element with the potential of being highly toxic. Arctic soils are considered a globally significant Hg reservoir, estimated to hold twice the amount of Hg compared to all other soils, the atmosphere and the ocean combined (Obrist et al., 2017; Schuster et al., 2018). With temperatures rising faster at the poles than the global average, concerns have been raised regarding the fate of Hg released from Arctic soils under climate change (IPCC, 2013). Mercury forms strong bonds to organic matter (OM) in soil. As OM is degraded, the bound Hg can be mobilized either by reduction to Hg^0 and revolatilization (Smith-Downey et al., 2010) or by complexation with mobilized OM (Bravo et al., 2018). Permafrost (PF) thaw water and runoff from Arctic soils transport nutrients and Hg from the soil to recipient surface waters and eventually the ocean (Ci et al., 2020; Holmes et al., 2012; Rydberg et al., 2010; Schuster et al., 2011). The largest concern is tied to the formation and dispersal of methylmercury (MeHg), which is the most toxic and readily bioaccumulated form of Hg (Engstrom, 2007; Morel et al., 1998; Wang et al., 2000). Methylmercury is a highly potent neurotoxin which quickly biomagnifies through aquatic food webs. Therefore, elevated concentrations of Hg and MeHg in Arctic waters can have a detrimental impact on ecosystems and human populations (AMAP, 2011). Particularly at risk are populations that consume large quantities of fish or marine mammals, such as indigenous communities in the North (Chan & Receveur, 2000). Populations at lower latitudes can also be affected, since much of the fish consumed globally originates from fisheries in the Northern Hemisphere (Douglas et al., 2012).

1.1 Cycling of Hg in the environment

Biogeochemical reactions cycle Hg through the biosphere, lithosphere and atmosphere (Selin, 2009). The main oxidation states of Hg in the environment are elemental mercury (Hg^0) and divalent mercury (mercuric ion; Hg^{2+}) (Jackson, 1998). Elemental mercury is highly volatile and emitted from geological sources (e.g. volcanic eruptions), land (e.g. fires or terrestrial Hg^{2+} reduction), and ocean surfaces (Selin, 2009). In addition, anthropogenic activities such as mining, and combustion of coal emit Hg to the atmosphere. The atmospheric lifetime of Hg^0 is estimated to be 1-2 years (Lin & Pehkonen, 1999). Thus, Hg^0 can travel long distances before it precipitates. The major sink of Hg^0 in the atmosphere is oxidation to Hg^{2+} (Selin, 2009).

Mercuric ion is considerably more surface reactive than Hg^0 and is therefore more readily deposited in ecosystems through wet and dry deposition (Lin & Pehkonen, 1999). However, it is estimated that 5-60% of newly deposited Hg^{2+} are reduced and reemitted to the atmosphere as Hg^0 (Selin, 2009). Reemission can be mediated by sunlight (heat and UV radiation), presence of reductants (e.g. Fe^{2+} or free radicals), or microorganisms harboring the *mer* operon which codes for mercuric reductase (MerA), the central enzyme in Hg reduction (Boyd & Barkay, 2012; Gabriel & Williamson, 2004; Morel et al., 1998). Mercury that does not re-volatilize becomes predominantly associated with vegetation and OM through strong binding of Hg^{2+} with reduced sulfur groups in the OM (Hintermann et al., 2002; Schuster, 1991). The binding immobilizes the Hg^{2+} until the OM material is decomposed or consumed by fire (Smith-Downey et al., 2010; Turetsky et al., 2006). Non-adsorbed nor re-volatilized Hg is prone to run off, associated with dissolved organic matter (DOM) or dissolved anions (e.g. OH^-, Cl^-), or to methylation (Gabriel & Williamson, 2004; Ravichandran, 2004).

Methylation of Hg is primarily mediated by microorganisms in anaerobic environments such as wetlands and lake sediments (Gabriel & Williamson, 2004). Various strains of sulphate reducers, iron reducers, methanogens, and fermenters have been found to methylate Hg (Compeau & Bartha, 1985; Gilmour et al., 2013). All strains of bacteria and archaea capable of Hg methylation harbor the *hgcAB* gene pair (Parks et al., 2013). Methylmercury can become demethylated by UV-radiation and microbial demethylation or it can be taken up by organisms and bioaccumulates in food webs (Morel et al., 1998).

1.2 Anthropogenic impacts on the Hg cycle

Anthropogenic activities have increased Hg concentrations in the environment since the Industrial Revolution. Approximately 2.5 Gg Hg $year^{-1}$ are emitted from anthropogenic sources, which account for about 30% of the total input to the atmosphere (UN Environment, 2019a). Soil bound Hg is estimated to have increased by 20% since the Industrial Revolution (Smith-Downey et al., 2010). Deposition has increased even in areas not affected by nearby anthropogenic emissions. Reported recent deposition rates are 2.7 ± 0.9 higher for lakes in the US and Canada and 2.0 - 2.6 higher for Scandinavia than in preindustrial times (Fitzgerald et al., 1998). Deposition in ice cores and accumulation in peat cores are reported to be 20 and 15-fold higher, respectively, than in preindustrial times (Roos-Barraclough et al., 2002; Schuster et al., 2002). In 2013, the Intergovernmental Negotiation Committee on mercury agreed to a

global treaty (the Minamata Convention) to diminish extraction and anthropogenic emission of Hg (UN Environment, 2019b).

1.3 Hg in the Arctic

Mercury is transported from lower latitudes to the Arctic by air currents, ocean currents, and rivers (AMAP, 2011). In coastal regions, temporary Hg enrichment is typically induced by so-called atmospheric Hg depletion events (AMDE) (Douglas et al., 2012). In Arctic terrestrial ecosystems, the main source of Hg is the uptake of Hg^0 from the atmosphere by vegetation (Obrist et al., 2017). Wet and dry deposition also occur, albeit to a lesser extent. Since decomposition of OM in colder ecosystems is slow, re-volatilization of mercury is less significant compared to warmer climates. In permafrost soil, Hg bound to OM has been buried by sedimentation or peat growth and remains frozen in the soil (Obrist et al., 2017).

The low turnover time combined with uptake of Hg^0 suggests that Arctic soils might be a globally important sink of Hg (Obrist et al., 2017). Northern Hemisphere PF regions have been estimated to store 1.656 ± 962 Gg Hg, where 793 ± 461 Gg Hg are reckoned to be frozen in permafrost soil (i.e. soil that has remained frozen (< 0°C) for at least two consecutive years) (Schuster et al., 2018). The Arctic is experiencing climate warming at a much higher rate compared to the rate of global average temperature rise, and between 37% (RCP2.6) and 81% (RCP8.5) of near-surface PF is estimated to vanish by the end of the 21st century (IPCC, 2013).

1.3.1 Implications of warming climate on Hg stored in Arctic permafrost

Permafrost thaw leads to increased erosion and altered hydrological connectivity in the landscape through ground subsidence and thermokarst formation (Vonk et al., 2015). Meltwater runoff and erosion transport Hg and other elements to recipient surface waters (Ci et al., 2020; Rydberg et al., 2010; Schaefer et al., 2020; Schuster et al., 2011; St Pierre et al., 2018). Elevated temperatures will also increase the rates of OM degradation (Harden et al., 2012). Consequently, Hg bound to OM is mobilized and can be transported to surface waters complexed to DOC (Braaten et al., 2014). Increased mobility and accessibility of Hg may also lead to elevated concentration of MeHg in Arctic ecosystems, since Arctic soils are found to be rich in the Hg methylation marker gene *hgcA* (Podar et al., 2015). Moreover, mercury methylation rates have been found to increase with higher temperatures in thawed PF (Yang et al., 2016). Alternatively, mobilized Hg can be reduced to Hg^0 and revolatilized (Ci et al., 2020;

Fahnestock et al., 2019). Reduction of Hg^{2+} can be driven by microbial activity, and Hg^0 production has been found to positively correlate with CO_2 production (Fritsche et al., 2008). Also, concentrations of DOM have been found to regulate the reduction of Hg^{2+} to Hg^0 in anoxic environments; low concentrations of DOM (>0.2 mg L^{-1}) promote reduction, whereas higher concentration inhibit production of Hg^0 due to complexation (Gu et al., 2011; Poulin et al., 2019). Hence, constraints and drivers of microbial OM degradation in tawed PF also control the mobilization and fate of Hg in Arctic permafrost.

1.3.2 Constraints of organic matter degradation in thawed permafrost

The general assumption is that PF thaw will lead to increased degradation of OM due to activation of the native microbial community and temperature-stimulated microbial processing (Harden et al., 2012; Jansson & Tas, 2014). However, CO_2 and CH_4 fluxes in discontinuous permafrost landscapes are highly variable in space and time, and physiochemical and microbial controls on OM degradation are complex (Estop-Aragonés et al., 2018; Waldrop et al., 2021). Carbon rich peat plateaus cover extensive areas of the Arctic and Subarctic regions (Gorham, 1991) and as they are rich in ice (palsa mires; peat mounds with a permanently frozen core), they tend to develop thermokarst ponds upon thaw. The rate and constraints of PF peat degradation in thermokarst ponds are uncertain (Estop-Aragonés et al., 2018). Peat quality prior to PF formation may differ between peat plateaus, exerting control on OM degradation upon PF thaw (Turetsky et al., 2020). Other factors such as soil moisture, temperature, availability of oxygen and alternative electron acceptors, dissolved C and N, and microbial functional limitations have also been found to be important factors controlling the degradation of OM in thawing PF peat plateaus (Estop-Aragonés et al., 2018; Jansson & Tas, 2014; Monteux et al., 2020; Sjögersten et al., 2016; Waldrop et al., 2021). However, the extent to which each factor impacts OM degradation and mobility of Hg, separate and in concert, remains unclear.

1.3.3 Vulnerability of Arctic ecosystems and communities to increased Hg levels

The levels of Hg in Arctic biota, particularly higher trophic level carnivores, have increased significantly over the past 150 years (AMAP, 2011). Some Arctic species show concentrations exceeding the threshold for biological effects. Human populations in the Northern Hemisphere also show elevated levels of Hg in hair and blood. This trend is particularly evident in indigenous communities, as seafood is a central component of their traditional diet (Chan & Receveur, 2000). Moreover, the majority of fisheries are located in the Northern Hemisphere,

which feed billions of people globally (Douglas et al., 2012). Therefore, more detailed insights are needed about the factors driving and constraining OM decomposition and associated Hg cycling, to predict the effect of PF thaw on environmental and human health locally and globally.

1.4 Aim of study

The original aim of study was to assess Hg methylation in thawing PF soils. Hence, field sampling and experimental setups were planned accordingly. The initial plan was to extract methylmercury from the soil with the method used by Braaten and de Wit (2016) which is based on Bloom et al. (1997). However, due to restrictions implemented to limit the spread of SARS-CoV-2, access to the NIVA laboratory, equipment and guidance was not available. Therefore, the plan was re-evaluated, and it was decided to focus on gaps in the understanding of links between Hg release and OM degradation in thawing PF.

Surface water and palsa cores from peat plateaus were sampled along a sea-to-inland gradient in Finnmark, Norway. The palsa cores consisted of peat from the active layer (AL; seasonally thawed), transition zone (TZ; possibly thawed in warm summers), and PF (frozen for 2 consecutive years or more). Additionally, the top layer of thermokarst bottoms, representing thawed and collapsed peat plateaus, and wet mires, representing newly accumulated peat without PF, were sampled. All TZ and PF samples were transferred frozen to the laboratory. To assess the geochemistry and concentration of Hg in the peat plateaus, the elemental composition of the peat samples was analyzed and compared to water chemistry in adjacent thermokarst ponds and nearby streams. Palsa samples from different layers were incubated as oxic or anoxic slurries over 96-108 days at 10°C to study the link between microbial OM degradation and Hg release. Additional incubation experiments were carried out to test the effect of readily decomposable C substrate (glucose), nutrients (NH_4^+, PO_4^{3-}), alternative electron acceptor (SO_4^{2-}), and Hg^{2+} concentration on Hg release and methylation.

We hypothesized that the concentration of Hg would follow the size of organic C pools in both soil and water due to the strong binding of Hg with OM. Secondly, Hg concentrations in peat and water were expected to decrease with increasing distance from the ocean due to the influence of AMDE (Douglas et al., 2012) and sea aerosols (Malcolm et al., 2003). Likewise, MeHg production rates (%MeHg of HgT; Tjerngren et al., 2012) in water were expected to be

higher closer to the ocean, due to deposition of SO_4^{2-} from sea aerosols stimulating sulphate reducing bacteria which are commonly found to methylate Hg. Finally, we expected the OM degradation rate and thereby mobilization of Hg to be higher in samples with added nutrients and in the presence of oxygen. Incubated samples amended with SO_4^{2-} and Hg^{2+} were expected to have the highest rates of MeHg production.

The specific objectives of the study were to:

1. map and compare three peat plateaus along a sea-to-inland gradient for depth profiles of pH, DOC, C, Hg, macro- and trace elements
2. compare Hg concentrations along a palsa to wet mire transect within each site
3. map water chemistry and determine concentrations of total (HgT) and methylated mercury (MeHg) in PF-affected ponds and streams
4. assess the effect of redox conditions (oxic *versus* anoxic) on release of Hg after PF thaw; released Hg was defined as water extractable dissolved HgT (dHgT) passing through a 0.45 μm filter after ~100 days of incubation at 10°C
5. investigate the effect of readily available nutrients (NH_4^+ and PO_4^{3-}), carbon (glucose), and alternative electron acceptors for anaerobic respiration (SO_4^{2-}) on release of Hg after PF thaw
6. test an alternative method for MeHg extraction from peat by comparing concentrations of MeHg in the water phase of peat slurries before and after incubation. This method only looks at dissolved MeHg (dMeHg).

An additional objective was to compare the microbial genetic potential for Hg methylation with microbial activity observed in incubations (production of MeHg and OM degradation). The microbial genetic potential is here defined as the abundance of the marker gene *hgcA*. Since DNA extraction from peat soil is challenging, particularly in PF soil, the work regarding the microbial genetic potential in this thesis must be regarded as preliminary.

2. Materials and methods

2.1 Description of field sites

Three peat plateaus at different locations in Finnmark, Norway (Fig. 1) were studied, all of which with a documented history of PF thaw and degradation (Borge et al., 2017). The region is situated north of the Arctic Circle (68-71°N) and covers an area of approximately 50 000 km^2 with a variable landscape characterized by alpine mountains in the northwest and plateau like topography at 300-500 m a.s.l. in the interior and south. Most of the plateau is covered by ground moraines, glaciofluvial and glaciolacustrine sediments from repeatedly being covered by ice during the Pleistocene (Borge et al., 2017; Kjellman et al., 2018). Low points in the landscape between ridges and moraines are often filled with wetlands or mires, covering approximately 850 km^2 of Finnmark county, some of which forming peat plateaus and 'palsas'. Palsas are peat mounds with a permanently frozen core in the peat or underlying mineral soil, and cover about 110 km^2 of Finnmark. Three field sites were chosen, representing typical peat plateaus. The vegetation at all three field sites consists of sedges (e.g. *Carex* spp.), cotton grass (*Eriophorum* spp.) and various *Sphagnum* species, common to wet fen areas of the region (Kjellman et al., 2018).

The climate in Finnmark county is influenced by the warm North Atlantic Current causing large climate variations from the coastal to the inland regions (Johannessen, 1970). The coastal region is characterized by mild winters and cool summers (NCCS, 2016). The inland plateau (Finnmarksvidda) has a typical subarctic continental climate with higher temperatures in summer and lower temperatures in winter as compared with the coastal climate. The mean annual temperature in Finnmark county is around 0°C, being slightly above for the coastal regions and slightly below for the inland plateau (Aune, 1993). On average, the coastal region receives more precipitation compared to the inland Finnmarksvidda (Olsen et al., 1996).

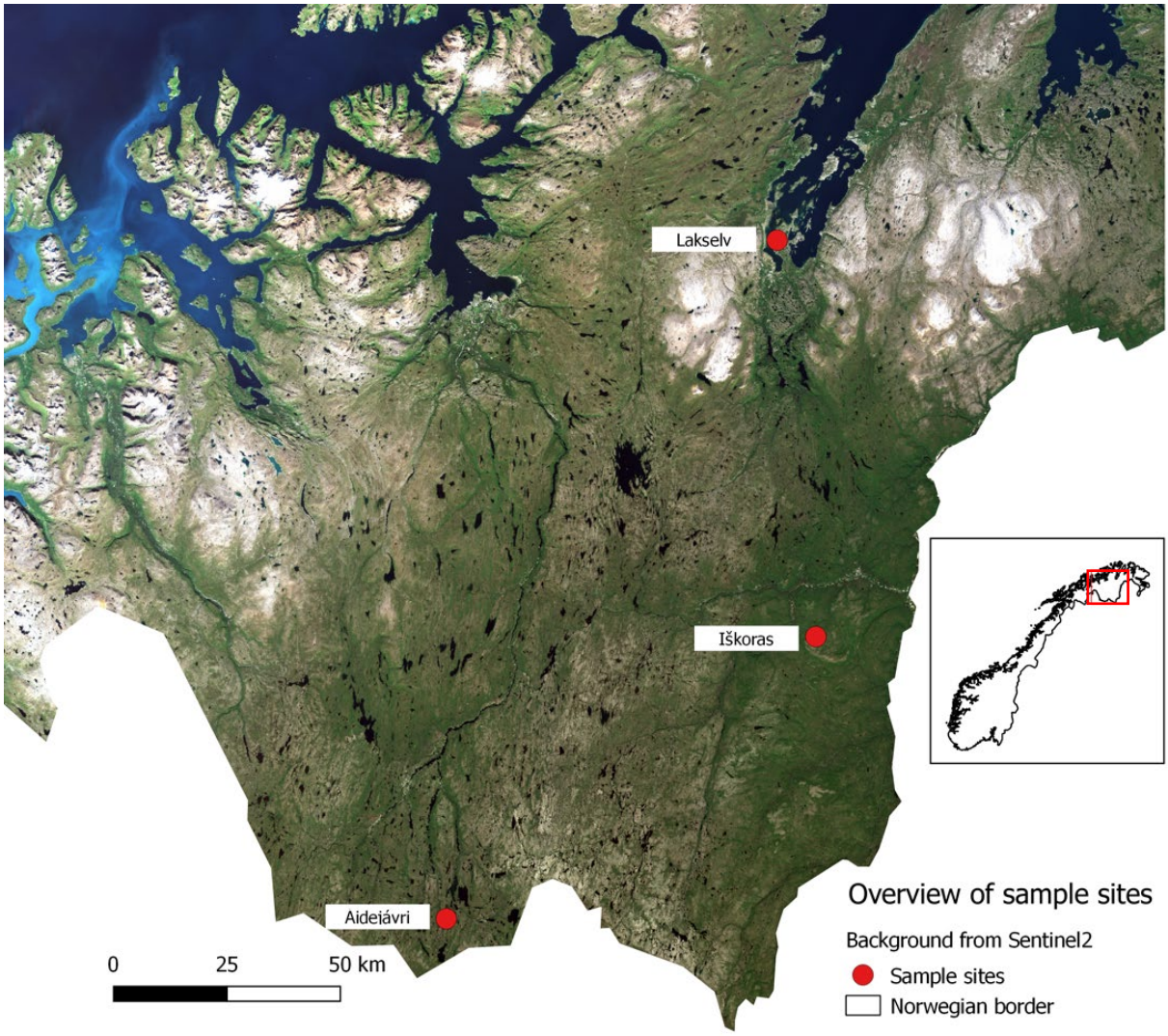

Figure 1. Locations of the three field sites in the present study, Lakselv, Iškoras, and Áidejávri, forming a gradient from sea to inland.

Finnmark county is located in the Subarctic and is unique in the light of permafrost research as the melting of permafrost happens contemporarily (Westermann, 2020). Therefore, the observations in Finnmark county may serve as a model system for the development of future permafrost thaw at high latitudes. The three field sites used in this study covered a gradient, from the warmer coastal regions in the North to the cooler inland regions in the South (Table 1).

Table 1. Climate and geographical data; distance to ocean, mean annual temperature and precipitation, elevation, and coordinates of each field site. MAT and MAP are based on data from the period 1991-2020 retrieved from MET (2021). Geographical data were collected in the field and from Kjellman et al. (2018).

Site	Distance to ocean (km)	Mean annual temperature (°C)	Mean annual precipitation (mm $year^{-1}$)	Elevation (m.a.s)	Coordinates
Lakselv	0	1.7	392	50	70°70'14 N 24°59'47 E
Iškoras	80	-1.3	433	381	69°20'27 N 25°17'44 E
Áidejávri	130	-1.9	478	398	68°44'59 N 23°19'06 E

2.1.1 Lakselv field site

The Lakselv field site (Fig. 2) is located on a peninsula in the Porsanger fjord outside of Lakselv village. The site is located below the marine limit and was suppressed by glaciation until about 11,200 ± 500 calibrated years before present (cal. yr BP; Stokes et al., 2014). The land raised around 9700 cal. yr. BP and peat started forming around 6150 cal. yr. BP (Kjellman et al., 2018). During the early stages of peatland formation, fen environments evolved and lasted for 4000 - 6000 years. The peatland then transitioned to a drier peat plateau around 150 cal. year BP, indicating initial appearance of permafrost.

The geomorphology of the Lakselv field site is classified by Miljødirektoratet (2020) as "moderate wave-exposed coastal plain with wetlands". The Lakselv site was chosen in the part of the coastal plain that is not directly exposed to open sea on a relatively flat terrain with more "inland-like" traits. In comparison to the other two field sites, the Lakselv peat plateau is smaller and shallower with concurrent palsa formation and degradation (Kjellman et al., 2018; Westermann, 2020). The bedrock at the study site consist of moraines, gravel, sand and clay (NGU, 2015). The surrounding elevated areas consist of white, light gray or yellow-green quartzite sandstone.

The climate is characterized as mild, coastal climate. The mean annual temperature is 1.7°C measured at the metrological station Banak, situated a few kilometers away (1991-2020; (MET, 2021)). The Lakselv field site is the warmest of the three field sites used in this study and the mean annual temperature is in the upper range of where permafrost can be found (Borge et al., 2017). The mean annual precipitation in the area is 392 mm year $^{-1}$ (1991-2020; (MET, 2021)). Precipitation in the form of rain during wintertime is common, and the area is prone to a high average wind speed of about 5 m s^{-1} (Borge et al., 2017). The thermal stability of the permafrost is likely attained both due to the high average windspeed and wintertime rain since the resulting reduction in snow cover decreases insulation.

Figure 2. Field work the peat plateau at the Lakselv field site. The mountains in the background are located on the opposite side of the Porsanger fjord.

2.1.2 Iškoras field site

The Iškoras field site (Fig. 3) is an inland peat plateau located on Finnmarksvidda, approximately 90 km from the coast (Martin et al., 2019). The elevation of the area is around 381 m a.l.s., which is above the marine limit (Kjellman et al., 2018). The area was glaciated until approximately 10,900-10,800 cal. yr BP and the initiation of peat formation is dated to around 9200 cal. yr BP (Kjellman et al., 2018; Stroeven et al., 2016). The first permafrost formation at the Iškoras site is estimated to have occurred around 800 cal. yr BP.

The area surrounding the Iškoras field site is characterized as "wooden inland plains with wetland" (Miljødirektoratet, 2020). The elevation differences in the area are less than 50 m within an area of 1 km. The peat plateaus underlain by permafrost are scattered and surrounded by large fen areas and small lakes (Kjellman et al., 2018). Areas that are not dominated by wetlands are usually covered with shrubland and mountain birch forest. The bedrock at the field site is dominated by quartz, feldspar, mica shale and calcareous shale (NGU, 2015). The immediate surrounding area consist of chlorite-amphibole rock originating from olivine-rich magma, or quartzite. The area is connected to the catchment of the Tana river and the Tana fjord (NVE, 2021).

The Iškoras field site has a mean annual temperature of -1.3°C (1991-2020; MET, 2021). The annual precipitation for the same period was 433 mm $year^{-1}$. Both temperature and precipitation are measured at Čuovddatmohkki weather station, located a few kilometers west of the Iškoras field site.

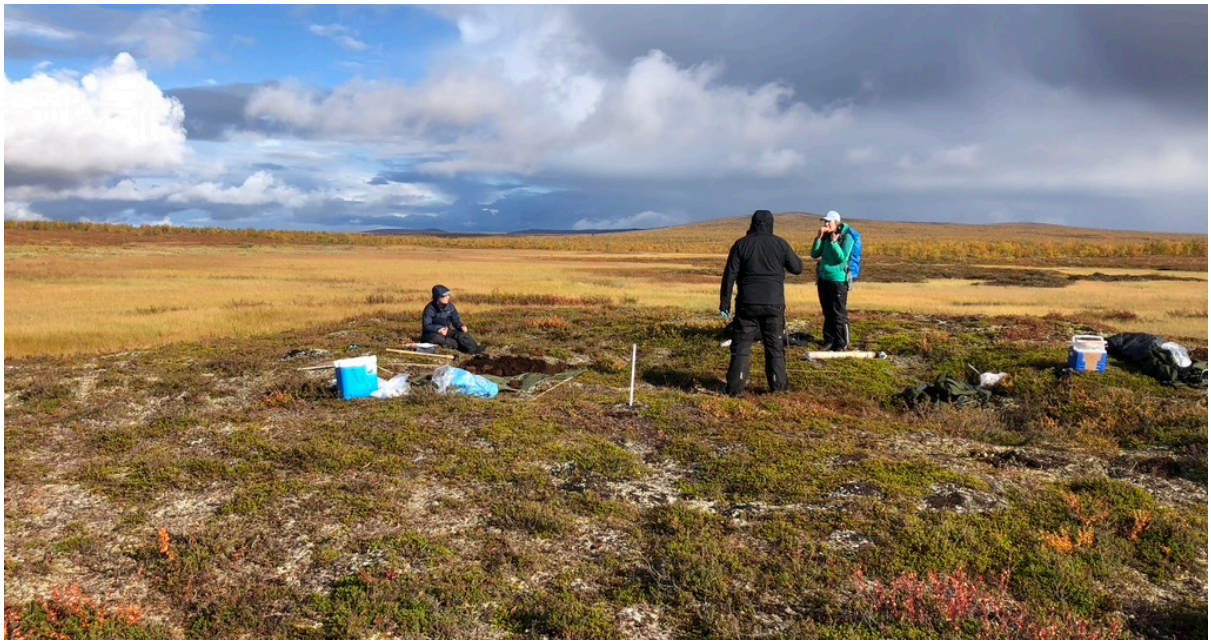

Figure 3. Field work at the peat plateau in Iškoras, with surrounding fen area in the background. The picture is taken facing northward, away from Iškoras mountain.

2.1.3 Áidejávri field site

The Áidejávri field site (Fig. 4) is located 30 km southeast of Kautokeino on the Finnmarksvidda plateau. The entire peat plateau covers an area of approximately 16.4 km^2 (Framstad et al., 2010), which makes it the largest peat plateau of the three field sites. The area is scarcely populated, however a road frequently used for commercial transport (E45), cuts through the peat plateau. The topography of the area is relatively flat and characterized as "wooded inland plain" (Miljødirektoratet, 2020). The landscape is covered with forest where it is not dominated by wetland, and rivers and streams are abundant in the area. The bedrock consists of medium-grained amphibolite with transitions to coarse-grained reddish feldspar rocks in certain places (NGU, 2015). The area is part of the catchment connecting to Altavassdraget and the Alta Fjord (NVE, 2021). Mean annual temperature and precipitation for the area are -1.9°C and 478 mm $year^{-1}$ (1991-2020; MET, 2021), measured at the Sihččajávri metrological station (382 m a.s.l.) approximately 9 kilometers east of Áidejávri.

Figure 4. Field work at the peat plateau in Áidejávri. Shown is an erosion edge feeding into a thermokarst pond. The picture is taken facing East.

2.2 Field sampling

2.2.1 Peat

Samples were collected to characterize the chemical composition of the peat and to determine its potential degradability in incubation experiments. The sampling sites were chosen based on knowledge from previous research in the area. A 0.6 × 0.6 m large area of the vegetated top of a peat plateau was cut with a saw as shown in Fig. 5A, leaving one square column intact for AL sampling. The top layer was kept intact to fill in the hole after sampling. All AL material was removed down to the PF and the AL core was sampled at three depths: top, middle, and bottom. To keep the samples as intact as possible, a saw was used to remove the AL column from the adjacent soil. After the samples were cut out, the sides were trimmed off to remove adhering peat from other depths. Both the knife and the cutting board used in this step were washed with 70% ethanol prior to use. Three sub-samples from each AL sample were cut vertically (from top to bottom), transferred to sterile cryotubes, and placed in a cooler containing crushed ice and salt. These samples were snap frozen in a dry shipper containing liquid nitrogen within 6 hours of sampling for later molecular analyses. The remaining AL samples were transferred to clean Tupperware boxes with rubber seal lids and stored dark and cold until further processing.

After sampling the AL, remaining peat was removed from the top of the permafrost layer. To sample PF, a 2 m long metal pipe with an outer diameter of 4 and inner diameter of 3 cm was placed on top of the permafrost (Fig. 5B). A heavy metal block was placed on top to create a counterweight and the pipe was hammered 5 cm into the permafrost using a sledgehammer. Thereafter the tube was taken up and the PF core pushed out of the pipe using a wooden broomstick (Fig. 5C). The broom stick had a piece of clean paper tissue at the end to avoid direct contact with the sample and to simultaneously rinse the pipe. Once out of the pipe (Figure 5D), the sample was placed on a clean cutting board. One side of the sample was trimmed off, to allow pushing the entire sample into a 50 ml centrifuge tube (VWR). The tubes were immediately placed in a cooler containing ice and salt to prevent thawing of the samples. The cutting board and knife were wiped off with a paper towel in between each sample and cleaned with ethanol between each new core. All PF samples were placed in a freezer (-20^{o}C) within 6 hours of sampling.

Figure 5. Stepwise sampling of palsa cores. (A) Removal of AL, leaving a protruding column for sampling undisturbed AL material. (B) Coring of permafrost using a metal tube. (C) Removing a sample from the cylinder by using a wooden broomstick. (D) Permafrost sample as it comes out from the cylinder. Shown is the bottom sample with transition to mineral soil.

In addition to palsa peat cores, the top layers of adjacent thermokarst sediment (TK) and wet mire (WM) were sampled at all three sites. The samples were collected by digging out peat, approximately 20 cm in depth, using clean gloves. Subsequently, the samples were treated and stored like AL samples.

Permafrost and AL samples were transported from Finnmark to Ås by airplane in coolers containing ice and salt. A temperature logger (iButton temperature loggers, Maxim integrated) was added to two of the coolers to document the thermal history of the samples. The cryotubes from the active layer remained in the dry shipper during transport. Back in Ås, the samples were immediately placed in a freezer holding -17.8°C (SD = ± 0.39°C; PF samples) or

refrigerated room holding 3.8°C (SD = ± 0.47°C; AL samples). The PF samples remained frozen during transportation.

2.2.2 Water

Water samples were collected for analysis of Hg and MeHg concentrations and general water chemical parameters. Water was sampled from thermokarst ponds at each field site according to USEPA Method 1669 'trace metal clean sampling technique'. The sampling equipment consisted of two fluorinated polyethylene bottles, one for MeHg sampling and one for HgT sampling. Both bottles were separately packed in double zip lock plastic bags. The bottle for MeHg contained concentrated hydrochloric acid to immediately preserve the sample. The bottle for HgT samples had no additions.

During the procedure, one person was defined as *Clean Hands* and the other person as *Dirty Hands*. Person *Dirty Hands* was only in contact with the exterior, whereas person *Clean Hands* in contact with the interior of the outer bag. Person *Dirty Hands* opened the exterior plastic bag, and person *Clean Hand* opened the interior bag, took out the bottle and preformed the sampling. The bottle for HgT was filled halfway and rinsed three times before filled up completely. The content was then poured over into the MeHg bottle for MeHg sample, and the HgT bottle was filled again for HgT sample. The bottles and zip lock bags were closed, and the samples were stored cold and dark until analysis.

2.3 Characterization of peat

2.3.1 Preparation of samples

Scintillation vials were weighed and marked with their respective sample ID, to be able to calculate the dry weight of the peat after freeze-drying. Knives, cutting boards, and ambient surfaces were cleaned with 70% ethanol and ultrapure DI water (>18.0MΩ) prior to sample preparation to avoid contamination. Clean gloves were worn at all times when in contact with the samples. The sample preparation always started from the top and followed the depth sequentially to simulate a natural vertical drift of elements in case of contamination between layers. The equipment was wiped off with a paper tissue between each sample from the same core, and cleaned off with 70% ethanol and DI water before preparation of each new core to avoid cross contamination. For the AL samples, the entire process was carried out in a refrigerated room (3.8 ± 0.47°C) where the samples were stored to avoid unnecessary exposure

to warmer temperatures and UV-radiation. The scintillation vials containing the samples, were weighed again to determine the fresh weight of the samples, before being placed in a freezer over night until frozen (approximately 24 hours) to prepare for freeze-drying. The PF samples were prepared right before the incubation experiments (section 2.3). The samples, each approximately 5 cm long, were divided into 6 equally large subsamples while still being frozen. The subsamples were used for elemental and isotope analysis (1 sample; section 2.3.3; 2.3.4), incubation experiments (4 samples; oxic and anoxic soil slurries, described in section 2.5.1, and oxic and anoxic treatment without added water for the master thesis of Sigrid T. Kjær, 2021), and a sample to represent pre-incubation material (1 sample; section 2.5.2). The samples for elemental and isotope analysis were then placed into scintillation vials, weighed, and placed back into the freezer immediately. Once all AL and PF samples were frozen, they were put into a freeze drier (SP Scientific VirTis BenchTop Pro with Omnitronics™). The samples were dried with a program holding -48.3°C and a vacuum of 180 mT. After approximately 2-4 days, all samples were completely dry. The scintillation vials were then weighed again to assess water content. Replicates for elemental composition analysis were not prepared due to the large quantity of samples and low mass for each individual PF sample.

All peat samples had to be decomposed prior to chemical analysis. The freeze-dried material was first ground into fine particles by Agate mills (Retsch RM 200) to obtain homogeneous subsamples. The mills were pre-cleaned by grinding silica sand followed by thorough vacuuming. The freeze-dried samples were then applied and ground for approximately 3 minutes. The same agate mill was used for the same core throughout the process to minimize cross contamination between samples from different sites. In addition, the top layer of each core was always ground first followed by samples in sequential order to mimic natural drift in nutrients, if any. The agate mills were rinsed with thorough vacuuming and paper tissue between each sample from the same peat core. Between each new core, the agate mills were cleaned with silica sand and deliberate vacuuming in addition. The samples were put back into their original containers after grinding to minimize the potential loss of trace elements and contamination. The samples were not sieved prior to grinding, and a plastic spoon was used throughout to eliminate metal contamination.

2.3.2 Elemental analysis

The peat samples were analyzed for elemental composition and Hg concentration. First, 0.20-0.25 g of finely ground sample and reference material (Bush Branches and Leaves (NCS DC 73349); Peach Leaves (1547); Pine Needles (1575); River Sediment (LGC6187); Spinage (NCS ZC73013)) were weighed into acid washed Teflon tubes. The Teflon tubes and scintillation vials were placed in an electric field prior to handling to neutralize their static charge and thereby prevent loss of material from sticking to the sides of the tube.

After all samples were weighed into Teflon tubes, 2 ml of ultrapure DI water and 5 ml ultra-pure concentrated nitric acid (HNO_3) were added for decomposition. Some of the samples precipitated when the HNO_3 was added, and additional hydrofluoric acid (HF) was added to some replicates to test the effect of precipitation on measured elemental composition. The HF dissolves the precipitated silicates which might bind nutrients that would otherwise escape detection. Results from analysis with and without HF were not statistically different (data not shown), and it was decided that treatment with HNO_3 only was sufficient.

After all Teflon tubes were prepared, the lids were put back on and the samples were left to incubate over-night under a fume hood at room temperature. The incubation ensures that all sample material is moisturized prior to further treatment. The following day, the samples were decomposed in an ultraCLAVE (Milestone) with a program running at 48.7 bar, 114°C for 1h 57 min. The samples were cooled down for approximately one hour after autoclavation. Thereafter, 20 ml ultrapure DI water and 1 ml concentrated HCl was added to new 50 ml centrifuge tubes. The HCl was added to conserve the sample. Once the centrifuge tubes were prepared, the sample material was poured over from the Teflon tubes. To ensure all sample material was transferred, the Teflon tubes were rinsed three times with ultrapure DI water that was discarded into the centrifuge tubes. The volume of the centrifuge tubes was then filled up to 50 ml with ultrapure DI water. Last, all centrifuge tubes were inverted ten times, to ensure sufficient mixing of the material. The samples were analyzed with inductively coupled plasma mass spectrometry (ICP-MS; Agilent Technologies 8800 ICP-MS Triple Quad) and inductively coupled plasma optical emission spectroscopy (ICP-OEC; PerkinElmer FIMS) by lab technicians.

Briefly described, the principle behind the analysis is as follows; droplets of the sample are vaporized in a high temperature plasma (ICP). The high temperature ionizes the elements in the samples. In ICP-MS, the ions pass through a quadrupole mass spectrometer which filters out everything except the target ions, based on their mass to charge ratio (m/z) (Vanhaecke, 2015). Subsequently, the target ions enter a detector where they are quantified. In ICP-OES, the elements are analyzed based the light emitted from the excited ions when returning to ground state (Boss & Fredeen, 2004). The light has a wavelength that is specific to each excited atomic species. An optical system receives the light, and the elements are distinguished and quantified based on wavelength and light intensity.

2.3.3 Quantification of carbon and nitrogen

Remaining freeze-dried peat was used to analyze for C and N content by a flash-combustion elemental analyzer (EA) coupled to an isotope ratio mass spectrometer (EA-IRMS; Finnigan DELTAplus XP, Thermo Fisher Scientific). Natural abundance of ^{13}C and ^{15}N was analyzed simultaneously, since this was relevant for the master thesis of Sigrid T. Kjær, 2021. In brief, a finely ground sample is combusted in the EA which converts all C to CO_2 and all N to N_2. The gases are then flushed through an open split to the source of the mass spectrometer, where they are ionized electrically and accelerated through a flight tube before they enter a magnetic field. The magnetic field changes the flight path of the molecules based on their atomic mass to charge ratio (m/z); the lighter ions bend more than the heavier ions. The ions are received in Faraday cups based on their flight paths and quantified as ion beam (mV).

The ^{15}N and ^{13}C ratios of CO_2 and N_2 were calibrated against certified standards (IAEA-N1 USGS-CO8). For quantification of C and N content, the peak areas of the abundant isotopocules (m/z 44 for CO_2 and m/z 28 for N_2) were calibrated against known amounts of ehtylenediaminetraacetic acid (ETDA). Ehtylenediaminetraacetic acid was also used as a running standard to monitor drift and linearity of the isotope measurements.

All materials (reference standards, running standards, samples and blanks) were prepared in the same manner. The weight was reset with the small tin capsule used for the respective sample before the material was weighed in using a spatula. Once the appropriate weight was achieved, the tin capsule was folded carefully with tweezers.

A calibration curve (Eq. 1) was found for both C and N based on EDTA samples.

$$mass\ (mg) = \frac{a*pa+b}{soil\ (mg)} \qquad \text{Equation 1}$$

Where pa is the measured peak area, a is the slope and b is the interception with the y-axis. The mass is the corrected mass expressed as mg per g dry weight peat.

2.4 Analysis of water samples

Water samples were analyzed for HgT, MeHg, and general chemical parameters (pH, conductivity, DOC, Ca, Mg, TotP, TotN, NO_3, SO_4^{2-}). Most of the water samples were collected in collaboration with the Norwegian Institute for Water Research (NIVA). These samples were transported and stored in a refrigerator at the NIVA laboratory in Oslo until they were analyzed by lab technicians. Three samples (values marked with * in Table 7) were sampled without NIVA and transported back to Ås in a similar manner to the peat samples (section 2.2.1). Once the samples were back in the lab at NMBU, they were immediately placed in a dark, refrigerated room holding 3.8 ± 0.47°C. Selected samples were delivered to NIVA shortly after for analysis of MeHg and HgT. The samples delivered for HgT analysis later had to be transported back and analyzed at NMBU due to instrument problems at NIVA.

2.4.1 Analysis of methyl mercury in water

All samples for MeHg quantification were analyzed at the NIVA laboratory in Oslo. The samples had to be analyzed by lab technicians due to restriction implemented to reduce the spread of SARS-CoV-2. The instrument used for the analysis was an automated methylmercury system (MERX-M, Brooks Rand, WA, USA) and the system follows US EPA Method 1630 for analysis of methylmercury (Telliard, 1998). In brief, specially designed fluoropolymer distillation vessels are filled with 50 ml of conserved (0.4% concentrated HCl) sample material, from which 40 ml is distilled into a receiving vessel. After transferring the samples to glass tubes in an autosampler, an acetate buffer is added to adjust the pH to 4.9, before adding an ethylating reagent. The sample is siphoned into a bubble vessel and flushed with N_2 to separate the ethyl analog of MeHg ($CH_3CH_3CH_2Hg$; MeEtHg) onto a carbo trap. After desorbing the

MeEtHg thermally into an inert gas stream, it is transported through a pyrolytic decomposition column, where it is converted to Hg^0. Lastly, the Hg^0 is transported to a cold-vapor atomic fluorescence spectrometer (CVAFS) for quantification.

2.4.2 Analysis of total mercury in water

Samples for HgT quantification were analyzed at NIVA and in the environmental chemistry lab at NMBU by lab technicians. At NIVA, a MERX-T system (Brooks Rand, WA, USA) was used and the procedure followed the same principles as EPA 1631 (Telliard & Gomez-Taylor, 2002). In short, a BrCl-solution is added to the sample while still in the original sampling bottle. The BrCl-solution is added to ensure that all Hg in the sample is oxidized to Hg^{2+} and does not stick to the walls of the bottle. Subsequently, a 25 ml aliquot is transferred to a glass tube in an auto sampler and NH_2OH•HCl and SnCl are added. The NH_2OH•HCl destroys the free halogens in the sample and SnCl releases the Hg by converting it to Hg^0. An autosampler flushes the sample with N_2 directly in the glass tube, by penetrating the lid with a double needle (allowing for ingestion and output at the same time). The N_2 flushing purges the Hg out of the solution, which is simultaneously ingested by the needle and led onto a gold-coated sand trap. Subsequently, thermal desorption releases the Hg into an inert gas which carries the Hg into a cold-vapor atomic fluorescence spectrometer (CVAFS) for quantification.

At NMBU, samples were analyzed for HgT using ICP-MS as described in section 2.3.2. The samples showed precipitation and therefore had to be decomposed prior to analysis, also described in section 2.3.2.

2.4.3 Analysis of DOC

All samples were filtered through a 0.45 µm glass fiber filters (VWR International) prior to analysis. The filtrates were analyzed for DOC by a lab technician on a total organic carbon analyzer (TOC-V_{CPN}, Shimadzu corporation, Japan). In brief, HCl is added to lower the pH to 2-3 which converts inorganic carbon to CO_2, which is then removed by flushing with synthetic air. The pH-treated sample is injected into a combustion tube (680°C) where the organic carbon is converted to CO_2 which is quantified by a near infrared detector (NDIR). All values are expressed as mg C per L sample.

2.4.4 Analysis of sulphate

Samples were filtered through a 0.45 µm filter prior to analysis. Sulfate was analyzed by a lab technician with an ion chromatograph (IC5000, Lachat/Zwegler analytics) connected to an autosampler (ASX500, Lachat/Zwegler analytics). The principle behind the method is to separate the anions in time and space so they can be quantified separately. In short, the system consists of a mobile (eluent) and a stationary phase (column). The column consists of a polymer with positive charges, which binds the anions. Ions with higher affinity (higher charge and smaller radius) will bind more firmly to the column. The eluate passed the sample through the column and competes with the anions exchange places in the column. The anions in the sample will then be replaced in order based on their respective binding affinity. Immediately after release, the anions are transported to a conductivity meter where they are quantified.

2.5 Incubation experiments

Selected samples from AL, TZ and PF cores were incubated after over-night thawing to measure post-thaw respiration kinetics and assess the release of total Hg from soil to water in relation to OM degradation under different conditions (oxic/anoxic, addition of substrate and/or nutrients). The release of Hg was defined by concentration of HgT in water phase after passage through a 0.45 µm filter, termed "dissolved total mercury" (dHgT) from here on. The net release of Hg during agitated slurry incubation was assessed as the concentration of dHgT in the water phase of the slurries post incubation minus the concentration measured after 1 h of stirring at 450 rpm pre incubation (section 2.5.2).

2.5.1 General procedure for setting up incubation experiments

Permafrost samples were taken out of the freezer (-17.8 ± 0.39°C) and prepared as described in section 2.3.1 before being transferred to 120 ml serum bottles equipped with Teflon stirring bars. Active layer samples were obtained directly from the container using clean gloves and a pre-cleaned knife. The serum bottles were immediately crimp-sealed with butyl rubber septa and washed with helium 6.0 (He; mild vacuum; 7 cycles of 30 s vacuum followed 10 s He filling) by a manifold (Fig. 6) to minimize exposure to oxygen during thawing. Bottles with PF samples were thawed in temperature adjustable incubation unit at 3.8 ± 0.47°C in the dark for approximately 20 h. After thawing, the bottles were placed in a water bath holding approximately 10°C and the amount of CO_2, CH_4 and N_2O released to the He-filled headspace

during thawing was quantified by a gas chromatograph. Thereafter, the samples received 50 ml of ultrapure DI water cooled to 4°C directly through the septum, before being placed on a magnetic stirrer submersed in a water bath (10°C) for one hour. In the following, the incubation samples are referred to as “slurries”. After one hour of stirring, the slurries were set aside for 10 min to sediment before sampling 1.6 ml of the supernatant directly through the septum for DOC analysis, using a 10 ml syringe (BD Plastipak) with a long 0.60 × 80 mm needle (B. Braun Melsungen AG). First, 0.5 ml of the sample was transferred to a 1.5 ml Eppendorf tube in which the pH was measured by inserting a pH meter (Hache H170) into the tube. Thereafter the rest of the sample was added and centrifuged at 10,000 rcf for 10 minutes to spin down particles. The supernatant was removed with a syringe and forced through a 0.45 µm filter (VWR international, Sterile Syringe Filter w/0.45 µm Polyethersulfone Membrane) into a clean Eppendorf tube. The obtained DOC samples were stored in a refrigerator until further analysis (usually within 48 h).

Following sampling of the slurries for DOC analysis, the bottles were washed with He or He/O_2 (80:20) with 5 cycles of 120s vacuum and 30s He- or He/O_2-filling using a manifold accommodating 14 bottles while stirring them in a water bath cooled with ice (Fig. 6). The purpose was to remove gases accumulated during thawing and to adjust fully anoxic or oxic conditions.

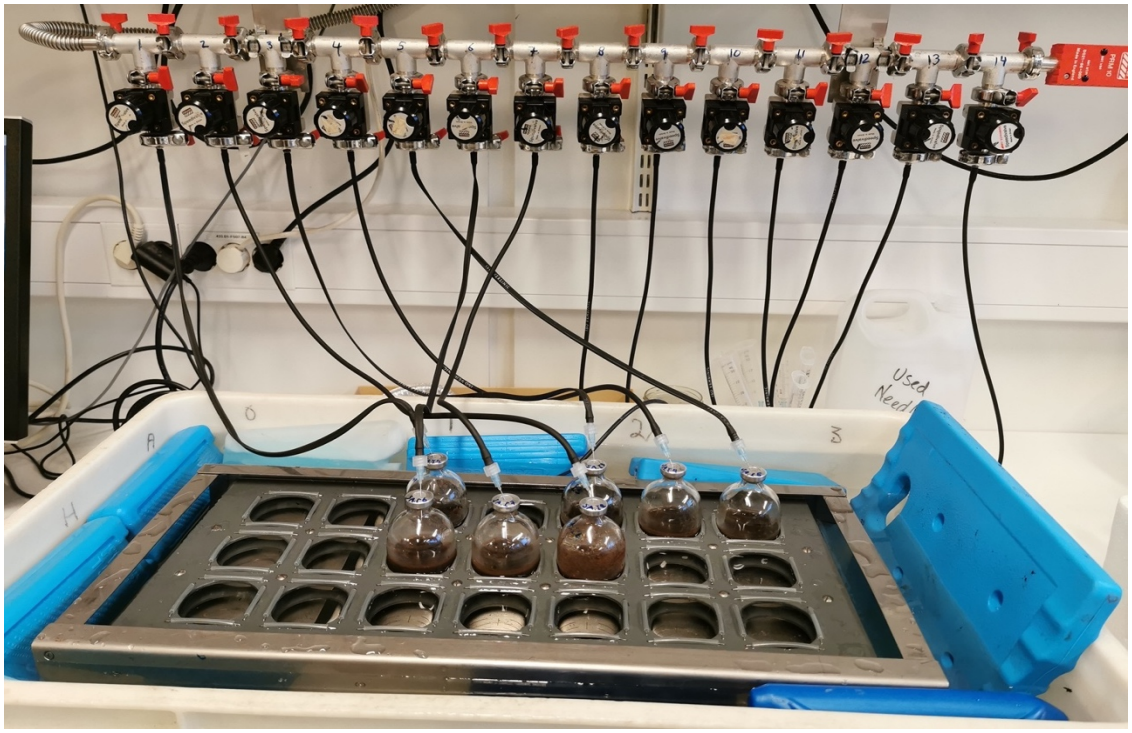

Figure 6. Manifold and ice bath with magnet stirrer used to wash crimp sealed flasks with He or He/O_2.

After washing, the bottles were placed into the water bath adjusted to 10°C on submersible stirring boards (Fig 7). A temperature of 10°C was selected for the incubation to speed up biochemical reactions while still being within the range suitable for growth of cryophiles (Jansson & Tas, 2014). After temperature equilibration, the overpressure resulting from He-washing was released by piercing the septa with a syringe without plunger filled with 2 ml of DI water. The bottles were covered with aluminum foil to keep out light. The water bath was placed under the robotic arm of an autosampler (GC-PAL, Switzerland), which is equipped with a hypodermic needle piercing the septa for repeated headspace sampling. Every four hours, appr. 1 ml of the headspace was pumped via a peristaltic pump (Gilsen Minipulse) to a gas chromatograph (Agilent Model 7890A, Agilent, Santa Clara, CA, USA) for analysis of CO_2, O_2, N_2, CH_4 and N_2O as described by Molstad et al. (2007). The bottles were incubated for three weeks, while constantly stirring the slurries at 300 rpm. Thereafter, the bottles were placed in a dark climate chamber set to 10°C, continuing the incubation off-line. The actual temperature was later measured to be 9.7 ± 0.04°C. Once a week the bottles were shaken for approximately 10 seconds to ensure gaseous equilibrium between slurry and headspace, before sampling 1 ml from the headspace using an airtight syringe. The gas samples were injected into 10 cc septum vials (Matriks) washed, filled and equilibrated to 1 atm with He. Before each

sampling, the syringe was washed with He. After a couple of rounds with sampling by hand, it was decided that direct headspace analysis in the incubation robot ensured better data quality and the samples were transferred weekly to bi-weekly to the incubator for headspace analysis. The total incubation time was approximately 100 days. The cumulative gas kinetics were used to determine microbial decomposition potentials under slurry conditions (no diffusion limitations).

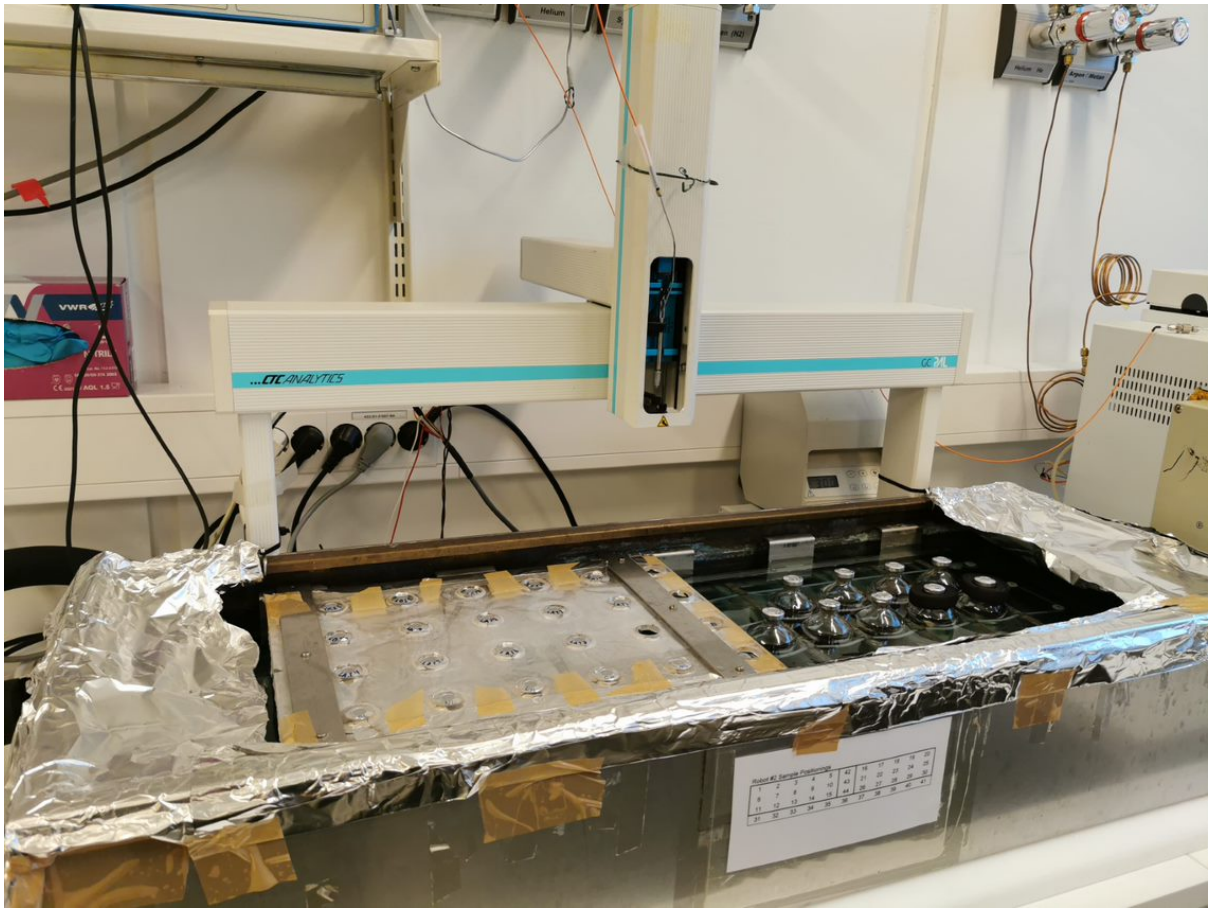

Figure 7. Water bath with bottles set up for online-incubation below an autosampler used for automated, semi-continuous (4-hourly) headspace analysis of O_2, N_2, CO_2, CH_4 and N_2O by gas chromatography. The bottles are placed on submersible magnetic stirring boards in the water bath which is held at constant temperature (here 10°C) by cycling water through a cryostat (not shown). All bottles were covered with aluminum foil to avoid penetration of UV-rays as shown for the samples to the left in the water bath.

After approximately 100 days of incubation, the experiments were terminated and sampled for chemical analysis. The samples were first shaken to mix the slurries before the entire sample was poured into 50 mL centrifuge tubes and centrifuged at 4100 rcf. Subsequently, the

supernatant was siphoned off and filtered through a sterile syringe filter with 0.45 µm polyethersulfone membrane (VWR international; Fig. 9). Immediately thereafter the filtrate was partitioned for further analysis of DOC (1.5 mL), dMeHg (> 40 mL) and dHgT (> 5 mL). Samples for dMeHg and dHgT analysis received 0.4% and 2% 11.6 M HCl, respectively, for conservation and to keep Hg in solution. The remaining incubated peat soil was frozen at -20°C for later DNA extraction.

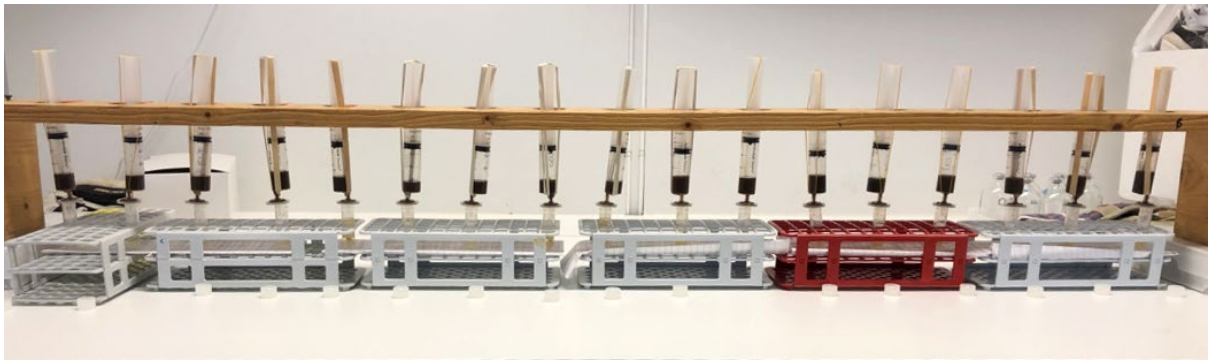

Figure 8. Set-up for filtration of samples.

2.5.2 Preparation of pre-incubation material

To compare pre-incubation with post-incubation extractable HgT, a subsample of peat material used for incubation was put aside and frozen to be analyzed alongside the incubated samples. The pre-incubation material was prepared in the same way as the incubated slurries for three reasons: (1) to ensure there is enough permafrost material to have the same soil/water ratio as in the incubated slurries, (2) to allow for the entire peat sample to be used for DNA extraction if necessary, and (3) to ensures that the initial treatment would not affect the comparability of pre- and post-incubation samples. For this, the pre-incubation samples were put into identical bottles containing magnets (known weight). The bottles were then capped, evacuated, and He-washed before thawing at 3.8 ± 0.47ºC overnight. The next day, 50 ml of pre-cooled (4.0 ºC) ultrapure DI water was added, and the slurries were stirred for one hour. Thereafter, the slurries were treated the same way as the incubated samples upon termination of the incubation experiments, described in the previous paragraph.

2.5.3 Incubations testing effects of field site, depth, and redox conditions on Hg mobilization

Three depths each of AL and PF, and the TZ were selected to represent one core from each peat plateau (Table 2). The samples were prepared as described in section 2.5.1. After the initial

24 hours of thawing in crimp sealed bottles under anoxic condition, one sample from each depth was washed with He, the other sample with He/O_2; as part of oxygen was consumed throughout the incubation, some of the bottles became anoxic eventually, thereby testing the effect of oxic-anoxic transition on OM decomposition activity and Hg release. The incubations lasted for 106 days for Iškoras and 98 days for Áidejávri and Lakselv.

Table 2. Depths of incubated samples from each field site. The respective depths are presented as cm from the top (left) and bottom (right) of the sample to the surface.

Site	Layer	Depth from surface, top (cm)	Depth from surface, bottom (cm)
Lakselv	AL1	2	12
Lakselv	AL2	20	35
Lakselv	AL3	40	60
Lakselv	TZ	60	70
Lakselv	PF1	70	80
Lakselv	PF2	80	85
Lakselv	PF3	85	95
Iškoras	AL1	0	15
Iškoras	AL2	25	35
Iškoras	AL3	45	55
Iškoras	TZ	60	73
Iškoras	PF1	80	86
Iškoras	PF2	106	118
Iškoras	PF3	150	162
Áidejávri	AL1	0	15
Áidejávri	AL2	20	35
Áidejávri	AL3	40	50
Áidejávri	TZ	50	60
Áidejávri	PF1	69	80
Áidejávri	PF2	89	100
Áidejávri	PF3	104	110

2.5.4 Effect of substrate stoichiometry

To find out whether OM degradation and hence Hg mobilization in peat plateaus are sensitive to the availability and stoichiometry of substrates, an experiment was set up covering different C:N:P stoichiometries by adding C (glucose), N (NH^{4+}) and P (PO_4^{3-}) alone or in combination. Since the original aim of the experiment was to investigate Hg methylation, additional

treatments supplemented with sulphate (SO_4^{2-}) and Hg^{2+} were set up to enhance Hg methylation. The concentrations of elements for each treatment were selected to ensure no limitations and reasonable stochiometric relationships of approximately 1:12 between C and N, P, and S, respectively. The amount of Hg^{2+} added was based on an incubation experiment by Yang et al. (2016), increasing native Hg concentration by approximately +25% . Stock solutions were made for each element added. Selected sections from a permafrost core (Iškoras, 71-139 cm from surface) were pooled, thawed and mixed in a clean glass beaker using a glass bar. The sample material was then divided equally into 24 vials and set up in triplicates with the following treatment combinations (final concentrations in parentheses):

1. No elements added (Control)
2. Glucose (C; 60 mM)
3. Ammonium chloride (N; 5 mM)
4. Monopotassium phosphate (P; 5 mM)
5. Sodium sulphate (S; 5 mM)
6. Mercuric ion (Hg; 3 nM)
7. N (5 mM) + P (5 mM)
8. C (60 mM) + N (5 mM) + P (5 mM) + S (5 mM) + Hg (3 nM)

The total volume of liquid added to each sample was approximately 50 mL. Three subsamples of the slurries were transferred to scintillation vails and frozen for elemental analysis to evaluate how well the PF material was mixed. Initially, all bottles were incubated anoxically and shifted to oxic conditions after 180 hours due to low microbial activity (CO_2 and CH_4 cumulation) with no appreciable effect of nutrient addition. The incubation lasted for 70 days.

2.6 DNA extraction

To investigate the abundance of genes important for mercury cycling, DNA was extracted from the soil samples. The initial intent was to target the marker gene for Hg methylation, *hgcA*, using the primer described by Gionfriddo et al. (2020) with the potential of also looking at other marker genes (e.g. for carbon cycling or Hg^{2+} reduction). DNA from various samples from all three field sites (both AL and PF) was extracted with DNeasy® PowerSoil® from Qiagen or with a method using phenol-clorophorm developed by Griffiths et al. (2000) and modified specifically for peat soil by Lim et al. (2016).

2.6.1 Preliminary test with DNeasy® PowerSoil® from Qiagen

In the first round, DNA extraction from intact organic rich active layer samples were tested with DNeasy® PowerSoil® from Qiagen. Since the samples contained a lot of water, one freeze dried sample was tested as well. The DNA was extracted following the manufacturer's protocol, without modification. First, 0.25 g of sample material was added to PowerBead tubes followed by 60 µl of a solution containing anionic detergents and other disrupting agents (Solution C1). The anionic detergent breaks down fatty acids and lipids associated with the cell membrane and is therefore necessary for complete cell lysis. Thereafter, the samples were placed in a FastPrep®-24 bead beater for cell lysis and ran at 6 m s^{-1} for 45 seconds. Some samples were ran 2 × 45 seconds, to test the effect of increased bead beating. The samples were put on ice for five minutes in between the runs to avoid overheating. All samples were put on ice immediately after, before centrifugating them at 10,000 g for 30 seconds. The supernatant was transferred to a clean 2 ml Collection Tube, and 250 µl of a solution containing a patented Inhibitor Removal Technology (IRT; Solution C2) was added. The IRT helps remove non-DNA organic material and inorganic material such as humic acids and proteins. The samples were then incubated at 2-8°C for 5 minutes, before they were centrifuged at 10,000 × g for 1 min. The supernatant was transferred to a clean Collection Tube and 200 µl of a solution containing a second patented IRT (Solution C3) was added. Once again, the samples were incubated at 2-8°C for 5 minutes and centrifuged at 10,000 rcf for 1 minute. Up to 750 µl of the supernatant was transferred to clean Collection Tubes and 1200 µl of a high-concentration salt solution (Solution C4) was added. The samples were then vortexed for 5 seconds. The solution, 675 µl each round, was transferred to an MB Spin Column and centrifuged at 10,000 rcf for 1 minute. The MB Spin Column contains a silica membrane, allowing DNA in the high-concentration salt solution to bind and remain in the column, while contaminants pass through the membrane. This step is repeated until all the sample is ran through the column. Subsequently, 500 µl of an ethanol-based solution (Solution C5) is added to wash the DNA additionally. The sample is centrifuged for 30 seconds at 10,000 g, and the flow-through is discarded. To ensure that all remaining ethanol is removed from the sample, it is centrifuged again for 1 minute at 10,000 g. Last, the MB Spin Column is placed in a clean Collection Tube and 100 µl elution buffer (Solution C6) is added to the center of the filter membrane, before centrifuging for 30 seconds at 10,000 g. The DNA was now in the Collection Tube. The quality and quantity of the DNA was measured with NanoDrop (1000 Spectrometer, Thermo Fisher

Scientific). Amplifiability was tested with PCR, as described in section 2.6.4, and the samples were stored at -20°C until further use.

2.6.2 Test of optimization of DNA extraction with DNeasy® PowerSoil® from Qiagen

In an attempt to increase the quantity, quality, and amplifiability of the DNA extract, optimization steps according to the manufacturers protocol were taken. First, to remove excess water, 0.25 g sample material were weighed into the PowerBead Tube. All the content of the PowerBead Tube was then transferred to clean centrifuge tubes and ran at 10,000 rcf for 30 s at room temperature. The samples were centrifuged after being weighed in to make it possible to later relate all results to per g dry weight soil, based on the known soil to water ratios for the samples. After centrifugation, the excess water was removed with a sterile pipette. Care was taken not to touch or remove any of the soil particles.

After removal of excess water, the content was transferred back to the original PowerBead Tube. Solution C1 was then added. The samples were incubated for 10 minutes at 70°C prior to bead beating to facilitate lysis of cells. The standard procedure was resumed at step 3 in the protocol, bead beating, and followed as described in section 2.6.1 until the last elution step. When adding Solution C6, the volume was decreased to 50 µl to up-concentrate the extracted DNA. Due to the low volume, great care was taken when applying solution C5 to ensure that the membrane in the MB Spin Column was completely moisturized. After the DNA was eluted, the quality and quantity of the DNA was measured with NanoDrop. The amplifiability was then tested with PCR, as described in section 2.6.4, and the samples were stored at -20°C until further uses.

2.6.3 Test of DNA extraction with phenol-chloroform

Another DNA extraction method specifically developed for peat soil by Griffiths et al. (2000) and modified by Lim et al. (2016) was tested. First, 0.5 g sample was weighed into a clean Eppendorf tube. 500 µL of CTAB extraction buffer was added and mixed with the sample by pipetting. After careful mixing, 500 µL phenol-chloroform-isoamyl alcohol (25:24:1) was added before the entire sample was transferred to micro centrifuge tubes containing 0.5 g glass beads. The samples were then run in FastPrep®-24 at 6.5 m s^{-1} for 3 × 30 seconds for bead beating, cooled on ice for approximately 5 minutes in between each round of bead beating.

Thereafter, the samples were centrifuged at 16,000 g for 5 minutes at 4°C. The topmost part of the aqueous phase (300-500 µL) was transferred to a new, clean Eppendorf tube and kept on ice. An equal volume (300-500 µL) of chloroform-isoamyl alcohol (24:1) was added and mixed by inverting the tube several times. Afterwards, the sample was centrifuged at 16,000 g for 5 minutes at 4°C. The aqueous phase was transferred to a clean Eppendorf tube, and 1 µL of RNAse A was added to remove RNA from the sample. The samples were incubated for 1 hour at 37°C.

After incubation, the DNA was purified to remove inhibitory compounds, using the *OneStep* Inhibitor Removal Kit (ZymoResearch) according to the manufacturer's protocol. First, the Zymo-Spin III-HRC Columns were prepared by adding 600 µL of Prep-solution and centrifuging them at 8,000 rcf for 3 minutes. The Collection Tube was discarded, and the column was transferred to a clean 1.5 ml tube. The sample material was then transferred to the prepared Zymo-Spin III-HRC Columns and centrifuged at 8,000 rcf for 1 minute. The column was discarded, and the tube containing the DNA sample was put on ice.

To further purify the DNA sample, 600 µL DNA Binding Buffer were added to 200 µL sample and mixed by brief vortexing. The solution was transferred to the Zymo-Spin IC-XL Column and centrifuged at 16,000 rcf for 30 seconds at room temperature. The flow-through was discarded and 200 µL Wash Buffer was added to the column. The sample was centrifuged at 16,000 rcf for 1 minute at room temperature. The flow through was discarded and the sample was treated with Wash Buffer one more time, following the same procedure. Afterwards, the sample was centrifuged once more at 16,000 rcf for 1 minute at room temperature. The column was transferred to a clean tube, and 25 µL nuclease-free water was added to the column matrix. After waiting for 1 minute to ensure that the matrix was thoroughly moist, the sample was centrifuged at 16,000 rcf for 30 seconds at room temperature. The final procedure was repeated once again to obtain a final volume of 50 µL of eluted sample. The sample was immediately put on ice. Quality and quantity of the DNA extract was measured with NanoDrop, and amplifiability was verified with PCR as described in section 2.6.4.

2.6.4 Verification of amplifiability

To verify the amplifiability of the extracted DNA, a polymerase chain reaction (PCR) was run followed by gel electrophoresis. The PCR was run in two different labs with different primers

(Table 3). The extracts from the preliminary test described in section 2.6.1 were tested at the University of Oslo (UiO). The products of the following two rounds of DNA extraction (section 2.6.2 and 2.6.3) were tested in the microbiology lab at NMBU for practicality reasons.

2.6.4.1 PCR at UiO

First, the samples were prepared for the PCR in the ratio described in Table 3. Four sets of primers were tested in the combinations displayed in Table 4. The PCR cycling times are given in Table 5.

Table 3. Components and volumes used in the PCR at UiO.

Component	Volume (µL sample^{-1})
Q5® High-Fidelity 2x MasterMix	10
10 µM Forward Primer	0.5
10 µM Reverse Primer	0.5
Template DNA	2
MilliQ water	7

Table 4. Primers tested in the first round of PCR run at UiO.

Combination ID	Forward primer	Reverse primer
1	340F_arc	803R_uni
2	519F_bac	803R_uni
3	SSU1ArF	SSU520R
4	341F	805R

Table 5. Temperatures, cycle times, and number of cycles of the PCR ran at UiO. The first test was run 30 cycles with denaturation, annealing, and elongation, the second round was run 30+15, and the last round was run 45 rounds.

Cycle	Temperature (°C)	Time	Repetitions of cycle
Initiation	98	30 s	1
Denaturation	98	10 s	30/30+15/45
Annealing	50	30 s	
Elongation	72	1 min	
Final elongation	72	7 min	1
Final hold	6	∞	1

The PCR conditions displayed in Table 4 were used for all samples, except for samples with primer combination 4. For samples with primer combination 4, the annealing temperature were set to 48°C. The rest of the procedure remained identical.

To verify the success of the PCR, the PCR products were separated by gel electrophoresis. The samples were first mixed with 1 µL of loading buffer to 5 µL of PCR product and applied to the wells of the agarose gel. Subsequently, the samples were then run for 40 minutes at 120V. The PCR products of primer combination 1, 2, and 3 (Table 4) were run for another 15 cycles of denaturation, annealing, and elongation. The rest of the procedure remained identical to the previous run (Table 5). In addition, a new set of samples were prepared with primer combination 1, 2, and 3, run for 45 cycles, with otherwise identical conditions as Table 5.

2.6.4.2 PCR at NMBU

The amplifiability of the DNA extracts from the procedures described in section 2.6.2 and 2.6.3 were tested in the microbiology lab at NMBU. The samples were prepared as described in Table 6.

Table 6. Components and volume of components used for the PCR solution ran at NMBU.

Component	Volume (µL sample^{-1})
Dream Taq Green PCR Master Mix (x2)	10
100 µM Forward Primer (27F)	0.1
100 µM Reverse Primer (518R)	0.1
Template DNA	9.8

Only the solution containing template DNA was used to complete the total volume of 20 µL and no MilliQ water was added due to low concentration of DNA in the extract. Once all PCR tubes were prepared, the PCR was run with the procedure described in Table 7.

Table 7. Temperatures, times, and repetitions of cycle of the PCR ran at NMBU.

Cycle	Temperature (°C)	Time	Repetitions of cycle
Initiation	95	5 min	1
Denaturation	95	30 s	35
Annealing	58	30 s	
Elongation	72	30 s	
Final elongation	72	10 min	1
Final hold	4	∞	1

After the PCR was finalized, the products were separated by gel electrophoresis. The PCR product was mixed with loading buffer in an approximate ratio of 1 µL of loading buffer to 5 µL of PCR product. Subsequently, the mix was applied to the agarose gel and run at 120V for 35 minutes.

2.7 Statistical analysis

Statistical analyses were run in RStudio 1.3.1073. Samples from the bottom of the cores containing mineral soil were excluded from the analysis.

2.7.1 PCA

Principal component analysis (PCA) was used to explore overall differences in peat chemistry between the sites. All PCA were run with the prcomp() function and the variables were scaled during the analysis due to large variations in the values of the dataset.

2.7.2 Regression

The data were subjected to regression analysis to investigate correlations. Data were transformed to obtain normal distribution, either by inverting (1/x) or logarithmizing (ln(x)) them. When distribution was deemed normal (verified by QQ-plots and the Shapiro-Wilk normality test ($p>0.05$)), correlation tests were run using the lm() function ($p<0.05$).

2.7.3 T-test

To test for significant differences between two groups, a t-test was used. The samples were first tested for equal variance within each population using the var.test() ($p>0.05$). Subsequently, the data were investigated for normal distribution, using QQ plots and the Shapiro-Wilk normality test ($p>0.05$). When the criteria were met, an independent sample t-test was run (t.test()) with a level of significance at $p < 0.05$.

2.7.4 ANOVA

To test for significant differences between more than two groups, an ANOVA was performed. The normal distribution of the data was verified using QQ plots and Shapiro-Wilk normality test ($p > 0.05$). Subsequently, the homogeneity of variance was tested using a Barlett test ($p >$

0.05). The data were then tested for significant differences using One Way ANOVA, with a subsequent TurkeyHSD post-hoc test.

2.7.5 Data visualization

All PCA analysis were visualized using the autoplot() function in the ggplot package in R. All other graphs were made in Microsoft Excel 16.48.

3. Results

3.1 Elemental composition and pH

3.1.1 Peat plateaus

The elemental composition of the collected peat samples was analyzed to infer differences in peat quality. The method of decomposition and analysis was selected based on the most essential elements for this study, namely S, P, and Hg. Other elements were selected based on extractability with the selected method, and their role in peat chemistry and microbial physiology. The optimal decomposition method for S, P, and Hg did not yield accountable results for K and Na. Consequently, K and Na were excluded from the analysis despite being important components in soil chemistry and microbial physiology. For each peat plateau, depth profiles of pH and extractable DOC were determined (Fig. 9).

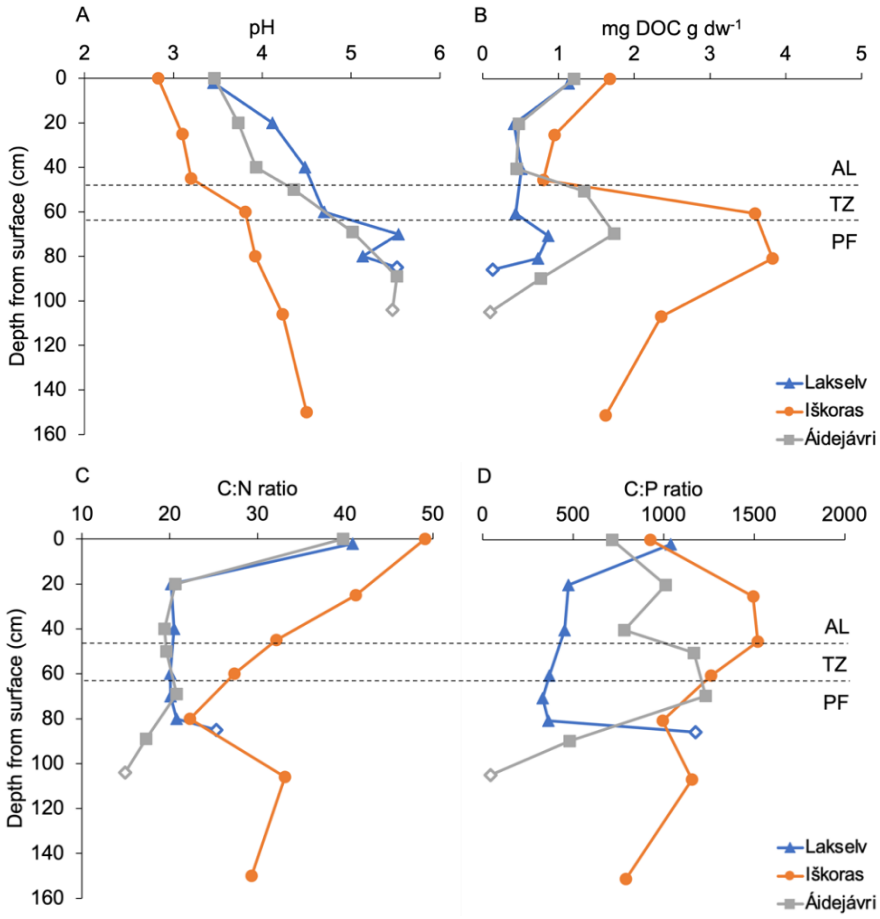

Figure 9. Depth profiles of pH (A), DOC (B), C:N (C) and C:P (D) in the peat plateaus at Lakselv, Iškoras and Áidejávri. The stippled lines denote the transitions between the AL (top section), TZ (middle section), and PF (bottom section). Open symbols for deepest PF layers at Lakselv and Áidejávri indicate influence from mineral soil.

Peat at Iškoras had the lowest pH, the highest concentrations of extractable DOC, and the highest C:N and C:P ratios among the three peat plateaus. In addition, concentrations of the metals Mg, Ca, Fe (Fig. 10D, E, F), and Mn (Tbl. A.1, appendix) were lowest. Carbon content (Fig. 10A) and DOC concentrations were lowest at Lakselv, which also had extraordinarily low C:P ratios reflecting its low C and high P contents (Table A.1). Concentrations of metals, particularly those of Mg (Fig. 10D), Zn (Fig. 11), Cu, and Ni (Tbl. A.1, appendix) were found to be highest in Lakselv, likely due to the influence of sea aerosols. Áidejávri had the highest concentrations of N, S, and Ca (Fig. 10B, C and E). C:N ratios were similar for Lakselv and Áidejávri.

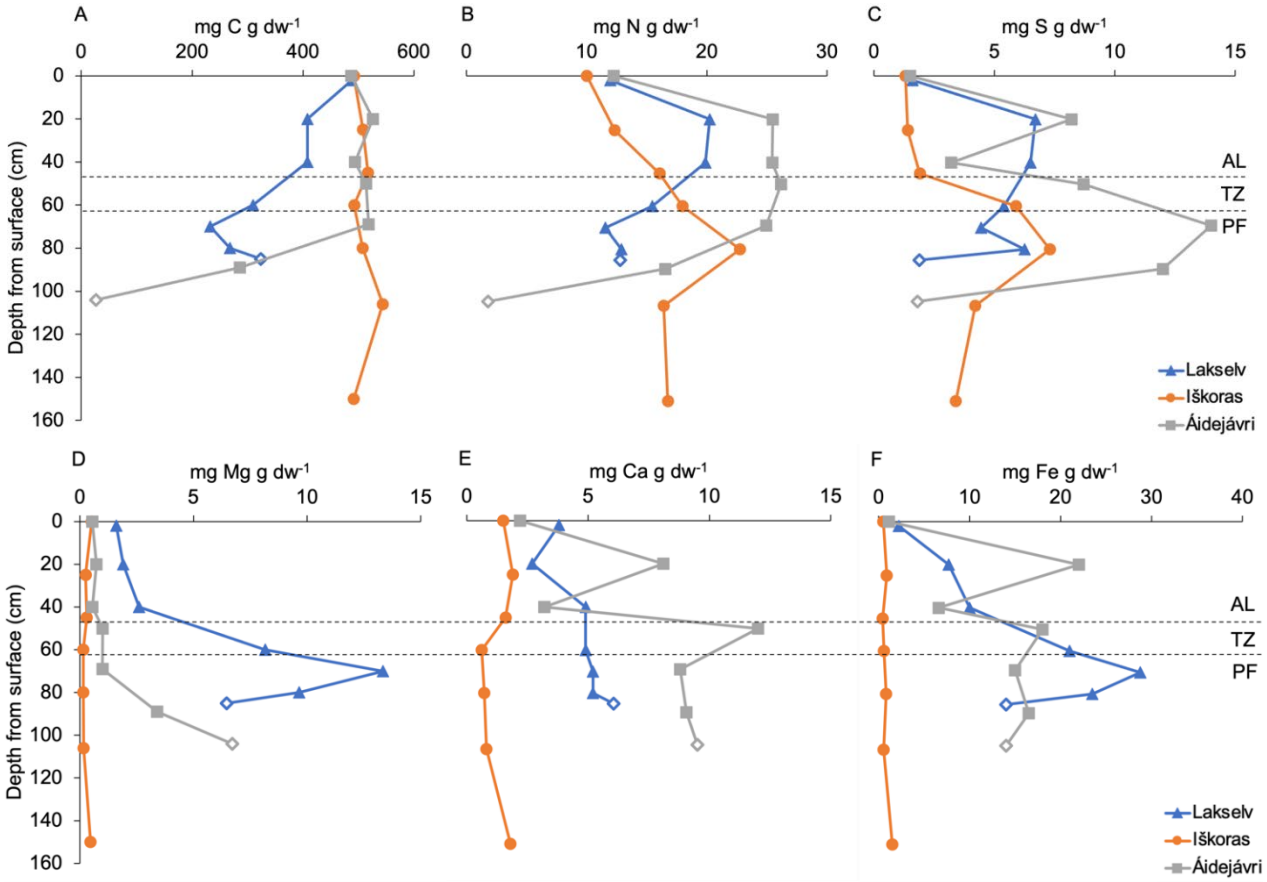

Figure 10. Depth profiles of the essential elements C (A), N (B), S (C), Mg (D), Ca (E), and Fe (F) in the peat plateaus at Lakselv, Iškoras, and Áidejávri. The stippled lines denote the transitions between the AL (top section), TZ (middle section), and PF (bottom section). Open symbols for deepest PF layers at Lakselv and Áidejávri indicate influence from mineral soil.

In **Iškoras,** concentrations of the essential macro-elements N, P, S, and the trace elements Zn, Ni, Cu, and Se (Fig. 11; Tbl A.1) were lower in AL than PF peat. By contrast, concentrations of other essential elements, such as C, Mg, Ca, Fe, and Mn were more evenly distributed with depth. Carbon content was persistently high, and the four latter elements persistently low. Of the non-essential metals, the concentration of Al was generally low throughout the core, whereas As, Pb, and Cd showed elevated concentrations in AL1 and a maximum in PF3 (Table A.1).

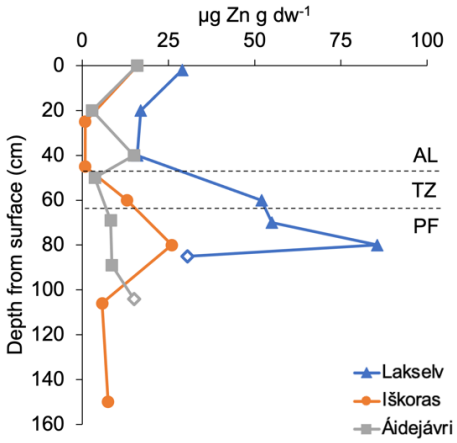

Figure 11. Depth profile of Zn concentration in peat plateaus at Lakselv, Iškoras, and Áidejávri. The horizontally stippled lines indicate transitions between AL (top), TZ (middle) and PF (bottom). Open symbols for deepest PF layers at Lakselv and Áidejávri indicate influence from mineral soil

In **Lakselv**, the concentrations of most elements in AL1 and the top of the PF (PF1) stood out from the rest of the core. For the essential non-metals N, P, S, and Se, the concentrations were lower in AL1 compared to the rest of the AL. Most essential metals, namely Fe, Mn, Ni, Cu, Zn, and Mg showed a general increase in concentration with depth, with a sudden rapid increase in TZ and PF1. The Ca content was rather stable over depth, while the concentrations of Al, As, and Pd followed a similar depth profile as those of the essential metals. Trends in concentrations of Cd with depth were more similar to the essential non-metals.

In **Áidejávri**, element contents varied greatly throughout AL and TZ with similar concentrations in AL1 and AL3, while many elements were enriched in AL2 (e.g. Ca, S, and Fe in Fig. 10, Ni, Cu and Se in Tbl. A.1). Element composition of AL2 appeared to be more similar to that of TZ. On the contrary, the elements P and Zn showed the opposite trend, with higher concentrations in AL1 and AL3 compared to AL2 (e.g. Fig. 11). The depth profiles of N and Mn differed from those of other elements, with lower concentrations in AL1, and stable concentrations through AL2 and AL3 (e.g. Fig 10). In the permafrost, C, N, and S generally decreased with depth, and P, Mg, Ni, Cu, and Se increased, while Ca, Fe, Mn, and Zn were fairly stable. Of the non-essential elements, As, Pb, and Cd showed similar trends as Zn. The

concentration of Al was generally low at Áidejávri, with a slightly enrichment in the permafrost (Table A.1).

To summarize differences in elemental composition, pH, and C:N ratios between the peat plateaus, the data were subjected to PCA. To avoid disproportionate weight of micro-elements in the analysis, Cu and Ni were excluded due to similar chemical properties and visually similar distribution to that of Zn. When including all other essential elements (C, N, P, S, Ca, Mg, Fe, Mn, Zn, Cu), C:N ratios, and pH values, there was a clear clustering of sites irrespective of depths except for AL1 samples, which formed a group on its own (Fig. 12). The superimposed loading plot reveals that Iškoras differs from the other two sites in that it is more acidic, carbon-rich, and has higher C:N ratios, suggesting a different peat quality. Also, Lakselv and Áidejávri differ in peat chemistry, with Lakselv having higher concentrations of Mg, Fe, Mn, and Zn, and Áidejávri higher concentrations of N, S, and Ca. Samples from AL1 of all three sites formed a separate group, due to their higher C:N ratios, lower pH values, and lower Mn, Fe, Ca, and S contents. The clustering of AL1 suggests similar organic matter quality in the top layer across all three sites.

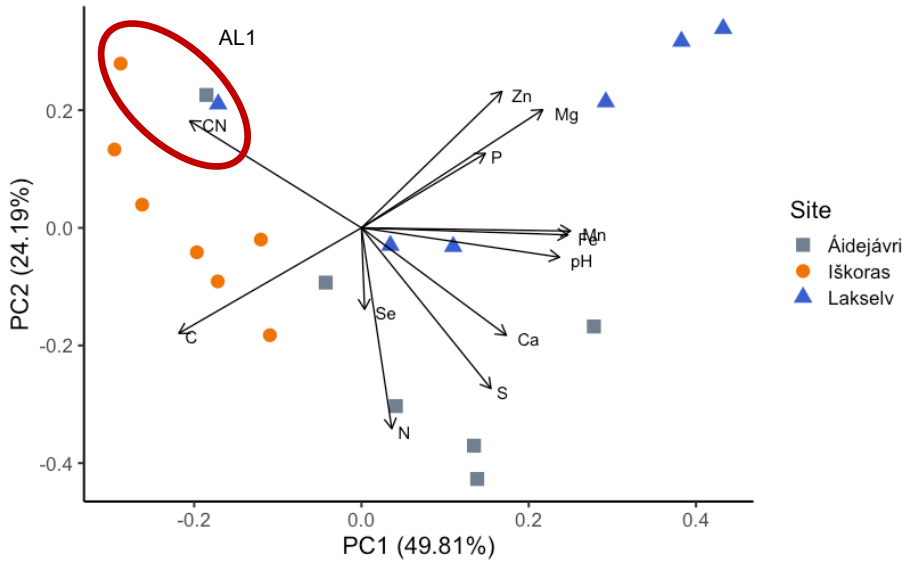

Figure 12. Score and loading plot (superimposed) of a PCA with the biologically essential elements (C, N, P, S, Ca, Mg, Fe, Mn, Zn, Se), C:N ratio, and pH. The red circle indicates the clustering of AL1 samples from all three sites. The analysis included samples from peat plateaus at Lakselv (0-85 cm), Iškoras (0-162 cm), and Áidejávri (0-100 cm). Samples with mineral soils were excluded.

3.1.2 Transects

The C:N ratios and elemental composition of the top 10 cm (n = 1 per landscape feature per site) of the peat plateaus (AL1), and adjacent thermokarst sediment (TK1) and a wet mire without underlying permafrost (WM1) from each site are shown in Fig. 13 and Table A.2. Except for Áidejávri, the C:N ratio of AL1 was higher than that of TK1, implying increased OM decomposition upon TK formation. The C:N ratio of WM1 differed across sites, showing an extraordinarily high value at Lakselv (> 90).

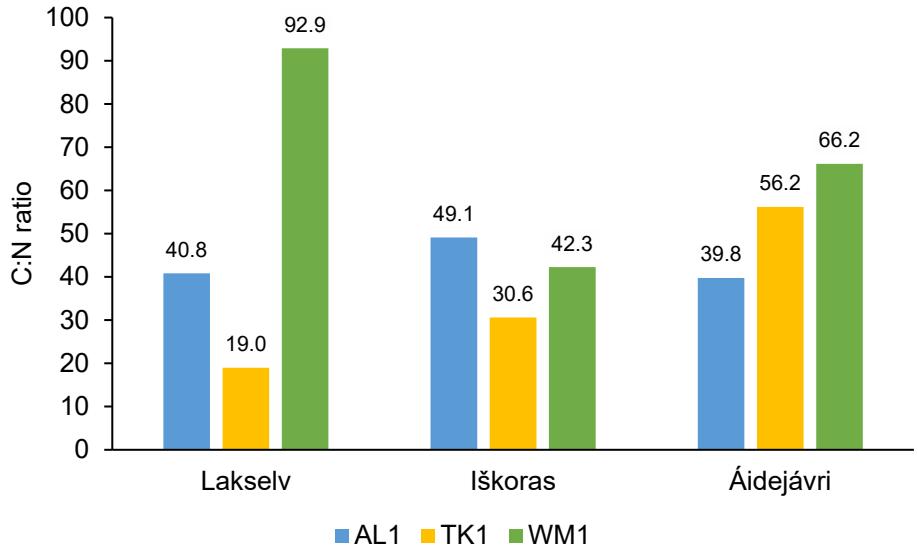

Figure 13. The C:N ratio in the top 0-10 cm of palsa peat (AL1), adjacent thermokarst sediment (TK) and an adjacent wet mire (WM1) at Lakselv, Iškoras and Áidejávri.

3.1.3 Mapping of Hg in peat

Concentrations of Hg were generally highest in AL1 at all three sites (Fig.14A), reflecting the increased Hg deposition over the last century. In Lakselv, the concentrations decreased gradually with depth, except for a slight increase in the middle of the permafrost (PF2). In Iškoras, AL3 had the lowest concentration of Hg, followed by an increase in the TZ and PF. When excluding AL1, the Hg concentration in Iškoras was generally higher in the PF than AL. In Áidejávri, the concentration of Hg showed a trend similar to that of P, Zn, and Pb, with a similarly high concentration in AL3 to that of AL1. The remainder of the core from Áidejávri had relatively low and stable Hg concentrations.

Since Hg readily binds to C and S, the Hg concentrations were normalized for the respective elements (Fig. 14 B, C). The Hg:C ratio at Lakselv was more evenly distributed with depth than the Hg content, suggesting that Hg followed C distribution in this peat plateau. By contrast, the normalization for C resulted in a larger difference between Lakselv and Iškoras in the AL. In the PF, however, the difference between Lakselv and Iškoras decreased, whereas the difference between Lakselv and Áidejávri increased.

When normalized for S content, the Hg:S ratio at all three sites became more evenly distributed with depth (Fig. 14C), particularly for the PF, suggesting that the S content of peat is a strong predictor for Hg concentrations.

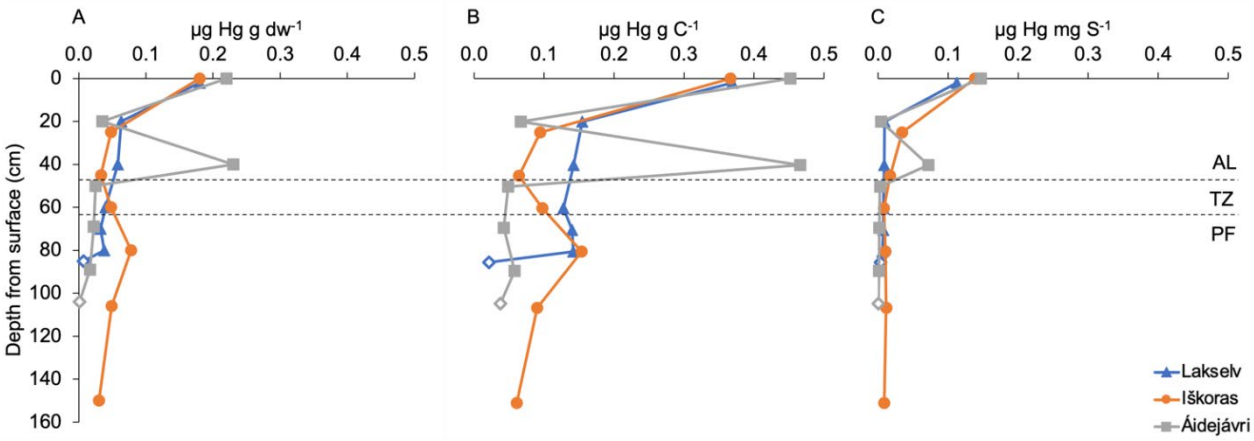

Figure 14. Depth distribution of Hg in peat plateaus at Lakselv, Iškoras and Áidejávri. Shown are (A) µg Hg contents per g dry weight peat, (B) Hg content normalized for C content and (C) Hg content normalized for S content. Markers without fill indicate mixing with mineral soil. The horizontal stippled lines indicate transitions between AL (top), TZ (middle), and PF (bottom).

To further investigate intercorrelations between Hg, other elements, pH, and C:N ratios, several PCA were run. In addition to the elements included in the PCA shown in Fig. 12, the non-essential elements Al, Cd, Pb, and As were included to unmask potential correlations between Hg and other biologically non-essential metals. The PCAs were first run separately for each site (Fig. A.1-3, appendix). A commonality for all three sites was that Hg was positively correlated with the C:N ratio, and negatively with the S content (Fig. 15), likely due to the

persistently high Hg concentration and C:N ratio, and low S concentration in AL1 across sites. In comparison to other metals, Hg showed the highest intercorrelation with Pb, which was positively intercorrelated at Iškoras and Áidejávri, but not at Lakselv.

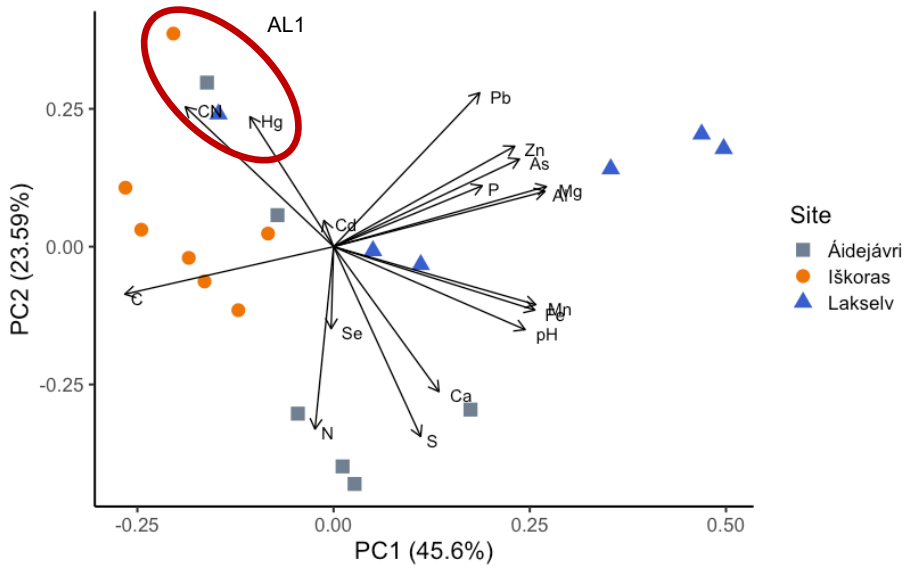

Figure 15. PCA score and loading plots (superimposed) including essential elements and metals (C, N, P, S, Mg, Ca, Fe, Mn, Se, Zn, Ni, Cu), common pollutants (Pb, As, Cd, Hg), C:N ratio, and pH. The red circle indicates a clustering of AL1 from all three sites. The analysis is based on samples from all depth at Lakselv (0-85 cm), Iškoras (0-162 cm), and Áidejávri (0-100 cm). PF3 from Lakselv and Áidejávri were excluded from the analysis due to mineral influence.

The average concentrations of Hg in the permafrost were compared between sites by pooling data for PF1 and PF2 at each site (Fig. 16). Samples from PF3 were excluded because they contained mineral soil at Lakselv and Áidejávri. The averages revealed that Iškoras has the highest concentration of Hg in the PF (0.06 µg g dw peat^{-1}) followed by Lakselv (0.04 µg g dw peat^{-1}) and Áidejávri (0.02 µg dw peat^{-1}). When comparing the Hg concentration normalized for C concentration, however, Lakselv showed a slightly higher ratio (0.14 µg Hg g C^{-1}) than Iškoras (0.12 µg Hg g C^{-1}) followed by Áidejávri which had the lowest Hg:C ratio with 0.05 µg Hg g C^{-1}. Significance of differences was not tested statistically, since the criteria of independent sampling were not fulfilled (there was only one core from each site and samples from the same core are not independent).

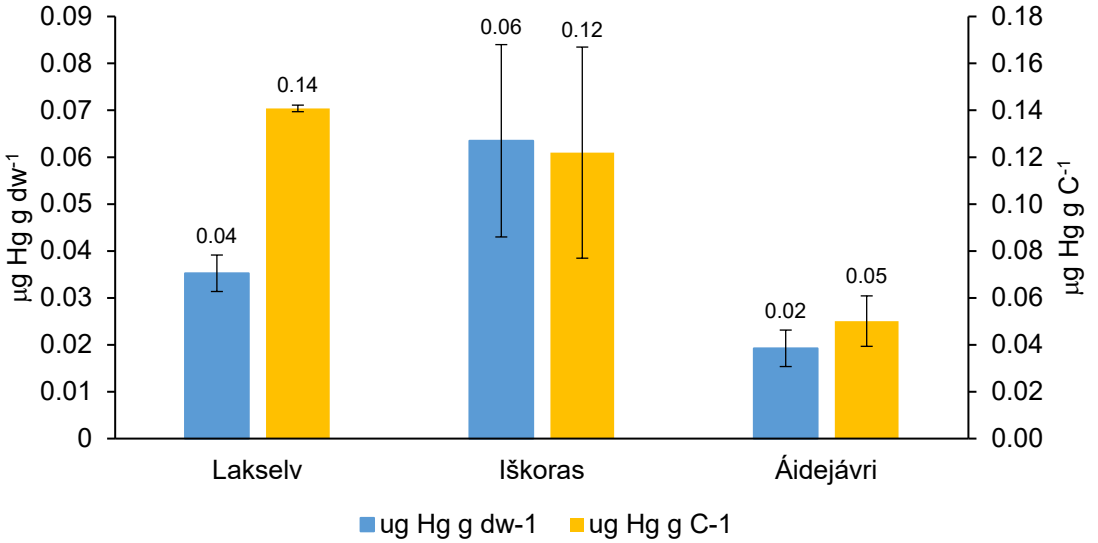

Figure 16. Average Hg concentrations and µg Hg g C^{-1} in permafrost peat (average of PF1 and PF2) at Lakselv (n = 2), Iškoras (n = 2), and Áidejávri (n = 2). Error bars are standard deviation.

To compare Hg concentrations in peat plateaus with those in adjacent landscape features, Hg concentrations in AL1 were averaged across all three sites and plotted together with those of the sediment of adjacent thermokarsts (TK1) and the top layers of adjacent wet mires (WM1) (Fig. 17). The content of Hg in AL1 was significantly larger than in TK1 ($p < 0.05$) and WM1 ($p < 0.001$), while TK1 held significantly more Hg than WM1 per g dry weight peat ($p < 0.05$). When comparing Hg:C ratios, there was no significant difference between AL1 and TK1 ($p = 0.076$), however WM1 was found to be significantly lower than both AL1 ($p = 0.0012$) and TK1 ($p = 0.015$).

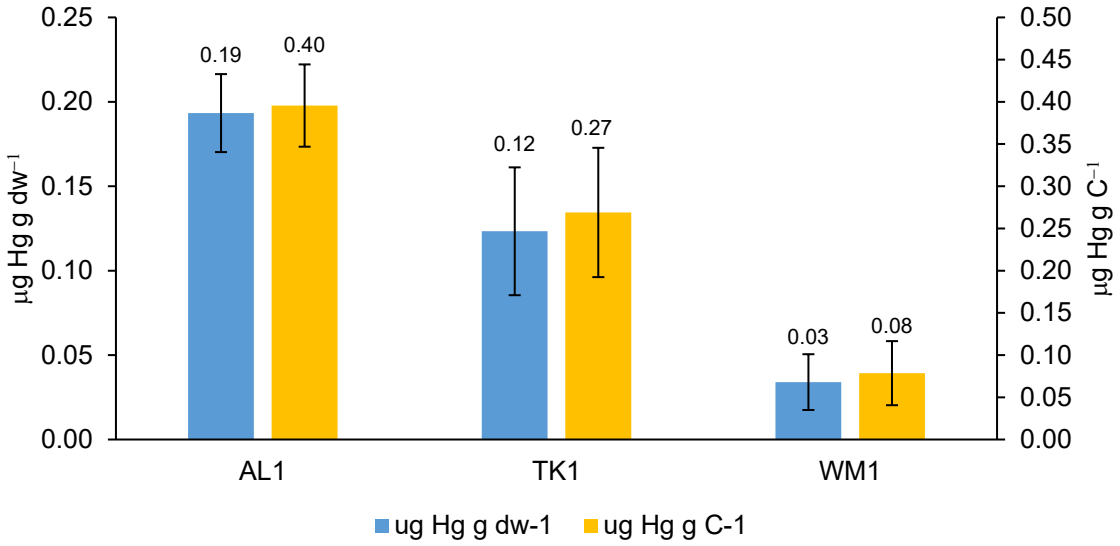

Figure 17. Average Hg concentrations and Hg:C ratios in the top layer (0-10 cm) of AL (n=3), TK (n=3), and WM (n=3). The values were averaged across Lakselv, Iškoras, and Áidejávri. Error bars are standard deviation.

3.1.4 Water chemistry

To obtain a general overview of the elements dissolved in water and to look for geochemical coupling between peat plateaus and surrounding water bodies, water chemistry was analyzed in thermokarst lakes and streams (Table 7). Thermokarst lakes in Iškoras had Ca concentrations roughly one order of magnitude smaller than at Lakselv and Áidejávri, well reflecting the differences in ambient peat chemistry. Waters at Iškoras had also lower conductivity than at Áidejávri (no data for conductivity were available for Lakselv). Lakselv waters had highest Mg concentrations, similar to what was found in ambient peat, likely reflecting the influence of sea aerosols. Concentrations of potential electron acceptors for anaerobic respiration (NO_3^- and SO_4^{2-}) were generally low, with the exception of the large thermokarst pond in Áidejávri.

When comparing smaller and larger thermokarst ponds, smaller ponds showed a tendency of having higher conductivity and concentrations of DOC, and lower pH. There were no clear differences in element concentrations between small and large thermokarst ponds.

To explore the differences in elements transported in and out of the catchments, the water chemistries in inlet and outlet at Iškoras were compared, in addition to a stream that leaches from the peat plateaus into a wet mire. No inlet data were available for Áidejávri and Lakselv.

The inlet water at Iškoras had slightly higher pH, and higher concentrations of DOC, Ca, Mg, P, and SO_4^{2-} than the outlet water. The concentration of total N however, appeared to be higher in the outlet than the inlet. The stream within the peat plateau area had higher concentrations of DOC and N, and lower pH, conductivity, and Mg and Ca compared to inlet or outlet. The lower pH, Ca and Mg and higher concentration of N in the outlet would be consistent with a contribution of water from the peat plateaus. However, the high DOC in the stream coming from the peat plateau did not leave a DOC signal in outlet water. It should be noted that we only sampled once and that a robust comparison should comprise several samplings in different seasons.

Table 8. Water chemistry of thermokarst ponds and streams in Lakselv, Iškoras, and Áidejávri. Values marked with * were analyzed in the environmental chemistry lab at NMBU.

	Type	DOC mg L^{-1}			pH			Conductivity mS m^{-1}			TotCa mg L^{-1}			TotMg mg L^{-1}			SO_4^{2-} mg L^{-1}			NO_3 µg L^{-1}			TotP µg L^{-1}			TotN µg L^{-1}		
		LA	IŠ	ÁI	LA	IŠ	ÁI	LA	IŠ	ÁI	LA	IŠ	ÁI	LA	IŠ	ÁI	LA	IŠ	ÁI	LA	IŠ	ÁI	LA	IŠ	ÁI	LA	IŠ	ÁI
Thermokarst Ponds	Small, erosion edge	N/A	N/A	46*	N/A	N/A	N/A	N/A	N/A	N/A	N/A	N/A	1.9*	N/A	N/A	0.5*	N/A	N/A	1.0*	N/A	N/A	N/A	N/A	N/A	*210**	N/A	N/A	N/A
	Small, in palsa	37*	35	71	N/A	3.9	3.7	N/A	5.5	9.1	2.1*	0.2	1.9	2.2*	0.06	0.2	0.7*	0.1	0.7	N/A	2	1.5	*<40**	3	3	N/A	980	950
	Large, in palsa	N/A	27	20	N/A	4.2	4.7	N/A	3.2	2.2	N/A	0.7	1.1	N/A	0.3	0.3	N/A	0.07	1.1	N/A	1.5	34	N/A	<1	3	N/A	860	1700
	Transition to wetland	N/A	19	N/A	N/A	4.5	N/A	N/A	2.3	N/A	N/A	0.6	N/A	N/A	0.3	N/A	N/A	0.08	N/A	N/A	1.5	N/A	N/A	3	N/A	N/A	440	N/A
	Upstream lake, old thermokarst	N/A	N/A	6.4	N/A	N/A	7.0	N/A	N/A	4.0	N/A	N/A	4.0	N/A	N/A	1.2	N/A	N/A	0.7	N/A	N/A	1.5	N/A	N/A	2	N/A	N/A	600
Streams	Inlet	N/A	9.4	N/A	N/A	6.8	N/A	N/A	2.5	N/A	N/A	2.2	N/A	N/A	1.1	N/A	N/A	0.8	N/A	N/A	1.5	N/A	N/A	7	N/A	N/A	200	N/A
	Palsa	N/A	35	8.2	N/A	4.8	7.0	N/A	1.6	3.4	N/A	0.6	3.9	N/A	0.3	1.1	N/A	0.1	0.7	N/A	1.5	1.5	N/A	3	2	N/A	430	190
	Outlet	41*	7.7	N/A	N/A	6.6	N/A	N/A	2.4	N/A	1.9*	2.0	N/A	2.2*	0.9	N/A	4.3*	0.6	N/A	N/A	1.5	N/A	*<40**	2	N/A	N/A	370	N/A

3.1.4 Hg in water

Concentration of HgT and MeHg were highest in Lakselv, followed by Áidejávri and Iškoras (Table 8). When normalizing the HgT concentration for DOC concentration, HgT and its methylated fraction were clearly highest in the small thermokarst pond at Lakselv. However, this high MeHg signal was not detected in outlet water. Also, HgT:DOC ratios for stream water were similar at all sites. Waters at Iškoras had the lowest concentrations of HgT and MeHg and the lowest values of %MeHg of HgT in ponds. It should be noted that the samples analyzed for HgT from Lakselv and thermokarst pond by erosion edge in Áidejávri (marked with * in Table 8) were stored for a prolonged period and Hg may have been lost due to reduction and evaporation, possibly resulting in an underestimation of HgT concentration for these samples.

Small thermokarst ponds had generally higher concentrations of dissolved HgT than large thermokarst ponds. Differences in MeHg concentrations among thermokarst ponds were more ambiguous with a tendency of higher MeHg concentrations in large ponds, except for the small pond by the active erosion edge in Áidejávri, which showed the highest MeHg value for this site.

Comparing HgT concentrations in inlet and outlet at Iškoras revealed no measurable difference (1.4 ng HgT L^{-1}). The concentration of MeHg, however, was much higher in the outlet compared to the inlet (0.05 and 0.12 ng MeHg L^{-1}, respectively). The concentration of MeHg in the stream in direct contact with the peat plateau was intermediate of that in the inlet and outlet (0.08 ng MeHg L^{-1}). Again, this would be consistent with a contribution of MeHg from the peat plateau to the outlet water. The higher MeHg concentration in the outlet could also be related to MeHg production in the wet mire.

Table 8. Distribution of Hg and MeHg, and Hg:DOC ratio and %MeHg of HgT in ponds and streams in Lakselv, Iškoras and Áidejávri. Samples marked with * were analyzed at the environmental chemistry lab at NMBU, the remainder at NIVA. The HgT samples from the environmental chemistry lab at NMBU were decomposed prior to analysis due to precipitation in some samples

	Type	HgT ng L^{-1}			Hg:DOC ratio ng mg^{-1}			MeHg ng L^{-1}			%MeHg of HgT		
		LA	IŠ	ÁI	LA	IŠ	ÁI	LA	IŠ	ÁI	LA	IŠ	ÁI
Thermokarst Ponds	small, by erosion edge	*N/A*	*N/A*	12.3*	*N/A*	*N/A*	0.27	*N/A*	*N/A*	1.41	*N/A*	*N/A*	11.5
	small, in palsa	8.6*	4.7	6.6	0.23	0.14	0.092	2.4	0.04	0.17	28.2	0.9	2.6
	large, in palsa	*N/A*	2.3	3.0	*N/A*	0.086	0.15	*N/A*	0.06	0.20	*N/A*	2.8	6.7
	transition to wetland	*N/A*	2.5	*N/A*	*N/A*	0.13	*N/A*	*N/A*	0.05	*N/A*	*N/A*	1.9	*N/A*
	upstream lake, old thermokarst	*N/A*	*N/A*	0.8	*N/A*	*N/A*	0.12	*N/A*	*N/A*	0.03	*N/A*	*N/A*	3.7
Stream	Inlet	*N/A*	1.4	*N/A*	*N/A*	0.15	*N/A*	*N/A*	0.05	*N/A*	*N/A*	3.6	*N/A*
	Palsa	*N/A*	1.7	1.7	*N/A*	0.047	0.092	*N/A*	0.08	0.05	*N/A*	4.9	6.1
	Outlet	5.4*	1.4	*N/A*	0.13	0.18	*N/A*	0.3	0.12	*N/A*	5.6	9.0	*N/A*

To look for intercorrelations between HgT and water chemistry, several PCAs were performed. A PCA including data from all three sites showed that the concentration of dissolved HgT in ponds strongly depended on DOC concentration and that MeHg was positively correlated with the concentration of SO_4^{2-} (Fig. 20A). In streams, MeHg appeared to be more coupled to HgT concentration (Fig. 20B), but both HgT and MeHg correlated positively with DOC and SO_4^{2-}.

The concentration of N, pH and conductivity were not analyzed in the water samples analyzed for HgT at NMBU (HgT concentrations marked with * for the respective samples in table 8). This included all samples from Lakselv. Therefore, the site could not be included in the PCA where N concentration, pH, and conductivity were incorporated. Concentrations of MeHg in ponds and HgT in streams were found to be positively correlated with N in the analysis excluding Lakselv (Figure A.4-5, appendix).

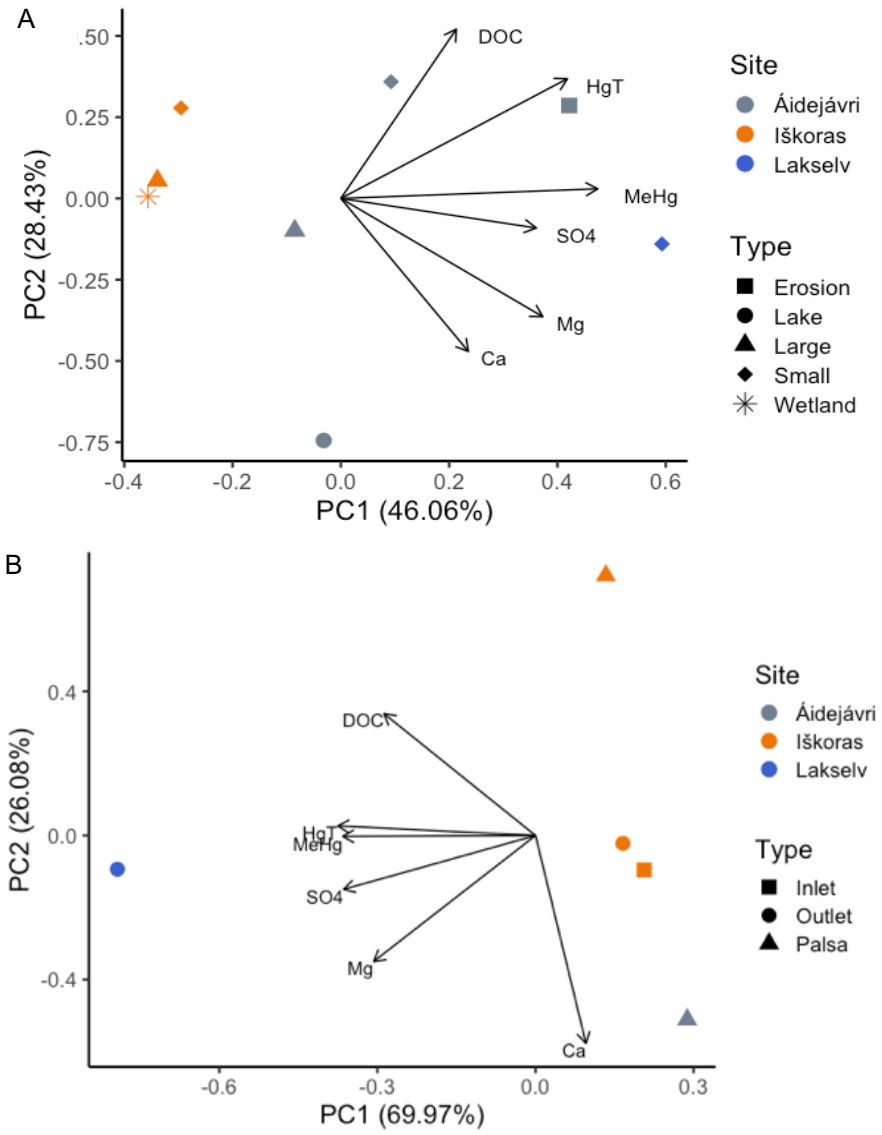

Figure 18. PCA of HgT, MeHg, DOC, SO_4^{2-}, Mg, and Ca for ponds (A) and streams (B) in different waters at Lakselv, Iškoras, and Áidejávri. pH, conductivity, NO_3, TotN, and TotP, were excluded, due to missing data for samples from Lakselv.

The dependency of dissolved HgT on DOC was confirmed by correlation analysis. Log transformed concentrations of HgT and DOC were found to have an almost perfect correlation ($R^2 = 0.99$, $p < 0.0001$) (Fig. 21).

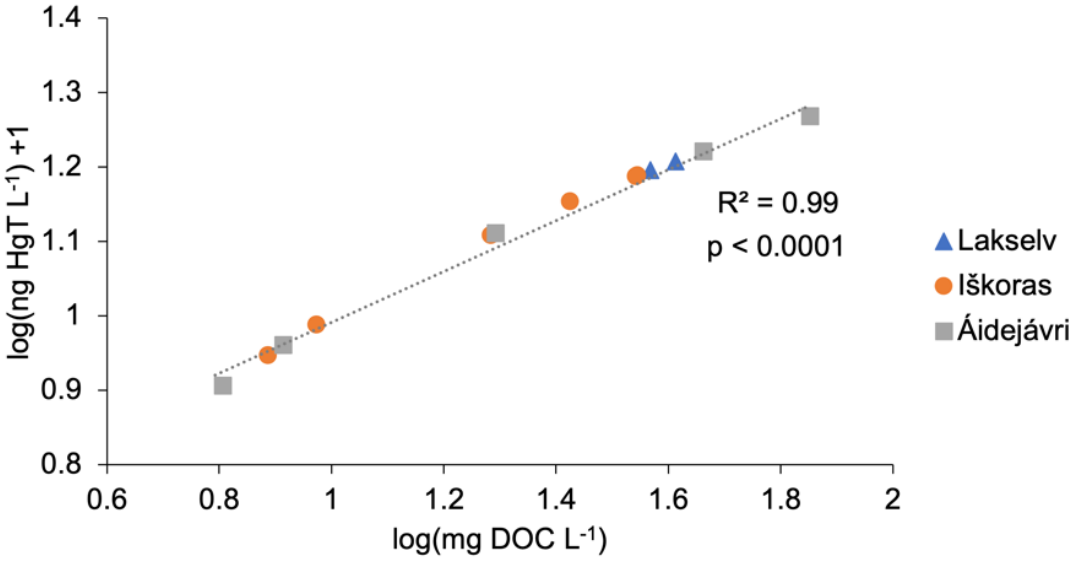

Figure 19. Correlation between HgT and DOC in streams and ponds across Lakselv, Iškoras, and Áidejávri. The concentrations of DOC are displayed on the x-axis as log(mg DOC L^{-1}) and the concentrations of HgT along the y-axis as log(ng HgT L^{-1}) + 1.

3.2 Release of Hg upon incubation of permafrost peat: effect of depths and redox conditions

To test whether Hg would be released gradually from the PF during post-thaw decomposition, samples were incubated as stirred slurries at 10°C under oxic and anoxic conditions for up to 108 days. To assess water-extractable dHgT at the beginning of the incubation, permafrost material was thawed overnight, amended with DI water, and stirred for 1 h at 10°C, before subsampling and filtering (0.45 µm) an aliquot from the suspension for analysis. Concentrations of dHgT in TZ and PF samples analyzed with incubation start were all below LOQ (<3.0 ng L^{-1}). In comparison, AL1 and AL2 showed detectable concentrations of dHgT at the start of the incubation (Tbl. A.4, appendix). The same procedure was applied after 96-108 days of incubation (17 days of which the slurry was stirred continuously). The measured dHgT concentration at the end of the incubation minus the concentration at the start (if above LOQ) thus represent the net release of Hg to the water during incubation. To normalize for varying incubation times, the net released dHgT was divided by the number of days incubated and expressed as rates (ng HgT kg dw^{-1} d^{-1}).

Release rates of Hg from peat to water were largest in AL samples, irrespective of site, and larger in anoxically than oxically incubated samples (Fig. 22; upper panel). For PF, the effect of initial redox conditions was ambiguous; Lakselv showed the highest release rates under anoxic conditions, Áidejávri under initially oxic conditions, whereas Iškoras had the highest release rates under anoxic conditions in PF1 and under initially oxic conditions in PF3.

Similar to Hg release, the production rates of DOC and CO_2 were generally higher in the AL compared to the rest of the peat profile. The accumulation rates of DOC (Fig. 20) and sum of DOC and CO_2-C, was slightly higher under anoxic than oxic conditions (Fig. A.6). Therefore, mobilization of HgT seemingly followed the production rates of DOC. The accumulation rates of CO_2-C appeared to be higher under initially oxic conditions, suggesting higher microbial activity.

The accumulation rates of DOC and CO_2 showed a similar depth profile than the release rates of HgT. To unmask the relationship between HgT release and degradation of OM, rates of HgT release were plotted against rates of CO_2 production and DOC release, respectively (Fig. 23). Rates of HgT release and DOC accumulation correlated positively across the three sites in both the oxic ($p = 0.005$) and anoxic ($p = 0.00005$) incubations, when omitting three outliers from Áidejávri with inconsistently low HgT release rates (Fig. 23; Fig. A.7, appendix). A significant correlation was also found between dHgT and CO_2 production in both oxic ($p = 0.05$) and anoxic ($p = 0.01$) incubations when removing the same outliers. No significant correlation was found between dHgT and native HgT concentration.

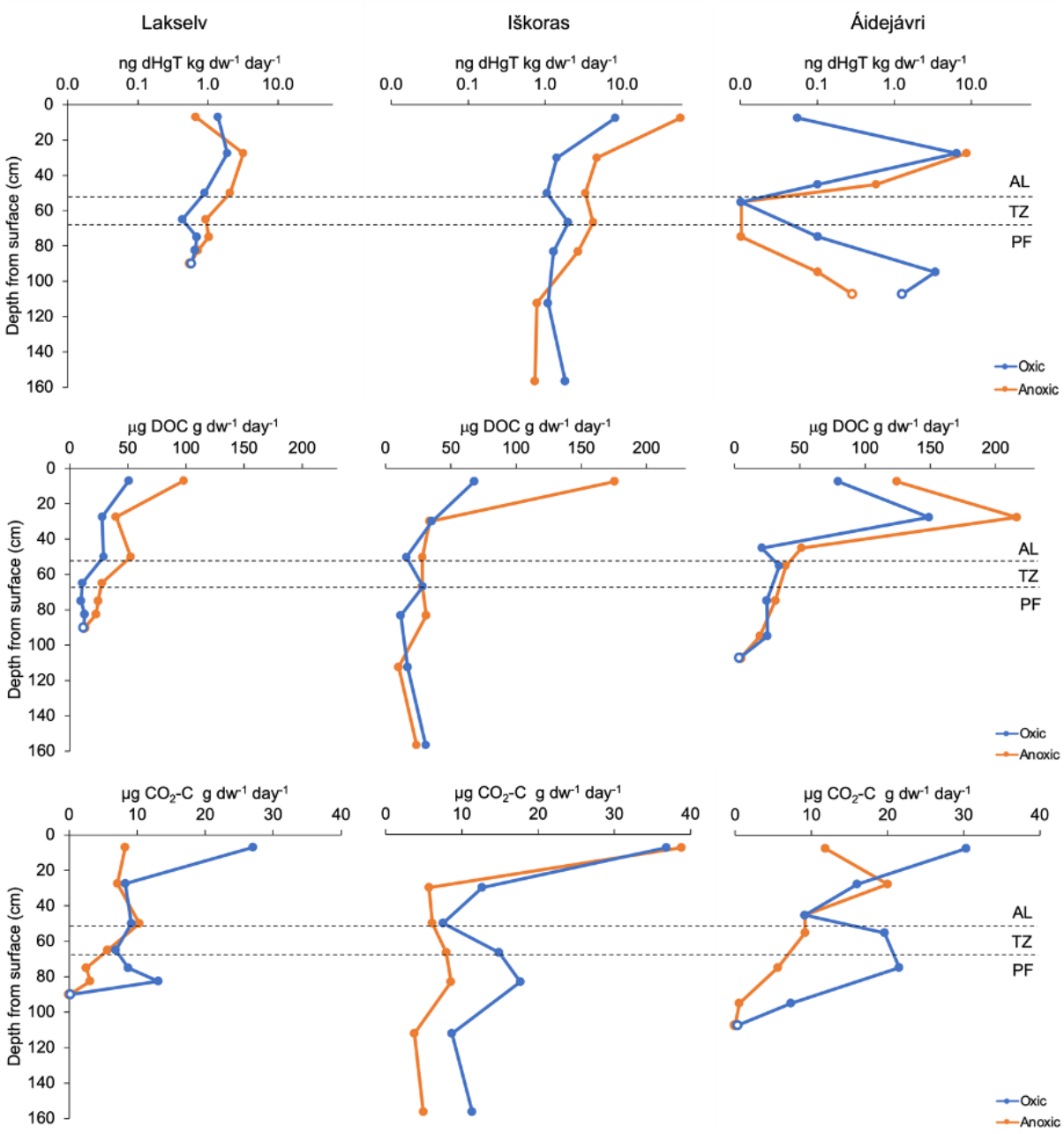

Figure 20. Daily rates of net release of HgT, DOC, and CO_2 production with depth during 96 days of initially oxic or anoxic incubation. The upper panel shows Hg mobilization rates in ng dHgT g dw^{-1} day^{-1}, the middle panel DOC production in µg DOC g dw^{-1} day^{-1}, and the bottom panel CO_2 production as µg C g dw^{-1} day^{-1}. Markers without fill indicate mixing with mineral soil. The dotted horizontal lines mark the approximate transition between AL (top), TZ (middle) and bottom (PF). Note logarithmic x-axis scale in the upper panel.

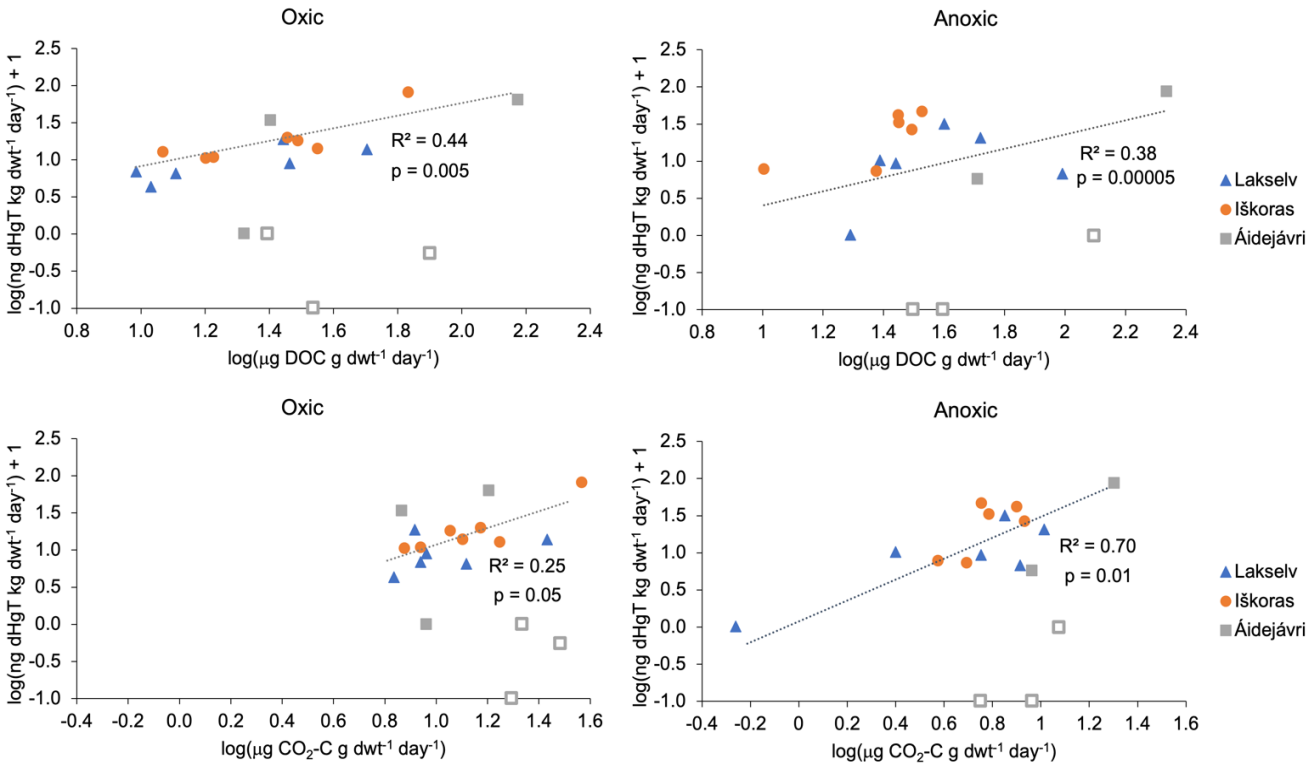

Figure 21. Correlation between rates of HgT release and DOC production in samples incubated oxically (left) and anoxically (right) across the three sites (Lakselv, Iškoras, Áidejávri) and different depths (PF3 was excluded from Lakselv and Áidejávri due to mixing with mineral soil). Log-log plots with dHgT displayed as log(ng dHgT kg dwt^{-1} day^{-1}) + 1. Three outliers from Áidejávri were excluded and are indicated by markers with no fill.

When tested individually for site and incubation treatment, Iškoras was the only site that showed positive correlations between dHgT and DOC, dHgT and CO_2 production, and dHgT and native HgT concentration in the peat (described in section 3.1.2). To investigate whether HgT release depends on both, DOC production and native HgT concentration in the peat, the variables were tested by multiple regression analysis. The analysis revealed that more of the variance of dHgT values of Iškoras samples could be explained if including both DOC and native HgT for oxic ($R^2 = 0.91$, $p = 0.008$) and anoxic ($R^2 = 0.90$, $p = 0.01$) incubations. For Lakselv and Áidejávri, no correlation was found. As shown in figure 24, HgT release rates became more evenly distributed with depth when normalized for native HgT or production of DOC and CO_2 for Iškoras, but not for Lakselv and Áidejávri.

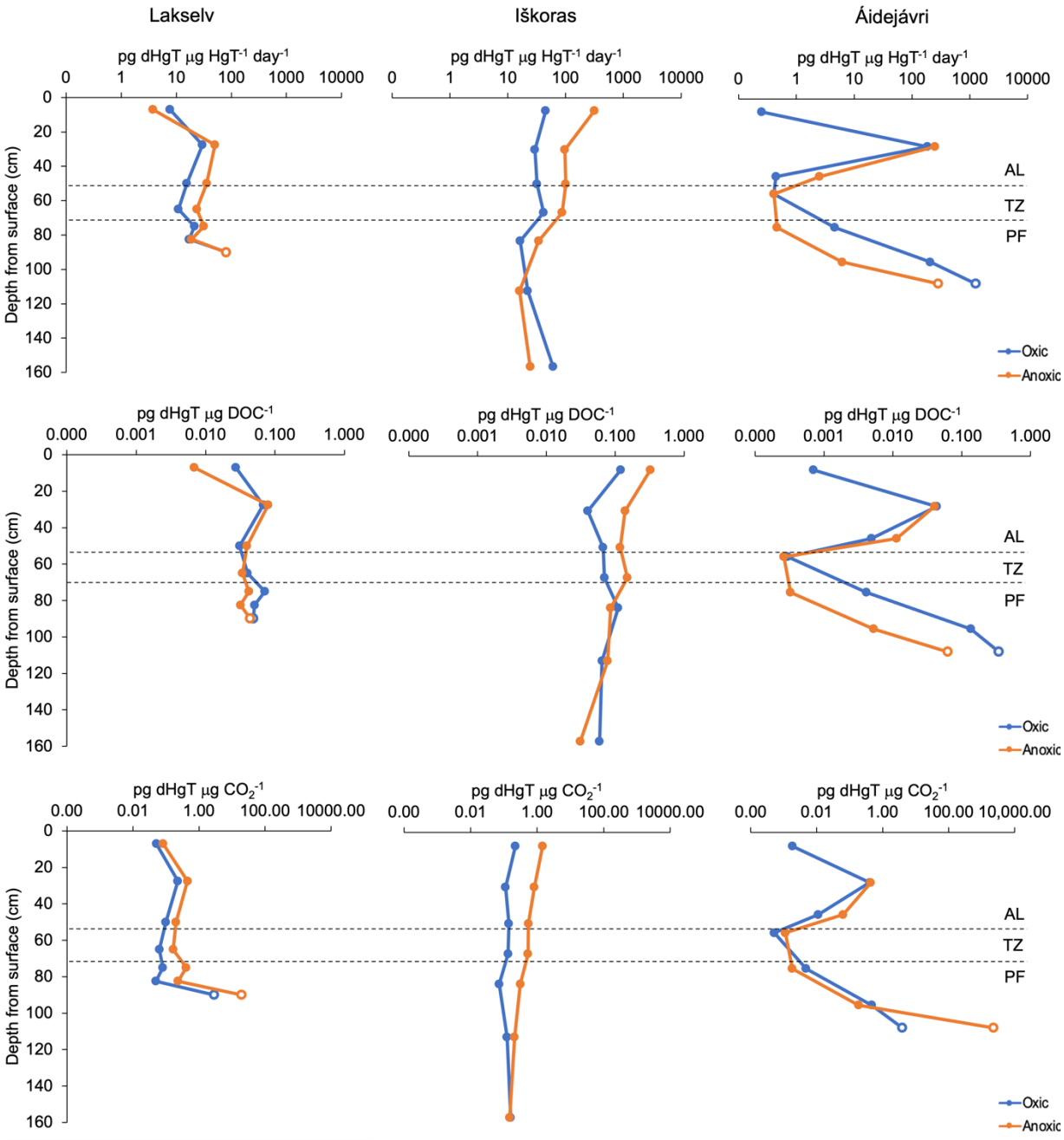

Figure 22. Depth distribution of daily rates of net release of dHgT in relation to native HgT in Lakselv, Áidejávri and Iškoras (upper panel), DOC production (middle panel), and CO_2-C production (bottom panel) during 96-108 days of initially oxic or anoxic incubation. Markers without fill indicate mixing with mineral soil. The dotted horizontal lines mark the approximate transition between AL (top), TZ (middle) and bottom (PF). All x-axes are log transformed.

3.3 Effect of nutrients on release of mercury

An additional incubation experiment with added nutrients (N and/or P), electron acceptors (S), and substrate (C and/or Hg; the latter added due to the original aim of study being to test effect on methylation) was set up to test whether stimulation of microbial activity would increase Hg release during incubation. No dHgT above LOQ was detected in any of the samples amended with nutrients (C, N, P, S, and NP), neither at the start nor at the end of the experiment (after 70 days), suggesting no or minimal release of Hg. By contrast, control samples without nutrient addition showed an average Hg release rate of 0.9 ± 0.1 ng dHgT kg dw soil^{-1} day^{-1}, which is comparable to the dHgT rates observed for Iškoras PF peat in the 108-day slurry incubation (Fig. 22). Since correlation between Hg release and OM degradation was established in section 3.2.1, CO_2 accumulation and change in DOC concentration were compared to unmask whether the lack of detectable dHgT in the treated samples was caused by low microbial activity. Due to widely differing variances between the treatments (Bartletts test; $p < 0.0001$), the samples were separated into groups, and treatments were tested against each other within each group. The groups were 1) samples with or without added essential nutrients (Control, N, P, NP), 2) samples with or without addition of readily available C (Control, C, CNPSHg), and 3) samples with or without an added alternate electron acceptor (Control, S).

In group 1, the treatment with added N (as NH^{4+}) had a significantly higher CO_2 accumulation rate than the Control ($p = 0.008$) and the treatment with added N and P ($p = 0.017$) (Fig. 25). There was no significant difference between the remaining nutrient treatments. In group 3, there was no significant effect of sulfate addition on CO_2 accumulation ($p = 0.052$). All samples having received glucose (group 2) accumulated significantly more CO_2 than the Control, irrespective whether glucose was given alone ($p = 0.0002$) or in combination with other nutrients (CNPSHg; $p < 0.0001$). The latter treatment produced more CO_2 than the treatment with glucose alone ($p = 0.009$) (Fig. 26).

Unlike CO_2 accumulation, DOC concentrations showed a conspicuous pattern with all nutrient treatments depleting DOC during incubation (Fig. 25, 26), whereas the Control produced DOC at similar rates as seen in the 108 days incubations (Fig. 22). Treatments with glucose (C and CNPSHg) had a significantly higher rate of DOC loss than nutrient treatments without glucose or the Control ($p < 0.0001$). Moreover, the rate of DOC loss was significantly higher in

CNPSHg than in C ($p < 0.0001$). Comparing the other treatments, the only significant difference was found between S and P ($p = 0.008$).

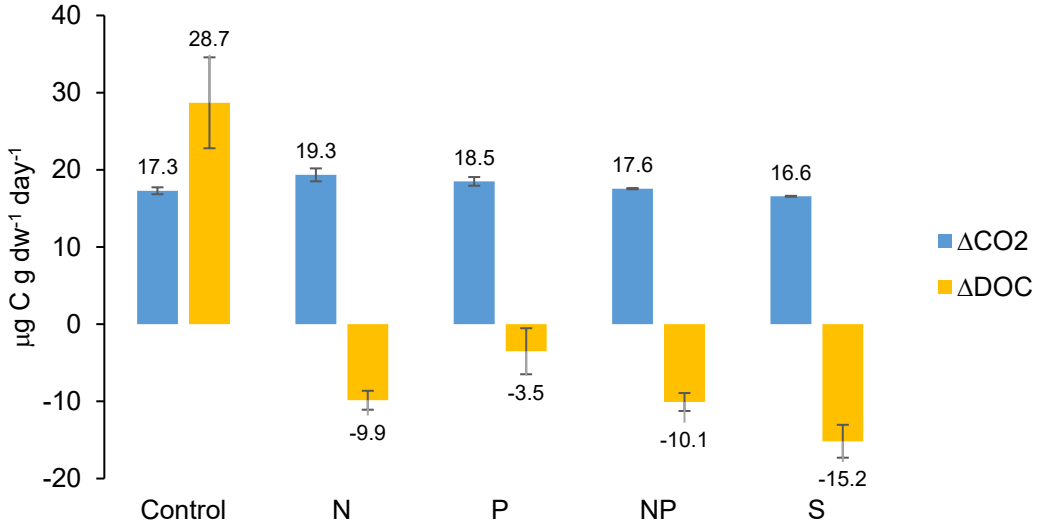

Figure 23. Average rates of CO_2 accumulation and DOC accumulation/depletion (n=3) in nutrient addition experiments without glucose throughout 70 days of anoxic/oxic incubation as stirred peat slurries. Error bars are standard deviation.

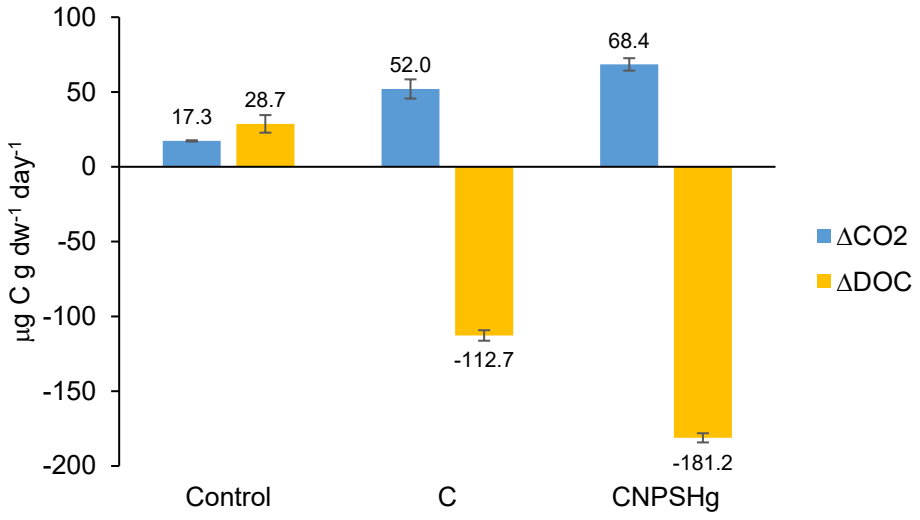

Figure 24. Average rates of CO_2 accumulation and DOC accumulation/depletion (n=3) in nutrient addition experiments with glucose throughout 70 days of anoxic/oxic incubation as stirred peat slurries. Error bars are standard deviation.

A noteworthy observation during the experiment was that the samples with added N, P, and S developed a clear phase separation after stopping the stirring (Fig. 27). The phase separation was particularly pronounced in the treatments with added N.

Figure 25. Incubated soil slurries treated with P (left), NP (middle) and Control (right). The treated samples showed a clear phase separation, whereas the untreated samples did not.

To further evaluate the potential reason for dHgT concentrations below LOQ in the treated samples, treatments with added Hg^{2+} (Hg and CNPSHg) were compared with the Control (Fig. 28). There was no difference in rates of HgT loss between Hg and CNPSHg. However, post incubation concentrations of dHgT were found to be significantly higher in the Hg than the CNPSHg treatment ($p = 0.0006$) and the Control ($p = 0.0007$) (Fig. 28). No statistically significant difference in post incubation dHgT was found between Control and CNPSHg. To refute that the difference in end concentration between Hg and CNPSHg were caused by variations in start concentrations, the initial dHgT concentrations of Hg and CNPSHg were analyzed and found to be statistically equal, hence the difference in post-incubation concentrations of dHgT between the two treatments were likely due to the additions of nutrients. This finding adds to the observation in section 3.2.1 that release of Hg is tightly correlated with OM degradation and signifies that removing DOC also removes dHgT.

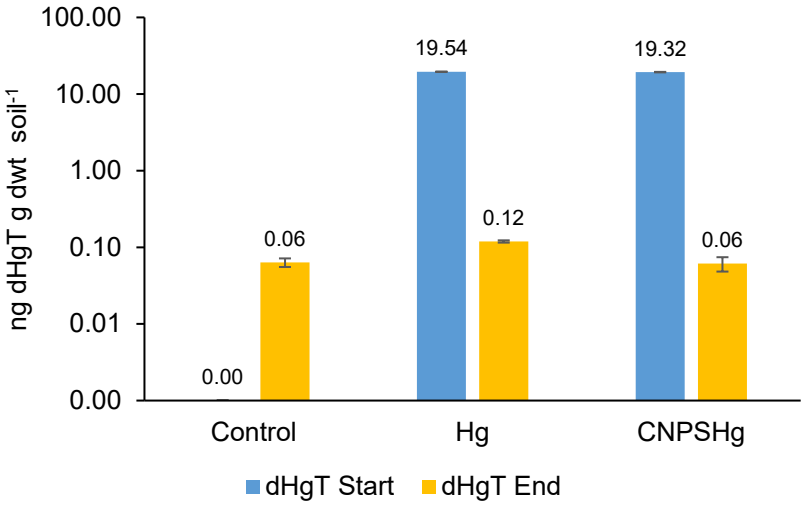

Figure 26. Mean concentrations of dHgT pre- and post-incubation (n=3) for Control, and samples treated with Hg and CNPSHg. Error bars are standard deviation.

3.4 Detection of MeHg in soil slurries

Since the original plan of organic phase MeHg extraction was deemed unfeasible, MeHg concentrations were analyzed directly in the filtered (0.45 µm) water phase of the incubated slurries. Due to the large number of incubated samples, a smaller subset of samples was tested first. Untreated permafrost samples from each field site were selected based on concentrations of native HgT in the soil (Fig. 14A) and observed CH_4 production rates during incubation (Table A.4, appendix), namely TZ from anoxic and oxic incubation from Iškoras, and samples from upper PF layers at Lakselv and Áidejávri incubated anoxically. In addition, samples from the nutrient addition experiment were tested, namely Control, +C, +N, +P, +S, +Hg, and +CNPSHg. None of the tested samples had concentrations of MeHg above LOD (0.002 ng L^{-1}).

3.5 Microbial genetic potential for Hg methylation

Amplifiable DNA was extracted from the AL of Lakselv and Áidejávri, and from the PF of a newly growing peat plateau at Lakselv (not discussed further in this study) using the DNeasy® PowerSoil® Kit from Qiagen (Fig. 29). The sample from AL (Áidejávri) displayed a strong band when run 45 cycles with the archaeal primer 340F_arc. The samples from new peat plateau in Lakselv showed weak bands when run with the archaeal primer SSU1ArF for 30 + 15 cycles. None of the samples showed any band for the bacterial (519F_bac) and universal

(27F) primers tested. Neither the DNeasy® PowerSoil® Kit from Qiagen nor the phenol-chloroform method modified for difficult peat soils by Lim et al. (2016) yielded amplifiable DNA from the old PF (from Iškoras and Áidejávri). Since no amplifiable DNA was obtained from the studied PF samples (i.e. incubation experiments), and the main purpose of DNA extraction was to link abundance of functional genes (*hgcA*) to observed MeHg production, the work was not continued within the frame of this master thesis.

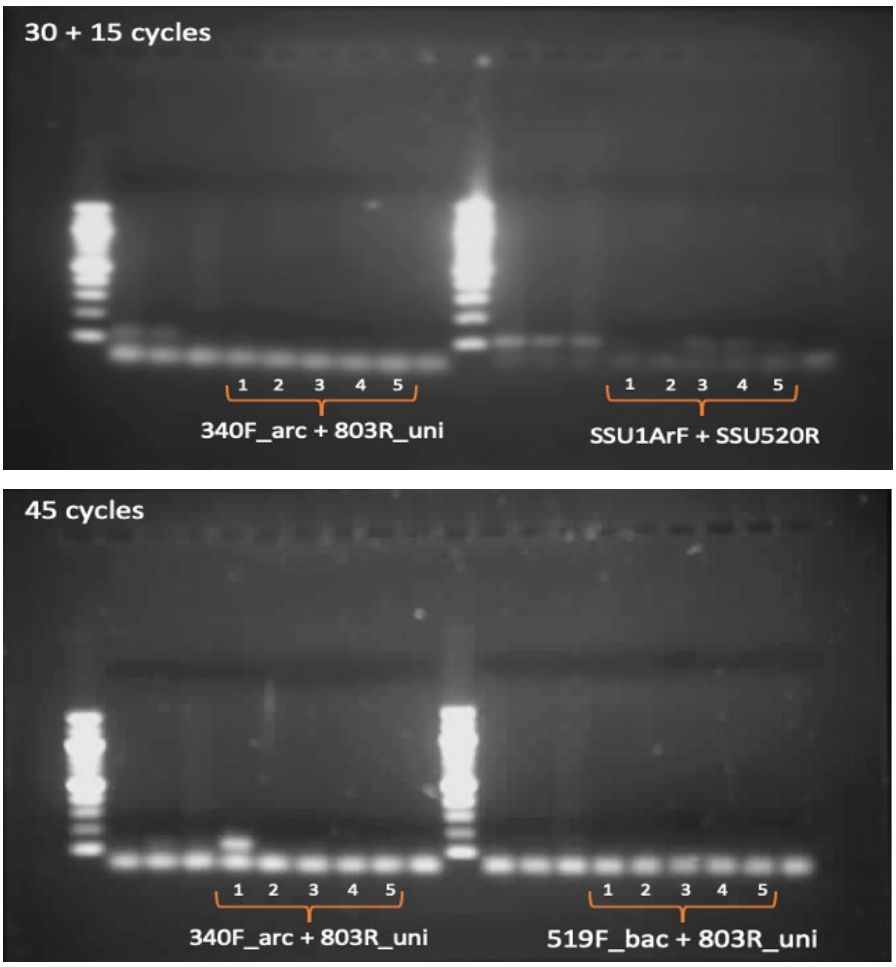

Figure 27. Gel electrophoresis of PCR products. The upper two gels show PCR runs with 30 + 15 cycles with the primers 340F_arc + 803R_uni (left) and SSU1ArF + SSU520OR (right). The lower two gels show PCR runs with 45 cycles with the primers 340F_arc + 803R_uni (left) and 519F_bac + 803R_uni (right). 1 is AL Áidejávri with one round of vortexing (4 ms^{-1}, 45 sec), 2 is AL Lakselv (6 ms^{-1}, 45 sec), 3 is Lakselv new palsa PF with one round of vortexing (4 ms^{-1}, 45 sec), 4 is Lakselv new palsa PF with two rounds of vortexing (4 ms^{-1}, 45 sec), 5 is Lakselv new palsa PF with two rounds of vortexing (6.0 ms^{-1}, 30 sec).

4. Discussion

4.1 Differences in peat and water chemistry between sites

The chemical properties and composition of the peat plateaus are important for Hg mobilization since they control the biogeochemical cycling of both, C and Hg (Poulin et al., 2019; Tjerngren et al., 2012; Treat et al., 2014). As indicated by the PCA, the peat cores below the top active layer differed clearly at the three sites in chemical composition (Fig.12). Since Lakselv is the only site that has been below the marine limit near to the ocean, the site was expected to differ in peat chemistry from Iškoras and Áidejávri. The results, however, showed that Iškoras is the most distinct peat plateau with distinctively low pH and base cation content, and highest C:N ratio. Lakselv and Áidejávri were more similar in pH and C:N ratio. Lakselv distinguished itself by generally higher concentrations of metals and P, while Áidejávri had more N, S, and Ca.

The differences in chemical composition between sites might be due to several factors, including location relative to the sea, geomorphology, bedrock, mire type and hydrologic connectivity. Lakselv stands out from Iškoras and Áidejávri as the youngest of the three sites (Kjellman et al., 2018) and the only site in close proximity to the ocean (Fig. 1). Thus, the high concentration of minerals in peat from Lakselv, particularly Mg, can be explained by influence of sea spray aerosols (Guasco et al., 2013). Relative to Iškoras and Áidejávri, Lakselv also displayed elevated concentrations of metals considered pollutants when present in larger quantities, namely Ni, Cu, Zn, Al, As, and Pb. Air currents in Finnmark tend to move north/north-east, especially in the winter (Berglen et al., 2014), and Lakselv is the only site located north of the of nickel-copper industries in Murmansk, Russia. Thus transport with air from Russia combined with input from the ocean, are the likely reasons for the elevated levels of metal pollutants in the AL in Lakselv (Hansen et al., 2017). The elevated levels of minerals in the PF, however, cannot be due to recent atmospheric deposition and are likely reflecting growth of minerotrophic *Sphagnum* species, as the area transitioned from minerogenic soil to fen environments around year 6150 ca. yr. BP (Kjellman et al., 2018).

The differences in peat chemistry between the two inland sites, Iškoras and Áidejávri, are likely caused by ambient geomorphology and hydrogeology. Peat plateaus in Áidejávri are situated in a more leveled terrain while the peat plateau in Iškoras is located in a depression surrounded by hills above the tree line. Consequently, the peat plateau in Iškoras has clear inlet and outlet,

whereas Áidejávri is surrounded by surface waters. The chemical parameters of the sampled waters revealed that waters in Iškoras have lower conductivity and concentrations of Ca compared to Áidejávri. These findings suggests that the peat plateau in Áidejávri has a different peat quality compared to Iškoras, probably because it is more affected by groundwater and/or ambient bedrock than the other sites (Racine & Walters, 1994). This corresponds with higher C:N ratios and lower concentrations of non-C elements in Iškoras. Although only small differences were found in pH for the thermokarst ponds at the two sites, the pH of the peat and the stream within the palsa were clearly lower in Iškoras compared to Áidejávri. Iškoras may be more similar to a 'raised bog' than the other sites, that is, that most nutrients are brought there by rainfall and not by groundwater which is generally richer in minerals.

In Iškoras, in and outlet waters had more Ca, higher conductivity and pH than the stream coming from the palsas, which implies that the surrounding fen area receives more input from the watershed and is therefore more minerotrophic. Even though the runoff from peat plateaus and its seasonal variation in chemistry are not known, the bog-like nature of the peat plateaus makes it unlikely to detect a significant signal of permafrost thawing at the outlet, since the chemical composition of the mainstream seems to be predominately controlled by minerotrophic fens surrounding the peat plateaus. It is important to note that all water analyzed for this study were sampled once in the fall. Further sampling in time and space, preferably year-round in more streams and ponds, are necessary to draw any conclusions.

4.2 Distribution of Hg in peat

All three sites showed elevated concentrations of Hg in in the top of the active layer (AL1) reflecting the increase of anthropogenic Hg emission since the industrial revolution (Biester et al., 2003; Hansen et al., 2017). Comparing HgT concentration in the permafrost (PF) among the three sites, showed that Iškoras contains more HgT than the other two sites on a gram dry weight basis (Fig. 14A). The higher HgT content of Iškoras peat likely reflects the higher peat quality with greater OM content and higher C:N ratios, complexing more Hg. This observation is supported by the positive association of these variables in the PCA (Fig. 15) and is in accordance with studies carried out by Biester et al. (2003), who argued that the concentration of Hg depends on the degree of humification and accumulation of carbon in peat. Thus, if assuming constant Hg deposition over time, the Hg content of peat will depend on the rates of OM accumulation and/or OM degradation. Since Iškoras has the deepest peat body and the

highest peat quality, it can be assumed that peat decays slower than at the other two sites, and thereby loses less Hg due to OM degradation.

Since Hg is strongly associated with OM, Hg concentrations were normalized to C content (Fig. 14B). Permafrost Hg:C ratios of Iškoras and Lakselv were similar and clearly higher than at Áidejávri. Since one of the transportation pathways of Hg is through ocean currents, the high Hg:C ratios of PF in Lakselv may be explained by its vicinity to the sea. In addition, the mire type may play a role as minerogenic peat has higher Hg concentrations than ombrotrophic peat (Franzen et al., 2004). Both Lakselv and Iškoras had minerogenic fens during early peat formation (Kjellman et al., 2018). No peat stratigraphy has been published for Áidejávri so far, and it is unknown what has caused the lower Hg:C ratios of PF peat in Áidejávri.

Type of ambient bedrock and local hydrogeology are also important factors for Hg concentrations and hence Hg:C ratios. For example, PF at Iškoras had higher levels of Cu, As, and Cd than Áidejávri, which may indicate that the relative enrichment of Hg at Iškoras origins from the bedrock (Jenner, 1996). The bedrock around Iškoras is more diverse than at Áidejávri, and contains e.g. transformed lava and tuff, which is not found in the immediate area around Áidejávri.

The PCA with elemental composition indicated a negative association between Hg and S for all three sites (Fig. 15). Since Hg is known to readily bind to reduced S groups in organic matter (Xia et al., 1999), the negative association was unexpected. When looking more closely at the concentrations of Hg and S with depth, however, it became evident that the concentration of Hg was highest in AL1, where the concentration of S is lowest, likely causing the negative association between Hg and S in the PCA. When excluding AL1, S and Hg showed similar trends with depth. Moreover, when normalizing the Hg concentration for S, it became evident that the two elements follow each other closely as the ratio became very evenly distributed with depth and between sites (Fig. 14C), signifying the role of S in binding Hg in OM.

The concentrations of Hg in the top layer of the peat (0-10 cm) decreased significantly along the transect from peat plateau (AL1) to thermokarst pond sediment (TK1) to new wet mire (WM1) (Fig. 17). The difference between AL1 and TK1 can likely be explained by loss of Hg after release from OM during degradation former AL peat in thermokarst ponds. To assess the degree of degradation of thermokarst sediment, the C:N ratios in AL1 and TK1 were compared across the three sites (Fig. 13). The ratios suggested that TK1 is more degraded than AL1 for

Lakselv and Iškoras, but surprisingly not for Áidejávri. The decrease in HgT content from the palsas to thermokarst sediments indicates that ground subsidence and formation of thermokarst ponds in waterlogged peat plateaus constitute a source for Hg release followed by volatilization and/or runoff with water.

Different Hg concentrations in AL1 and WM1 could be due to differences in growth and C accretion (Biester et al., 2003). The peat in wet mires grows more vigorously than on top of the peat plateau, which is lifted above the water table. This was also indicated by generally higher C:N ratios of WM1 (Fig. 13). Under constant Hg deposition, AL1 will therefore acquire higher concentrations of Hg relative to OM. Another explanation of differences in Hg content between AL1 and WM1 could be different fates of the Hg post deposition. Since uptake of Hg^0 in plants has been found to be the main pathway for Hg from the atmosphere to the terrestrial biosphere in the Arctic (Obrist et al., 2017), the uptake is likely greater in peat that is not submerged in water. Moreover, the initial reemission of deposited Hg has been found to be greater from water than from soil (Selin, 2009), which further diminishes the amount of Hg available for uptake by peat submerged by water. The latter is ambiguous, however, since palsas and bogs in peat plateaus are found to have higher rates of Hg^0 emissions compared to fens (Fahnestock et al., 2019). Nonetheless, the elevated Hg^0 emissions from palsas might be driven by PF thaw rather than reemission of recently deposited Hg, since Hg in PF thaw water is found to be highly photoreactive and readily reduced (Ci et al., 2020). Increased vertical transport of Hg^0 from PF thaw water could potentially also increase the immediate concentration and uptake of Hg in AL1.

4.3 Distribution of Hg in water

Lakselv and Áidejávri had slightly higher concentrations of HgT in thermokarst ponds than Iškoras, possibly indicating a larger influence of ground water discharge to the peat plateaus. Áidejávri is situated close to a highly trafficked road, and Lakselv to the ocean, which might be additional sources of Hg. The lower Hg concentrations in thermokarst ponds at Iškoras were matched by slightly lower HgT concentrations in the AL (Fig. 14). Thus, there is less Hg to be released from the upper part of the palsa at Iškoras upon thermokarst formations and subsequent OM degradation, as discussed in section 4.2.

Comparing the streams at Iškoras for HgT revealed that inlet and outlet had the exact same HgT concentrations, while concentrations of other elements such as Ca, Mg, and TotP were higher in the inlet than the outlet (Table 8). Difference in concentrations of other elements between inlet and outlet suggest that HgT in the outlet and inlet is likely of different origin; some of the dissolved HgT coming from outside the catchment may be lost from the water phase during the transport through the peat plateau and surrounding fen area, while old HgT released from palsas is added to the water originating from the peat plateau. This scenario is supported by the observation that the stream coming from the peat plateau had a higher concentration of HgT than both the inlet and outlet. More observations in space and time would be needed to confirm this idea and draw any conclusions about transport of HgT in general.

Another interesting observation is that the HgT correlated almost perfectly with DOC (R^2 = 0.99, $p < 0.0001$). Moreover, although the HgT:DOC ratio in water was slightly lower than the HgT:C ratio in soil, the two ratios were generally within the same order of magnitude, confirming the hypothesis that the Hg concentration would follow tightly the size of organic C pools. These results further illustrate the strong affinity of Hg to form complexes with OM, and the importance of DOC as a transport vector in aquatic environments as previously described by Braaten et al. (2014).

Of all thermokarst ponds, Lakselv had the highest concentration of MeHg and %MeHg of HgT, indicating the highest rates of Hg methylation. Lakselv also had the highest concentration of MeHg in the stream (outlet). Due to the proximity to the ocean, contribution of SO_4^{2-} and other minerals through sea spray (Guasco et al., 2013) could be plausible explanations (Tjerngren et al., 2012). Sulfate may trigger growth of sulphate reducing bacteria (SRB), which have been implicated to play an important role for Hg methylation (Compeau & Bartha, 1985). Lakselv is also the youngest of the three studied peat sites, and Hg methylation has been found to decrease with peatland age (Hu et al., 2020).

The potential of peat plateaus to act as hotspots for Hg methylation and subsequent transport to recipient streams was indicated by high MeHg concentrations in the outlets of Lakselv (0.3 ng L^{-1}) and Iškoras (0.1 ng L^{-1}). Moreover, although the concentrations of HgT were the same in Iškoras, the concentration of MeHg were twice as high in the outlet than the inlet (0.05 and 0.1 ng L^{-1}, respectively). These observations are supported by previous research conducted by

Fahnestock et al. (2019) concluding that rates of MeHg production increases in thawed peat plateaus. The study found particularly high MeHg production rates in thawed palsas entering the fen stage, likely due to favorable redox conditions, more labile OM, and increased relative abundance of Hg methylating microorganisms.

Scarcity of data, particularly for Lakselv, makes it difficult to draw any firm conclusion on what extent peat plateaus in Finnmark contributes with MeHg. For example, the amount of MeHg entering the Lakselv mires is unknown as the inlet was not sampled. Again, more frequent and spatial distributed sampling would be needed to shed light on this question.

4.4 Comparison of Hg concentrations to global averages and international standards

The Hg concentrations of permafrost found in the present study are withing the range of values reported from other peatlands (with and without permafrost) in subarctic and temperate regions (Patagonia, Chile; ON, Canada; AK, USA; northern Sweden), which typically have Hg concentrations between 10 and 123 ng Hg g^{-1}, with an average of 50 ng Hg g^{-1} (Biester et al., 2003; Skyllberg et al., 2003; Talbot et al., 2017; Yang et al., 2016). In the reported studies, Hg concentrations were highest in top layers and declined with depth. The top active layers investigated in the present study had higher values (~200 ng g^{-1}) than reported from arctic peatlands so far. This may point to higher deposition rates and/or lower rates of reemission in arctic peatlands. Even though Hg concentrations appear to be somewhat elevated in the studied peat plateaus, the concentrations are well below the effect threshold concentration for microbial processes of 1.47 μg g^{-1} (Gaudet et al., 1995). The values for Hg concentrations in water were found to be lower than the average concentration in drinking water and rain, which is approximately 25 ng Hg L^{-1} (WHO, 1996). The thermokarst pond in Áidejávri by the active erosion edge, was, however slightly above the former USEPA ambient water criterion of 12 ng Hg L^{-1} (EPA, 1984).

4.5 Potential release of HgT under different redox conditions during post-thaw incubation

The general trend across all sites was that anoxically incubated samples had higher rates of dHgT mobilization than oxically incubated samples (Fig. 20). The differences can likely be attributed to the DOC concentrations which correlated with dHgT (Fig. 21). Microbial

reduction and volatilization of Hg also may have contributed to lower concentrations of dHgT in the oxically incubated samples, since these samples showed higher microbial activity (measured in CO_2 production; Fig. 20) and expression of the *mer* operon responsible for biologic reduction of Hg^{2+} is higher in oxic than in anoxic environments (Boyd & Barkay, 2012; Fritsche et al., 2008; Schaefer et al., 2002). Volatilized Hg^0 may have accumulated in the headspace, adsorbed to septum (butyl rubber) and/or diffused through the septum during incubation (Ishimori et al., 2020).

Incubated AL peat mobilized dHgT at a higher rate than PF peat, suggesting that PF thaw resulting in thermokarst formations submerging the AL may be an important source of Hg to surface waters. Differences in mobilization rate between AL and PF were cancelled out, however, when normalized for the amounts of HgT present in the peat (Fig. 22), suggesting that PF peat released equally much dHgT per unit native HgT as AL peat. Yet, when comparing the release rates and their fraction of HgT between sites, differences became apparent. The anoxically incubated samples from Iškoras had the highest rates of dHgT production and pg dHgT of μg native HgT among the three sites. Mobility of Hg increases with decreasing pH, hence the higher release rates of Iškoras peat may be due to its lower pH. Surprisingly, thermokarst ponds at Iškoras had the lowest concentrations of HgT among the three sites. This finding suggests that peat plateaus which mobilize more Hg also lose more Hg, once the Hg reaches the water phase, presumably through reduction of Hg^{2+} to Hg^0, which then volatilizes. This effect could not be captured during this experiment.

In summary, the incubations confirmed the strong link between OM degradation and Hg mobilization as shown by the positive correlation between the rates of dHgT and CO2 as well as DOC production (Fig. 21). The effect of redox conditions was small and followed the trend of DOC production which was higher under anoxic conditions. Worth mentioning is that the mechanistic stirring of the incubated samples could have contributed to additional release of DOC and dHgT. Thus, the stirring might have affected the concentrations of DOC and dHgT observed at the end of the incubations. Nevertheless, all samples were treated equally hence it should not affect the comparability between samples.

4.6 Effect of substrate, nutrients, electron acceptors, and Hg^{2+} on Hg mobility and methylation

An incubation experiment with different substrate and nutrient additions with and without additional Hg^{2+} was carried out to explore limiting factors for Hg mobilization and methylation. The hypothesis was that increased access to essential nutrients would enhance microbial activity and thereby Hg mobilization and methylation. Slurries with PF peat from Iškoras amended with N (NH_4^+), C (glucose), and CNPSHg showed increased respiration but none of the slurries had dHgT concentration above LOQ neither pre nor post incubation (except slurries with added Hg, i.e. CNPSHg). Previous incubation experiments have found addition of glucose to boost Hg reduction and volatilization (Fritsche et al., 2008), which can remove Hg from the slurry. In the present study, the addition of nutrient salts resulted in a draw-down of DOC, removing dissolved HgT efficiently from the solution. This effect was absent in the Control (Fig. 23, 24) and confirms once again the tight association between dHgT and DOC. Apparently, the nutrient salts caused DOC to coagulate and precipitate, particularly in samples added N and P, as seen by the clear phase separation in Fig. 25.

A similar phenomenon was observed *in situ* by St Pierre et al. (2018), who found that the concentration of dHgT was higher upstream of a retrogressive thaw slump in the Western Canadian Arctic, while the total concentration of Hg was higher downstream of the thaw slump. However, most of the Hg downstream was particle bound, likely due to the enrichment of elements originating from the thaw slum. Together, these observations may indicate that despite increased microbial activity upon addition of nutrients, small changes in the ion balance affecting DOC override the effect of microbial activity on dissolved Hg, with ramifications for methylation.

4.7 Analysis of MeHg without organic phase extraction

Since the original plan for the incubation experiments was to test the effect of post-thaw conditions on Hg methylation, but the organic phase extraction (described in Bloom et al., 1997; Braaten & de Wit, 2016) was not available, an alternative method was tested. The MeHg was measured directly in the filtered supernatants of the soil slurries. Detectable concentrations of MeHg have been found in filtered porewater during this project (data not shown) and in previous research (e.g. Poulin et al., 2019), which suggests that detection of MeHg in the

filtered water extracted from the incubated slurries should have been possible. Nevertheless, none of the extracts from the incubated samples showed MeHg concentrations above LOD which means that either the incubation conditions were not conducive to Hg methylation or that MeHg was not stable.

Methylation and demethylation of Hg are biologically concurrent processes (e.g. Tjerngren et al., 2012) and rates of demethylation may equalize or exceed rates of methylation under certain condition, e.g. under oxic conditions in the presence of microorganisms harboring the *mer* operon (Boyd & Barkay, 2012; Schaefer et al., 2002). Hence, demethylation exceeding methylation may have been a possible reason for the absence of Hg above LOD in the incubations. The balance between methylation and demethylation can be studied by labelling different Hg pools with isotopically heavy Hg and following the dilution over time (Hu et al., 2020; Tjerngren et al., 2012). However, addition of Hg isotopes also adds additional substrate for methylation and may thus overestimate methylation. Isotopic approaches to study methylation/demethylation were beyond the scope of the present thesis.

Hg methylation has been reported previously from incubation experiments without Hg spiking (Yang et al., 2016). However, these studies used organic phase extraction (as described in Bloom et al. (1997)). The absence of a MeHg signal in the present study suggests that direct analysis in water is less sensitive than organic phase extraction for detecting MeHg.

Another reason for the absence of detectable MeHg in the water phase in our experiments might have been the small sample volume (approximately 50 ml water and 1-4 g dw/12-14 g fresh soil in 120 ml flasks). In comparison, the incubation experiment by Yang et al. (2016) used the sample sizes one order of magnitude larger (150 g fresh weight). On the other hand, Hu et al. (2020) used an even smaller sample size (30 mL slurry) than the present study, and measured Hg methylation. Hence, the sample size *per se* does not seem to play a role as long as MeHg is extracted quantitatively.

Tjerngren et al. (2012) concluded that wetlands with low to intermediate nutrient status have the highest net production of MeHg. Relative to the nutrient status given by Tjerngren et al. (2012), which was based on Ca content in porewater, Iškoras is nutrient poor, Lakselv intermediate, and Áidejávri nutrient rich. However, the sites studied by Tjerngren et al. (2012) had generally higher HgT concentration (113 – 287 ng Hg g dw^{-1}) than the peat plateaus studied

here. Thus, the absence of detectable MeHg in the present study might also have been due to low HgT concentrations in the peat.

The present experiment is similar to that of Yang et al. (2016), both in terms of peat type (PF), native Hg content (PF; 55.2 ±1.3 ng g dw^{-1}), and lack of Hg isotope addition. Therefore, a larger sample size and more advanced extraction (Bloom et al., 1997) seems to be necessary to obtain quantifiable concentrations of MeHg without addition of isotopes.

4.8 DNA extractions

Despite several attempts to extract DNA from peat material, DNA recoveries were insufficient for downstream sequencing. The present study focused on acidic permafrost soils rich in organic matter, which is particularly challenging for DNA extraction. First, acidic soils rich in organic matter contain inhibitory compounds (e.g. humic acids) (Lim et al., 2016), which have similar chemical properties as the DNA, and are therefore often co-extracted (Tebbe & Vahjen, 1993). Co-extracted inhibitory compounds interfere with downstream applications such as PCR amplification. Second, permafrost soils are particularly challenging in terms of DNA extraction due to low endogenous cell numbers and DNA abundance (Saidi-Mehrabad et al., 2020).

The further plan for DNA extractions during the present study was to test the ZymoBIOMICS DNA Microprep kit as described by Saidi-Mehrabad et al. (2020). The kit was ordered in October, however in February the kit had still not arrived, likely due to increased demands for microbial lab supplies in the light of the ongoing SARS-CoV-2 pandemic. In contrast, regular shipping time from the respective supplier is 1-2 weeks. Since the other methods tested during the present study did not work, the further DNA extractions was put to a halt in absence of the ZymoBIOMICS DNA Microprep kit.

5. Conclusion

The total concentration of Hg did not show a clear trend of decrease with increasing distance from the ocean as hypothesized. The Hg:C ratio in PF showed a vague trend of decrease with increasing distance from the ocean, however, the top of the AL in Áidejávri had the highest total Hg content and Hg:C ratio contradicting our hypothesis. These results suggest that air

transport of Hg from anthropogenic sources likely plays a larger role than transport with ocean currents and AMED events in the present-day environment. Our hypothesis that MeHg concentrations and production rates would be higher closer to the ocean was confirmed by strikingly high MeHg concentrations in Lakselv, up to 2.4 ng L^{-1}. These observations were based on a small number of water samples but support the idea that peat plateaus near the coast could be a hotspot for Hg methylation upon PF thaw.

The results from the slurry incubations did not support our hypothesis that Hg mobilization would be triggered by nutrient addition or alternative electron acceptors. However, this finding is likely an artefact; adding the nutrients as salts resulted in a 'salting-out' effect for DOC, removing associated dHgT from the solution. The highest rates of dHgT mobilization during incubation were generally found in the AL suggesting that abrupt thaw and water-logged thermokarst formation can be a significant source of Hg into surface water in arctic peat plateaus.

Field sampling and experiments on HgT mobilization largely confirmed our hypothesis that the concentration of Hg follows the size of organic C pools in peat and ambient water. Based on these observations, the studied transects across active layer, thermokarst and wet mire were expected to show similar Hg:C ratios. However, Hg:C ratios decreased along the transect, suggesting loss of Hg, likely through evaporation of Hg^0. Although these results are based on a small number of samples, the observed patterns propose that PF thaw may not only contribute to increased Hg loadings into surface waters but could also be a significant source of secondary Hg emission into the atmosphere.

The role of thawing peat plateaus as a secondary source of atmospheric Hg emission has been previously proposed (Ci et al., 2020; Fahnestock et al., 2019), and could potentially counteract current attempts of reducing Hg in the environments through the Minamata Convention. Since Arctic biota are already vulnerable to high Hg content in the food web (e.g. AMAP, 2011), increased loading of Hg from secondary sources can have severe effects on wildlife, fisheries and populations in these ecosystems. Further research, including extended sampling of soil, water, and Hg^0 fluxes, combined with sampling of biota, should be conducted for a deeper understanding of fate and cycling of Hg upon PF thaw.

References

AMAP. (2011). *AMAP Assessment 2011: Mercury in the Arctic*. Oslo, Norway: Arctic Monitoring and Assessment Programme (AMAP).

Aune, B. (1993). *Temperaturnormaler, Normalperiode 1961-1990*, 02/93. Oslo: Norwegian Meterological Institute.

Berglen, T. F., Dauge, F., Andersen, E., Haugsbakk, I., Nilsson, L. O., Ofstad, T., Tønnesen, D., Vadset, M. & Våler, R. L. (2014). *Air quality monitoring in the border areas of Norway and Russia - progress report April 2013 - March 2014*. In Berglen, T. F. (ed.). NILU OR, Scientific reports - OR, 33/2014, 978-82-425-2698-4: NILU.

Biester, H., Martinez-Cortizas, A., Birkenstock, S. & Kilian, R. (2003). Effect of Peat Decomposition and Mass Loss on Historic Mercury Records in Peat Bogs from Patagonia. *Environ Sci Technol*, 37: 32-39.

Bloom, N. S., Colman, J. A. & Barber, L. (1997). Artifact formation of methyl mercury during aqueous distillation and alternative techniques for the extraction of methyl mercury from environmental samples. *Fresenius J Anal Chem*, 358: 371-377.

Borge, F. A., Westermann, S., Solheim, I. & Etzelmüller, B. (2017). Strong degradatoin of palsas and peat plateaus in northern Norway during the last 60 years. *The Cryosphere*, 11: 1-16. doi: 10.5194/tc-11-1-2017.

Boss, C. B. & Fredeen, K. J. (2004). *Concepts, Instrumentation and Techniques in Inductively Coupled Plasma Optical Emission Spectrometry*. 3rd ed. Sciences, P. L. a. A. (ed.). Shelton, CT: PerkinElmer, Inc. pp. 1-1 - 1-6.

Boyd, E. & Barkay, T. (2012). The Mercury Resistance Operon: From an Origin in a Geothermal Environment to an Efficient Detoxification Machine. *Frontiers in Microbiology*, 3 (349). doi: 10.3389/fmicb.2012.00349.

Braaten, H. F. V., de Wit, H. A., Fjeld, E., Rognerud, S., Lydersen, E. & Larssen, T. (2014). Environmental factors influencing mercury speciation in Subarctic and Boreal lakes. *Science of The Total Environment*, 476-477: 336-345.

Braaten, H. F. V. & de Wit, H. A. (2016). Effects of disturbance and vegetation type on total and methylmercury in boreal peatland and forest soils. *Environmental Pollution*, 218: 140-149. doi: https://doi.org/10.1016/j.envpol.2016.08.029.

Bravo, A. G., Kothawala, D. N., Attermeyer, K., Tessier, E., Bodmer, P., Ledesma, J. L. J., Audet, J., Casas-Ruiz, J. P., Catalán, N., Cauvy-Fraunié, S., et al. (2018). The interplay between total mercury, methylmercury and dissolved organic matter in fluvial systems: A latitudinal study across Europe. *Water Research*, 144: 172-182. doi: https://doi.org/10.1016/j.watres.2018.06.064.

Chan, H. M. & Receveur, O. (2000). Mercury in the traditional diet of indigenous peoples in Canada. *Environmental Pollution*, 11: 1-2.

Ci, Z., Peng, F., Xue, X. & Zhang, X. (2020). Permafrost Thaw Dominates Mercury Emission in Tibetan Thermokarst Ponds. *Environmental Science & Technology*, 54: 5456-5466.

Compeau, G. C. & Bartha, R. (1985). Sulfate-Reducing Bacteria: Principle Methylators of Mercury in Anoxic Estuarine Sediment. *Appl Environ Microbiol*, 50 (2): 498-502.

Douglas, T. A., Loseto, L. L., Macdonald, R. W., Outridge, P., Dommergue, A., Poulain, A., Amyot, M., Barkay, T., Berg, T., Chételat, J., et al. (2012). The fate of mercury in Arctic terrestrial and aquatic ecosystems, a review. *Environ. Chem.*, 9: 321-355. doi: http://dx.doi.org/10.1071/EN11140.

Engstrom, D. R. (2007). Fish respond when the mercury rises. *PNAS*, 104 (42): 16394-16395.

EPA. (1984). *Ambient water quality criteria for mercury*: U.S. Environmental Protection Agency.
Estop-Aragonés, C., Cooper, M. D. A., Fisher, J. P., Aaron, T., Garnett, M. H., Charman, D. J., Murton, J. B., Phoenix, G. K., Treharne, R., Sanderson, N. K., et al. (2018). Limited release of previously-frozen C and increased new peat formation after thaw in permafrost peatlands. *Soil Biology and Biochemistry*, 118: 115-129.
Fahnestock, M. F., Bryce, J. G., McCalley, C. K., Montesdeoca, M. R., Bai, S., Li, Y., Discroll, C. T., Crill, P. M., Rich, V. I. & Varner, R. K. (2019). Mercury reallocation in thawing subarctic peatlands. *Geochem. Persp. Let.*, 11: 33-38. doi: 10.7185/geochemlet.1922.
Fitzgerald, W. F., Engstrom, D. R., Mason, R. P. & Nater, E. A. (1998). The Case for Atmospheric Mercury Contamination in Remote Areas. *Environmental Science & Technology*, 32 (1): 1-7.
Framstad, E., Blindheim, T., Erikstad, L., Thingstad, G. & Sloreid, S.-E. (2010). *Naturfaglig evaluering av norske verneområder*. Oslo: NINA.
Franzen, C., Kilian, R. & Biester, H. (2004). Natural mercury enrichment in a minerogenic fen-evaluation of sources and processes. *Journal of Environmental Monitoring*, 6 (5): 466-472.
Fritsche, J., Obrist, D. & Alewell, C. (2008). Evidence of microbial control of Hg0 emissions from uncontaminated terrestrial soils. *J. Plant Nutr. Soil Sci.*, 171: 200-209. doi: 10.1002/jpln.200625211.
Gabriel, M. C. & Williamson, D. G. (2004). Principal biogeochemistry factors affecting the speciation and transport of mercury through the terrestrial environment. *Environmental Geochemistry and Health*, 26: 421-434.
Gaudet, C., Lingard, S., Cureton, P., Keenleyside, K., Smith, S. & Raju, G. (1995). Canadian environmental quality guidelines for mercury. *Water , Air, and Soil Pollution*, 80: 1149-1159.
Gilmour, C. C., Podar, M., Bullock, A. L., Graham, A. M., Brown, S. D., Somenahally, A. C., Johs, A., Hurt, R. A. J., Bailey, K. L. & Elias, D. A. (2013). Mercury Methylation by Novel Microorganisms from New Environments. *Environ Sci Technol*, 47 (20): 11810-11820.
Gionfriddo, C. M., Wymore, A. M., Jones, D. S., Wilpiszeski, R. L., Lynes, M. M., Christensen, G. A., Soren, A., Gilmour, C. C., Podar, M. & Elias, D. A. (2020). An Improved hgcAB Primer Set and Direct High-Throughput Sequencing Expand Hg-Methylator Diversity in Nature. *Frontiers in Microbiology*, 11. doi: 10.3389/fmicb.2020.541554.
Gorham, E. (1991). Northern Peatlands: Role in the Carbon Cycle and Probable Responses to Climatic Warming. *Ecological Applications*, 1 (2): 182-195. doi: 10.2307/1941811.
Griffiths, R. I., Whiteley, A. S., O'Donnell, A. G. & Bailey, M. J. (2000). Rapid method for coextraction of DNA and RNA from natural environments for analysis of ribosomal DNA- and rRNA-based microbial community composition. *Appl Environ Microbiol*, 66 (12): 5488-91. doi: 10.1128/aem.66.12.5488-5491.2000.
Gu, B., Bian, Y., Miller, C. L., Dong, W., Jiang, X. & Liang, L. (2011). Mercury reduction and complexation by natural organic matter in anoxic environments. *PNAS*, 108 (4): 1479-1483.
Guasco, T. L., Cuadra-Rodriguez, L. A., Pedler, B. E., Ault, A. P., Collins, D. B., Zhao, D., Kim, M. J., Ruppel, M. J., Wilson, S. C., Pomeroy, R. S., et al. (2013). Transition Metal Association with Primary Biological Particles in Sea Spray Aerosol Generated in a Wave Channel. *Environ Sci Technol*, 48: 1324-1333. doi: dx.doi.org/10.1021/es403203d.

Hansen, M. D., Nøst, T. H., Heimstad, E. S., Evenset, A., Dudarev, A. A., Rautio, A., Myllynen, P., Dushkina, E. V., Jagodic, M., Christensen, G. N., et al. (2017). The Impact of a Nickle-Copper Smelter on Concentrations of Toxic Elements in Local Wild Food from the Norwegian, Finnish, and Russian Border Regions. *Int. J. Environ. Res. Public Health*, 14. doi: 10.3390/ijerph14070694.

Harden, J. W., Koven, C. D., Ping, C.-L., Hugelius, G., McGuire, A. D., Camill, P., Jorgenson, T., Kuhry, P., Michaelson, G. J., O'Donnell, J. A., et al. (2012). Field information links permafrost carbon to physical vulnerabilities of thawing. *Geophysical Research Letters*, 39 (15). doi: https://doi.org/10.1029/2012GL051958.

Hintermann, H., Harris, R., Heyes, A., Hurley, J. P., Kelly, C. A., Krabbenhoft, D. P., Lindberg, S., Rudd, J. W. M., Scott, K. J. & St. Louis, V. L. (2002). Reactivity and Mobility of New and Old Mercury Deposition in a Boreal Forest Ecosystem during the First Year of The METAALICUS Study. *Environ Sci Technol*, 36: 5034-5040.

Holmes, R. M., McClelland, J. W., Peterson, B. J., Tank, S. E., Bulygina, E., Eglinton, T. I., Gordeev, V. V., Gurtovaya, T. Y., Raymond, P. A., Repeta, D. J., et al. (2012). Seasonal and Annual Fluxes of Nutrients and Organic Matter from Large Rivers to the Arctic Ocean and Surrounding Seas. *Estuaries and Coasts*, 35 (2): 369-382. doi: 10.1007/s12237-011-9386-6.

Hu, H., Wang, B., Bravo, A. G., Björn, E., Skyllberg, U., Amouroux, D., Tessier, E., Zopfi, J., Feng, X., Bishop, K., et al. (2020). Shifts in mercury across a peatland chronosequence: From sulfate reduction to methanogenesis and syntrophy. *Journal of Hazardous Material*, 387. doi: https://doi.org/10.1016/j.jhazmat.2019.121967.

IPCC. (2013). *Climate Change 2013: The Physical Science Basis. Contribution of Working Group I to the Fifth Assessment Report of the Intergovernmental Panel on Climate Change*. In Stocker, T. F., Qin, D., Plattner, G.-K., Tignor, M., Allen, S. K., Boschung, J., Nauels, A., Xia, Y., Bex, V. & Midgley, P. M. (eds). Cambridge, United Kingdom and New York, NY, USA.

Ishimori, H., Suzuki, T., Sakanakura, H. & Ishigaki, T. (2020). Establishing soil adsorption testing methods for gaseous mercury and evaluating the distribution coefficients of silica sand, decomposed granite soil, mordenite, and calcium bentonite. *Soils and Foundations*, 20: 496-504.

Jackson, T. A. (1998). Mercury in aquatic ecosystems. In Langston, W. J. & Bebianno, M. J. (eds) *Metal Metabolism in Aquatic Environments*, pp. 77-158. Boston, MA: Springer US.

Jansson, J. K. & Tas, N. (2014). The microbial ecology of permafrost. *Nature*, 12: 414-425.

Jenner, G. A. (1996). *Trace Element Geochemistry of Igneous Rocks: Geochemical Nomenclature and Analytical Geochemistry*. Trace Element Geochemistry of Volcanic Rocks: Applications For Massive Sulfide Exploration. Newfoundland: Geological Association of Canada.

Johannessen, T. W. (1970). The Climate of Scandinavia. In Wallén, C. C. (ed.) *In Climate of Northern and Western Europe*, pp. 23-80. Amsterdam: Elviser Publishing Company.

Kjellman, S. E., Axelsson, P. E., Etzelmüller, B., Westermann, S. & Sannel, A. B. K. (2018). Holocene development of subarctic permafrost peatlands in Finnmark, northern Norway. *The Holocene*, 28 (12): 1855-1869.

Lim, N. Y. M., Roco, C. A. & Frostegård, Å. (2016). Transparent DNA/RNA Co-extraction Workflow Protocol Suitable for Inhibitor-Rich Environmental Samples That Focuses on Complete DNA Removal for Transcriptomic Analyses. *Frontiers in Microbiology*, 7.

Lin, C.-J. & Pehkonen, S. O. (1999). The chemistry of atmospheric mercury: a review. *Atmospheric Environment*, 33: 2067-2079.

Malcolm, E. G., Keeler, G. J. & Landis, M. S. (2003). The effects of the coastal environment on the atmospheric mercury cycle. *Journal of Geophysical Research: Atmospheres*, 108 (D12). doi: https://doi.org/10.1029/2002JD003084.

Martin, L. C. P., Nitzbon, J., Aas, K. S., Etzelmüller, B., Kristiansen, H. & Westermann, S. (2019). Stability Conditions of Peat Plateaus and Palsas in Northern Norway. *Journal of Geophysical Research: Earth Surface*, 124: 705-719. doi: https://doi.org/10.1029/2018JF004945.

MET. (2021). *Norsk Klimaservicesenter*. In Institutt, M. (ed.). Seklima: Observasjoner og værstatistikk. https://seklima.met.no/observations/: Meterologisk Institutt. Available at: https://seklima.met.no/observations/ (accessed: 03 Feb).

Miljødirektoratet. (2020). *Naturbase kart*. Available at: https://geocortex01.miljodirektoratet.no/Html5Viewer/?viewer=naturbase (accessed: 05 March).

Molstad, L., Dörsch, P. & Bakken, L. R. (2007). Robotized incubation system for monitoring gases (O_2 , NO, N_2O, N_2) in denitrifying cultures. *Journal of Microbiological Methods*, 71 (3): 202-211.

Monteux, S., Keuper, F., Fontaine, S., Gavazov, K., Hallin, S., Juhanson, J., Krab, E. J., Revaillot, S., Verbruggen, E., Walz, J., et al. (2020). Carbon and nitrogen cycling in Yedoma permafrost controlled by microbial functional limitaitons. *Nature Geoscience*, 13: 794-798. doi: https://doi.org/10.1038/s41561-020-00662-4.

Morel, F. M. M., Kraepiel, A. M. L. & Amyot, M. (1998). The Chemical Cycle and Bioaccumulation of Mercury. *Annual Review of Ecology and Systematics*, 29: 543-566.

NCCS. (2016). *Klimaprofil Finnmark - Et kunnskapsgrunnlag for klimatilpasning*: Norwegian Centre for Climate Services.

NGU. (2015). *Nasjonal berggrunnsdatabase*. Available at: http://geo.ngu.no/kart/berggrunn/ (accessed: 05 March).

NVE. (2021). *NVE Nedbørfelt (REGINE) Temakart*. Available at: https://temakart.nve.no/tema/nedborfelt (accessed: 05 March).

Obrist, D., Agnan, Y., Jiskra, M., Olson, C. L., Colegrove, D. P., Hueber, J., Moore, C. W., Sonke, J. E. & Hemling, D. (2017). Tundra uptake of atmospheric elemental merdury drives Arctic mercury pollution. *Nature*, 547: 201-204. doi: 10.1038/nature22997.

Olsen, L., Mejdahl, V. & Selvik, S. (1996). Middle and Late Pleistocene stratigraphy, chronology and glacial history in Finnmark, North Norway. *Nor. geol. unders.*, 429: 1-111.

Parks, J. M., Johs, A., Podar, M., Bridou, R., Hurt, R. A. J., Smith, S. D., Tomanicek, S. J., Qian, Y., Brown, S. D., Brandt, C. C., et al. (2013). The genetic basis for bacterial mercury methylation. *Science*, 339 (6125): 1332-1335. doi: 10.1126/science.1230667.

Podar, M., Gilmour, C. C., Brandt, C. C., Soren, A., Brown, S. D., Crable, B. R., Palumbo, A. V., Somenahally, A. C. & Elias, D. A. (2015). Global prevalence and distribuation of genes and microorganisms involved in mercury methylation. *Sci. Adv.*, 1: e1500675.

Poulin, B. A., Ryan, J. N., Tate, M. T., Krabbenhoft, D. P., Hines, M. E., Barkay, T., Schaefer, J. & Aiken, G. R. (2019). Geochemical Factors Controlling Dissolved Elemental Mercury and Methylmercury Formation in Alaskan Wetlands of Varying Trophic Status. *Environ Sci Technol*, 53: 6203-6213. doi: 10.1021/acs.est.8b06041.

Racine, C. H. & Walters, J. C. (1994). Groundwater-Discharge Fens in the Tana Lowlands, Interior Alaska, U.S.A. *Arctic and Alpine Research*, 26 (4): 418-426.

Ravichandran, M. (2004). Interactions between mercury and dissolved organic matter - a review. *Chemosphere*, 55: 319-331.

Roos-Barraclough, F., Martinez-Cortizas, A., García-Rodeja, E. & Shotyk, W. (2002). A 14500 year record of the accumulation of atmospheric mercury in peat: volcanic signals, anthropogenic influences and a correlation to bromine accumulation. *Earth Planet Sci. Lett.*, 202: 435-451.

Rydberg, J., Klaminder, J., Rosén, P. & Bindler, R. (2010). Climate driven release of carbon and mercury from permafrost mires increases mercury loading to sub-arctic lakes. *Science of The Total Environment*, 408: 4778-4783. doi: 10.1016/j.scitotenv.2010.06.056.

Saidi-Mehrabad, A., Neuberger, P., Cavaco, M., Froese, D. & Lanoil, B. (2020). Optimization of subsampling, decontamination, and DNA extraction of difficult peat and silt permafrost samples. *Nature*, 10. doi: https://doi.org/10.1038/s41598-020-71234-0.

Schaefer, J. K., Letowski, J. & Barkay, T. (2002). mer-Mediated Resistance and Volatilization of Hg(II) Under Anaerobic Conditions. *Geomicrobiology Journal*, 19: 87-102. doi: 10.1080/01490450231724619 2.

Schaefer, K. M., Elshorbany, Y., Jafarov, E., Schuster, P. F., Striegl, R. G., Wickland, K. P. & Sunderland, E. M. (2020). Potential impacts of mercury released from thawing permafrost. *Nature*, 11. doi: https://doi.org/10.1038/s41467-020-18398-5.

Schuster, E. (1991). The behavior of mercury in the soil with special emphasis on complexation and adsorption processes - a review of the literature. *Water, Air, & Soil Pollution*, 56: 667-680.

Schuster, P. F., Krabbenhoft, D. P., Naftz, D. L., Cecil, L. D., Olson, M. L., Dewild, J. F., Susong, D. D., Green, J. R. & Abbot, M. L. (2002). Atmospheric Mercury Deposition during the last 270 years: A glacial ice core record of natural and anthropogenic sources. *Environ Sci Technol*, 36: 2303-2310. doi: 10.1021/es0157503.

Schuster, P. F., Striegl, R. G., Aiken, G. R., Krabbenhoft, D. P., Dewild, J. F., Butler, K., Kamark, B. & Dornblaster, M. (2011). Mercury Export from the Yukon River Basin and Potential Response to a Changing Climate. *Environmental Science & Technology*, 45: 9262-9267. doi: dx.doi.org/10.1021/es202068b.

Schuster, P. F., Schaefer, K. M., Aiken, G. R., Antweiler, R. C., Dewild, J. F., Gryziec, J. D., Gusmeroli, A., Hugelius, G., Jafarov, E., Krabbenhoft, D. P., et al. (2018). Permafrost Stores a Globally Significant Amount of Mercury. *Geophysical Research Letters*, 45 (3): 1463-1471. doi: https://doi.org/10.1002/2017GL075571.

Selin, N. E. (2009). Global Biogeochemistry Cycling of Mercury: A Review. *Annual REview of Environment and Resources*, 34: 43-63.

Sjögersten, S., Caul, S., Daniell, T. J., Jurd, A. P. S., O'Sullivan, O. S., Stapelton, C. S. & Titman, J. J. (2016). Organic matter chemistry controls greenhouse gas emissions from permafrost peatlands. *Soil Biology and Biochemistry*, 98: 42 - 53. doi: http://dx.doi.org/10.1016/j.soilbio.2016.03.016.

Skyllberg, U., Qian, J., French, W., Xia, K. & Bleam, W. F. (2003). Distribution of mercury, methyl mercury and organic sulphur species in soil, soil solution and stream of a boreal forest catchment. *Biogeochemistry*, 64: 2003.

Smith-Downey, N. V., Sunderland, E. M. & Jacob, D. J. (2010). Anthropogenic impacts on global storage and emissions of mercury from terrestrial soils: Insights from a new global model. *Journal of Geophysical Research*, 115 (G3). doi: https://doi.org/10.1029/2009JG001124.

St Pierre, K. A., Zolkos, S., Shakil, S., Tank, S. E., St. Louis, V. L. & Kokelj, S. V. (2018). Unprecendent Increases in Total and Methyl Mercury Concentrations Downstream of Retrogressive Thaw Slumps in the Western Canadian Arctic. *Environ Sci Technol*, 52 (24): 14099-14109.

Stokes, C. R., Corner, G. D., Winsborrow, M. C. M., Husum, K. & Andreassen, K. (2014). Asynchronous response of marine-terminating outlet glaciers during deglaciation of the Fennoscandian Ice Sheet. *Geology*, 42 (5): 455-458. doi: 10.1130/g35299.1.

Stroeven, A. P., Hättestrand, C., Kleman, J., Heyman, J., Fabel, D., Fredin, O., Goodfellow, B. W., Harbor, J. M., Jansen, J. D., Olsen, L., et al. (2016). Deglaciation of Fennoscandia. *Quaternary Science Reviews*, 147: 91-121. doi: https://doi.org/10.1016/j.quascirev.2015.09.016.

Talbot, J., Moore, T. R., Wang, M., Dallaire, C. O. & Riley, J. L. (2017). Distribution of lead and mercury in Ontario peatlands. *Environmental Pollution*, 231: 890-898.

Tebbe, C. C. & Vahjen, W. (1993). Interference of Humic Acids and DNA Extracted Directly from Soil in Detection and Transformation of recombinant DNA from bacteria and a Yeast. *Appl Environ Microbiol*, 59 (8): 2657-2665.

Telliard, W. A. (1998). *EPA Method 1630: Methyl Mercury in Water by Distillation, Aqueous Ethylation, Purge and Trap, and Cold Vapor Atomic Fluorescence Spectrometry.* (4303), E. a. A. D. Washington DC: U.S. Environmental Protection Agency.

Telliard, W. A. & Gomez-Taylor, M. G. (2002). *EPA Method 1631, Revision E: Mercury in Water by Oxidation, Purge and Trap, and Cold Vapor Atomic Fluorescence Spectrometry*. Branch, S. a. A. S. Washington DC: U.S. Environmental Protection Agency.

Tjerngren, I., Karlsson, T., Björn, E. & Skyllberg, U. (2012). Potential Hg methylation and MeHg demethylation rates related to the nutrient status of different boreal wetlands. *Biogeochemistry*, 108: 335-350.

Treat, C. C., Wollheim, W. M., Varner, R. K., Grandy, A. S., Talbot, A. S. & Frolking, S. (2014). Temperature and peat type control CO2 and CH4 production in Alaskan permafrost peats. *Global Change Biology*, 20: 2674-2686. doi: 10.1111/gcb.12572.

Turetsky, M. R., Harden, J. W., Friedli, H. R., Flannigan, M., Payne, N., Crock, J. & Radke, L. (2006). Wildfires threaten mercury stocks in northern soils. *Geophysical Research Letters*, 33. doi: 10.1029/2005GL025595.

Turetsky, M. R., Abbott, B. J., Jones, M. C., Anthony, K. W., Olefeldt, D., Schuur, E. A. G., Grosse, G., Kuhry, P., Hugelius, G., Koven, C., et al. (2020). Carbon release through abrupt permafrost thaw. *Nature Geoscience*, 13: 138-143. doi: https://doi.org/10.1038/s41561-019-0526-0.

UN Environment. (2019a). *Global Mercury Assessment 2018*. In Chemicals and Health Branch (ed.), 978-92-807-3744-8. Geneva, Switzerland: UN Environment Programme.

UN Environment. (2019b). *Minamata Convention on Mercury - Text and Annexes*.

Vanhaecke, F. (2015). *Agilent 8800 ICP-QQQ Application Handbook*. 2nd ed. Ghent University, D. o. A. C. (ed.). Ghent, Belgium: Agilent Technology. p. 5.

Vonk, J. E., Tank, S. E., Bowden, W. B., Laurion, I., Vincent, W. F., Alekseychik, P., Amyot, M., Billet, M. F., Canário, J., Cory, R. M., et al. (2015). Reviews and synthesis: Effects of permafrost thaw on Arctic aquatic ecosystems. *Biogeosciences*, 12: 7129-71676. doi: 10.5194/bg-12-7129-2015.

Waldrop, M. P., McFarland, J. W., Manies, K. L., Leewis, M. C., Blazewicz, S. J., Jones, M. C., Neumann, R. B., Keller, J. K., Cohen, L., Euskirchen, E. S., et al. (2021). Carbon Fluxes and Microbial Activities From Boreal Peatland Experiencing Permafrost Thaw. *JGR Biogeoscience*, 126. doi: https://doi.org/10.1029/2020JG005869.

Wang, W., Clarkson, T. W. & Ballatori, N. (2000). y-Glutamyl Transpeptidase and l-Cysteine Regulate Methylmercury Uptake by HepG2 Cells, a Human Hepatoma Cell Line. *Toxicology and Applied Pharmacology*, 168 (1): 72-78.

Westermann, S. (2020). *Personal communication; explainations and descriptions given by S. Westermann before, during and after fieldwork.*
WHO. (1996). *Mercury in Drinking-water*. 2 ed. WHO Guidelines for Drinking-water Quality, vol. 2. Geneva.
Xia, Y., Skyllberg, U. L., Bleam, W. F., Bloom, P. R., Nater, E. A. & Helmke, P. A. (1999). X-ray absorption spectroscopic evidence for the complexation of Hg(II) by reduced sulfur in soil humic substances. *Environ Sci Technol*, 33 (2): 257-261.
Yang, Z., Fang, W., Lu, X., Sheng, G. P., Graham, D. E., Liyuan, L., Wullschleger, S. D. & Gu, B. (2016). Warming increases methylmercury production in an Arctic soil. *Environmental Pollution*, 214: 504-509.

Appendix

Table A.1. Elements analyzed in the palsa peat cores for each depth, additional to elements displayed in figures.

Site and depth (cm)	P mg g dw^{-1}	Al mg g dw^{-1}	Se µg g dw^{-1}	Mn µg g dw^{-1}	Cu µg g dw^{-1}	Ni µg g dw^{-1}	As µg g dw^{-1}	Pb µg g dw^{-1}	Cd µg g dw^{-1}	La µg g dw^{-1}	Ce µg g dw^{-1}	Pr µg g dw^{-1}	Nd µg g dw^{-1}	Sm µg g dw^{-1}	Eu µg g dw^{-1}	Gd µg g dw^{-1}	Dy µg g dw^{-1}	Ho µg g dw^{-1}	Er µg g dw^{-1}	Tm µg g dw^{-1}	Yb µg g dw^{-1}
Lakselv																					
2	0.5	2.2	0.3	60.0	7.0	4.8	0.6	4.7	0.0	0.0	0.0	0.0	1.4	0.3	0.1	0.2	0.2	0.0	0.1	0.0	0.1
20	0.9	16.0	0.8	51.0	54.0	29.0	1.0	4.5	0.2	31.0	66.0	7.3	28.0	4.5	0.9	3.6	2.5	0.4	1.2	0.2	1.0
40	0.9	16.0	0.7	121	60.0	24.0	1.1	5.0	0.2	30.0	63.0	6.6	26.0	4.1	0.8	3.4	2.3	0.4	1.1	0.1	0.9
60	0.8	34.0	0.6	205	94.0	47.5	1.7	9.7	0.2	47.5	89.0	10.5	39.0	6.0	1.2	4.8	3.2	0.6	1.4	0.2	1.2
70	0.7	45.0	0.5	280	94.3	63.7	1.8	10.0	0.2	52.7	94.7	11.7	42.0	6.2	1.2	4.8	3.2	0.6	1.5	0.2	1.3
80	0.7	34.5	0.6	230	93.5	54.0	2.7	9.6	0.1	49.5	91.5	10.5	38.5	5.9	1.2	4.7	3.1	0.5	1.5	0.2	1.3
85	0.3	34.0	0.1	180	27.6	27.5	1.6	3.8	0.0	19.0	35.5	4.2	15.6	2.5	0.6	2.1	1.5	0.3	0.8	0.1	0.7
Iškoras																					
0	0.5	0.6	0.3	10.0	4.6	2.8	0.8	8.1	0.3	0.4	0.8	0.1	0.4	0.1	0.0	0.1	0.0	0.0	0.0	0.0	0.0
25	0.3	1.8	0.3	1.8	3.5	4.5	0.1	0.4	0.0	0.0	0.0	0.0	1.8	0.3	0.1	0.3	0.3	0.1	0.2	0.0	0.1
45	0.3	2.5	0.3	2.3	6.5	7.0	0.2	0.3	0.1	4.8	7.5	1.0	4.0	0.7	0.2	0.7	0.5	0.1	0.3	0.0	0.3
60	0.4	3.2	1.3	6.6	37.0	10.0	0.7	0.4	0.1	5.5	9.0	1.4	5.5	1.1	0.3	1.0	0.9	0.2	0.5	0.1	0.4
80	0.5	4.0	1.7	11.0	76.0	14.0	0.8	0.6	0.3	10.0	17.0	2.8	11.0	2.3	0.6	2.2	1.9	0.4	0.9	0.1	0.8
106	0.5	5.1	1.2	6.7	51.0	14.0	0.5	0.3	0.0	0.0	0.0	0.0	18.0	3.3	0.8	3.2	2.5	0.5	1.4	0.2	1.1
150	0.6	9.2	1.2	24.0	46.0	31.0	1.3	1.0	1.0	22.0	50.0	6.1	24.0	4.6	1.1	4.3	3.4	0.6	1.6	0.2	1.4
Áidejávri																					
0	0.7	0.6	0.1	49.0	3.8	1.7	0.5	5.9	0.2	0.4	0.9	0.1	0.4	0.1	0.0	0.1	0.1	0.0	0.0	0.0	0.1
20	0.5	3.9	0.5	108	12.0	11.0	0.3	0.4	0.1	13.0	30.0	3.4	14.0	2.7	0.6	2.5	2.1	0.5	1.5	0.2	1.6
40	0.6	0.5	0.2	92.0	2.1	1.3	0.8	6.4	0.2	0.4	0.7	0.1	0.3	0.1	0.0	0.1	0.1	0.0	0.0	0.0	0.0
50	0.4	2.5	0.4	230	10.0	4.2	0.3	0.3	0.1	12.0	29.0	3.4	14.0	2.7	0.6	2.5	2.1	0.4	1.3	0.2	1.4
69	0.4	3.7	0.8	180	31.0	13.0	0.5	0.4	0.1	16.0	38.0	4.4	19.0	3.4	0.8	3.3	2.7	0.6	1.8	0.3	1.9
89	0.6	8.9	0.8	190	34.5	20.5	0.6	1.4	0.1	29.5	69.5	8.0	34.0	6.1	1.4	5.7	4.6	0.9	2.7	0.4	2.8
104	0.6	10.0	0.1	210	8.3	17.0	0.2	2.0	0.0	16.0	35.0	4.3	17.0	3.1	0.7	2.8	2.2	0.4	1.2	0.2	1.1

Table A.2. Additional elements analyzed in the top layer (0-10 cm) of thermokarst sediment (TK1) and wet mire (WM1) from Lakselv, Iškoras, and Áidejávri. The values below the stippled line are from core samples (70 -100 cm) from thermokarst sediment (TK) and wet mire (WM) from Áidejávri.

Site and type	C:N	C mg g dw^{-1}	N mg g dw^{-1}	P mg g dw^{-1}	S mg g dw^{-1}	Mg mg g dw^{-1}	Ca mg g dw^{-1}	Fe mg g dw^{-1}	Mn µg g dw^{-1}	Se µg g dw^{-1}	Ni µg g dw^{-1}	Cu µg g dw^{-1}	Zn µg g dw^{-1}	Pb µg g dw^{-1}	Cd µg g dw^{-1}	Al mg g dw^{-1}	As µg g dw^{-1}
Lakselv																	
TK1	19.0	424.0	22.3	0.8	14.0	1.9	5.0	15.0	111	0.7	39.0	33.0	34.0	8.5	0.4	8.7	1.1
WM1	92.9	441.6	4.8	0.4	0.8	1.4	1.7	0.4	126	0.1	0.9	2.1	18.0	1.0	0.0	0.5	0.1
Iškoras																	
TK1	30.6	510.9	16.7	0.5	2.2	0.2	0.8	1.4	12.0	0.5	5.6	7.4	5.8	4.9	0.2	1.6	0.7
WM1	42.3	437.1	10.3	0.5	1.2	1.1	3.0	2.2	100	0.2	4.8	2.7	25.0	3.0	0.1	0.7	0.4
Áidejávri																	
TK1	56.2	437.0	7.8	0.5	1.9	0.4	2.2	3.6	31.0	0.1	1.7	2.0	6.8	3.3	0.0	0.5	0.4
WM1	66.2	421.2	6.4	0.5	0.7	1.1	3.7	11.0	51.0	0.1	1.8	2.7	9.8	13.0	0.1	0.5	0.3

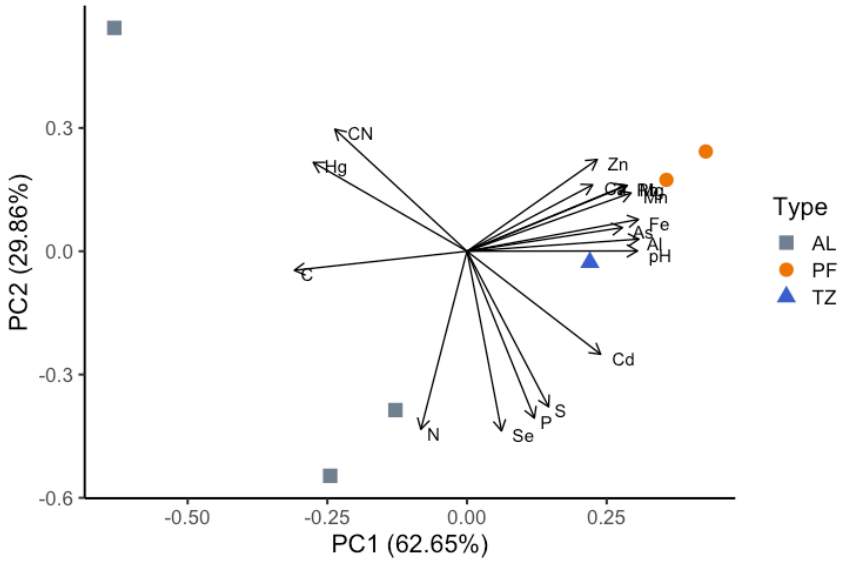

Figure A.1. PCA plot of Lakselv including C, N, P, S, Ca, Mg, Fe, Mn, Zn, Se, Al, Cd, Pb, Hg, C:N, and pH.

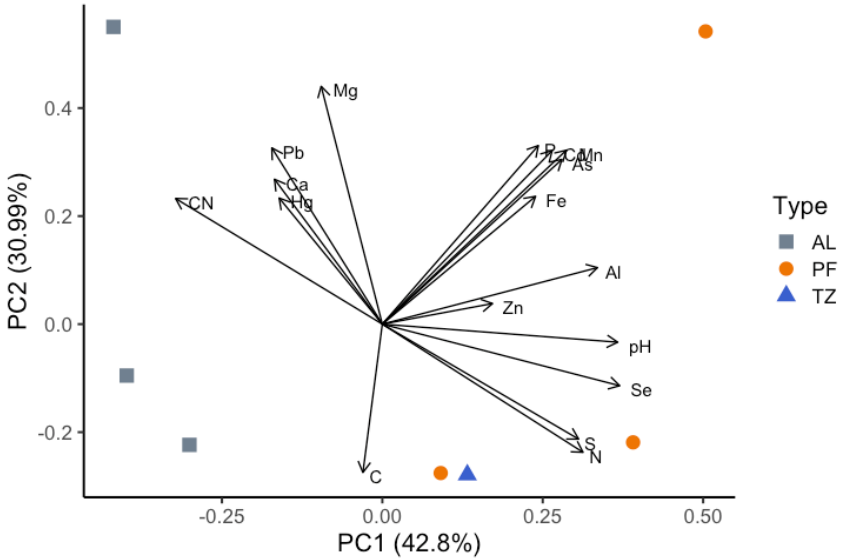

Figure A.2. PCA plot of Iškoras including C, N, P, S, Ca, Mg, Fe, Mn, Zn, Se, Al, Cd, Pb, Hg, C:N, and pH.

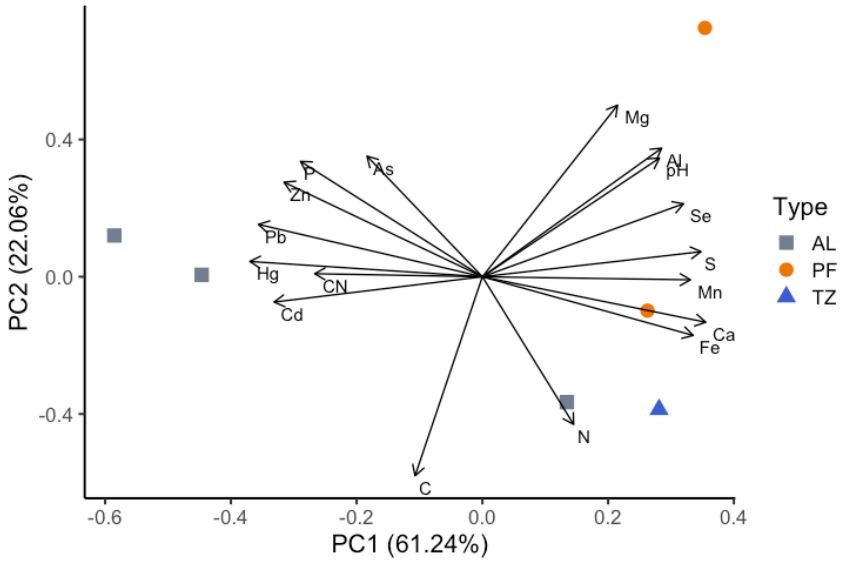

Figure A.3. PCA plot of Áidejávri including C, N, P, S, Ca, Mg, Fe, Mn, Zn, Se, Al, Cd, Pb, Hg, C:N, and pH.

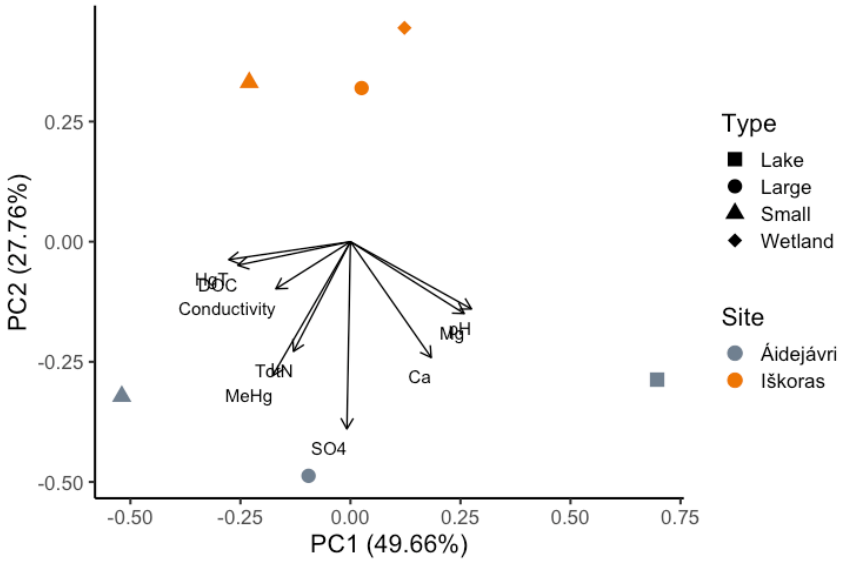

Figure A.4. PCA plots for thermokarst ponds in Iškoras and Áidejávri including HgT, MeHg, pH, conductivity, TotN, Ca, Mg, and SO_4.

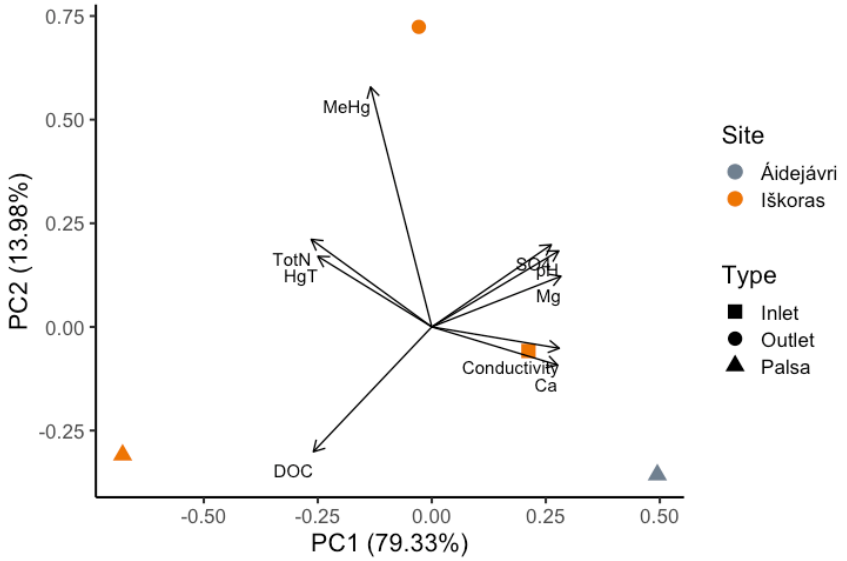

Figure A.5. PCA plot for streams in Iškoras and Áidejávri including HgT, MeHg, pH, conductivity, TotN, Ca, Mg, and SO_4

Table A.3. Dry weight and water content for the incubated samples from the palsa cores from each site.

Treatment and layer		Lakselv		Iškoras		Áidejávri	
		Fresh soil (g)	Dry soil (g)	Fresh soil (g)	Dry soil (g)	Fresh soil (g)	Dry soil (g)
Anoxic							
	AL1	10.39	2.40	9.05	1.03	11.56	2.36
	AL2	10.35	2.75	12.18	2.10	9.78	2.73
	AL3	11.68	2.89	11.64	2.11	14.91	2.52
	TZ	10.86	3.08	8.73	0.98	10.23	0.81
	PF1	11.73	2.35	7.37	0.98	10.32	0.75
	PF2	10.34	1.85	15.62	2.12	15.29	1.86
	PF3	17.82	7.69	13.15	1.55	10.19	5.98
Oxic							
	AL1	9.81	2.26	10.97	1.24	11.27	2.30
	AL2	9.76	2.59	12.05	2.08	11.21	3.13
	AL3	11.94	2.96	14.45	2.63	12.27	2.07
	TZ	10.88	3.09	10.78	1.20	9.97	0.79
	PF1	12.16	2.43	7.76	1.03	10.85	0.78
	PF2	9.47	1.69	14.49	1.97	14.63	1.78
	PF3	14.38	6.21	10.72	1.26	8.34	4.90

Table A.4. Overview over concentrations of dHgT and DOC pre- and post-incubation for each depth from each site and treatment (oxic/anoxic).

Site/Depth	Start dHgT ng g dw^{-1}	Oxic End dHgT ng g dw^{-1}	Anoxic End dHgT ng g dw^{-1}	Start DOC mg g dw^{-1}	Oxic End DOC mg g dw^{-1}	Anoxic End DOC mg g dw^{-1}	Oxic ΔCH_4 ng g dw^{-1} day^{-1}	Anoxic ΔCH_4 ng g dw^{-1} day^{-1}	Days incubated
Lakselv									
AL1	0.41	0.54	0.47	1.13	5.9	10.9	0.21	0.51	98
AL2	0.02	0.21	0.34	0.41	3.1	4.4	0.11	0.28	98
AL3	*N/A*	0.09	0.20	0.51	3.3	5.7	0.22	0.95	98
TZ	<LOQ	0.04	0.09	0.44	1.5	3.1	0.37	0.37	98
PF1	*N/A*	0.07	0.10	0.87	1.8	3.3	1.96	1.38	98
PF2	<LOQ	0.06	0.07	0.73	2.0	3.0	3.42	8.01	98
PF3	*N/A*	0.06	0.05	0.13	1.3	1.4	1.72	1.50	98
Iškoras									
AL1	0.46	1.32	6.47	1.68	8.66	20.50	0.60	2.22	106
AL2	0.07	0.22	0.56	0.95	4.66	4.56	0.19	0.12	106
AL3	*N/A*	0.11	0.35	0.80	2.48	3.80	0.13	0.08	106
TZ	<LOQ	0.21	0.45	3.59	6.59	6.61	6.56	7.24	106
PF1	<LOQ	0.14	0.28	3.82	5.09	7.10	5.41	5.58	106
PF2	*N/A*	0.12	0.08	2.36	4.14	3.43	0.78	0.63	106
PF3	*N/A*	0.19	0.08	1.62	4.94	4.09	0.79	0.58	106
Áidejávri									
AL1	0.58	0.59	0.55	1.20	9.02	13.35	0.88	1.40	98
AL2	0.06	0.69	0.91	0.48	15.02	21.74	0.09	0.06	98
AL3	*N/A*	0.01	0.06	0.45	2.52	5.45	0.12	0.09	98
TZ	<LOQ	0.00	0.00	1.34	4.79	5.10	0.52	0.30	98
PF1	*N/A*	0.01	0.00	1.73	4.13	4.83	0.91	19.23	98
PF2	<LOQ	0.34	0.01	0.77	3.22	2.70	1.22	4.35	98
PF3	*N/A*	0.12	0.03	0.10	0.45	0.55	1.03	1.11	98

Table A.5. Overview over the amount of soil applied in each of the flasks for the experiment testing effect of nutrients on mobilization of Hg.

Treatment	Fresh soil g	Dry soil g
Control 1	14.51	1.80
Control 2	14.07	1.75
Control 3	14.7	1.83
Carbon 1	14.35	1.78
Carbon 2	14.36	1.79
Carbon 3	14.9	1.85
Nitrogen 1	14.67	1.82
Nitrogen 2	14.73	1.83
Nitrogen 3	14.38	1.79
Phosphorus 1	14.26	1.77
Phosphorus 2	14.56	1.81
Phosphorus 3	14.3	1.78
Nitrogen + phosphorus 1	14.13	1.76
Nitrogen + phosphorus 2	14.45	1.80
Nitrogen + phosphorus 3	14.23	1.77
Sulphur 1	14.61	1.82
Sulphur 2	14.22	1.77
Sulphur 3	14.75	1.83
Mercury 1	14.22	1.77
Mercury 2	14.07	1.75
Mercury 3	14.19	1.76
All 1	14.31	1.78
All 2	14.22	1.77
All 3	14.43	1.79

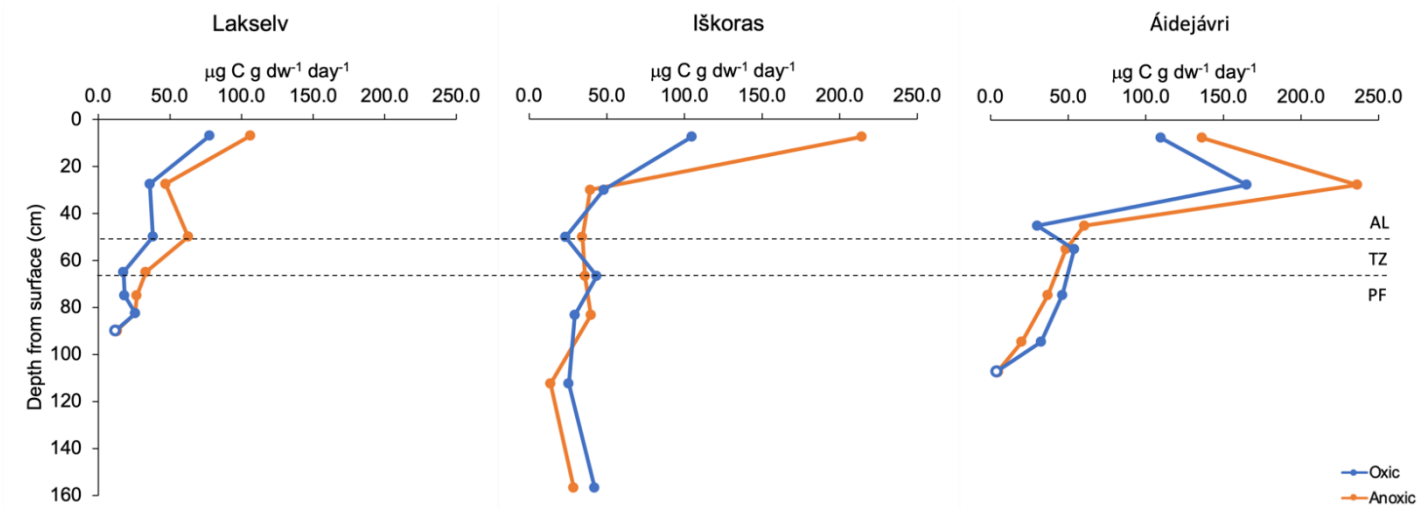

Figure A.6. Depth profiles for sum of DOC and CO_2-C accumulation rates for peat plateau samples incubated oxically (blue) and anoxically (orange), from Lakselv, Iškoras, and Áidejávri. The rates are expressed as µg C per g dry weight peat per day.

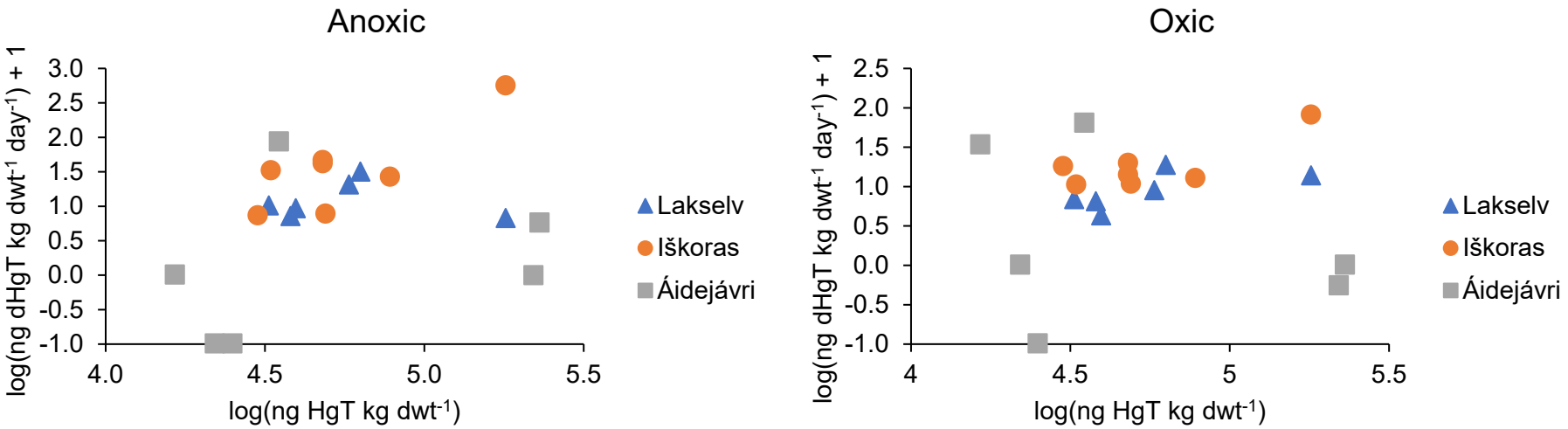

Figure A.7. Concentration of HgT in the peat soil plotted against the rate of mobilization of dHgT in samples incubated anoxically (left) and oxically (right) across the three sites (Lakselv, Iškoras, Áidejávri) and depths (AL1, AL2, AL3, TZ, PF1, PF2, PF3. PF3 was excluded from Lakselv and Áidejávri due to mixing with mineral soil). The concentration of HgT is displayed along the x-axis as log(ng HgT kg dwt^{-1}) and dHgT is displayed as log(ng dHgT kg dwt^{-1} day^{-1}) + 1 along the y- axis.

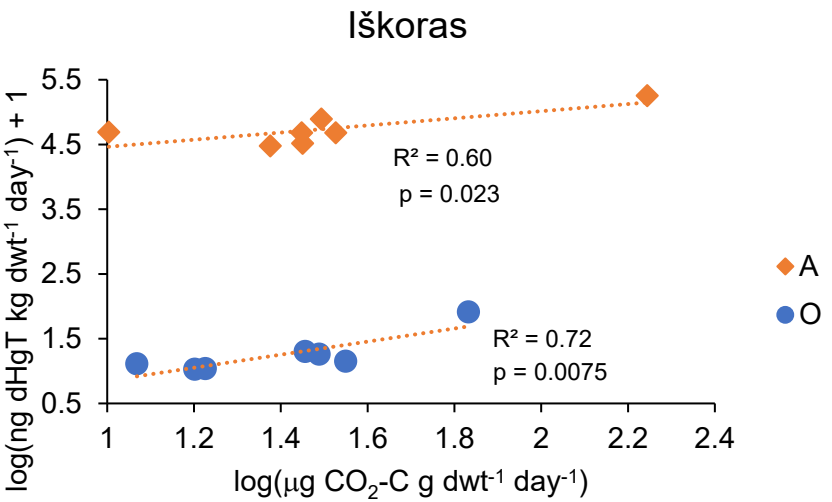

Figure A.8. Correlations between rates of dHgT and CO_2 accumulation in palsa core samples form Iškoras at different depths depth (AL1, AL2, AL3, TZ, PF1, PF2, PF3,) incubated anoxically (orange) and oxically (blue). Rates of CO_2 accumulation is displayed as log(µg CO_2-C g dwt^{-1} day^{-1}) along the x-axis, and dHgT are displayed as log(ng dHgT kg dwt^{-1} day^{-1}) + 1 along the y- axis. The linear correlation is calculated excluding the three outliers from Áidejávri indicated with no fill.

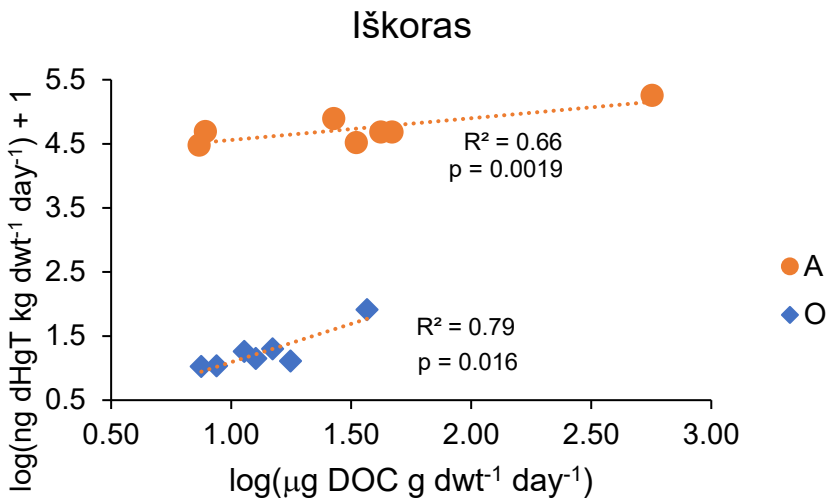

Figure A.9. Correlations between rates of dHgT and DOC accumulation in palsa core samples form Iškoras at different depths depth (AL1, AL2, AL3, TZ, PF1, PF2, PF3,) incubated anoxically (orange) and oxically (blue). Rates of DOC accumulation are displayed as log(µg DOC g dwt^{-1} day^{-1}) along the x-axis, and dHgT is displayed as log(ng dHgT kg dwt^{-1} day^{-1}) + 1 along the y- axis. The linear correlation is calculated excluding the three outliers from Áidejávri indicated with no fill.

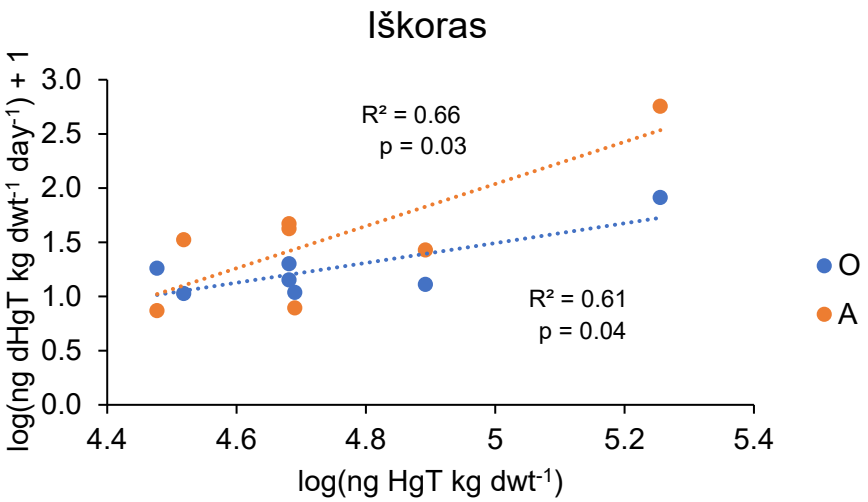

Figure A.10. Correlation between rates of mobilization of HgT and native HgT concentrations in peat for oxically and anoxically incubated samples from Iškoras. The x-axis displays the concentration of native HgT in peat as log(ng HgT kg dw^{-1}) and the y-axis displays the mobilization rate of HgT as log(ng dHgT kg dwt^{-1} day^{-1}) + 1.

Norges miljø- og biovitenskapelige universitet
Noregs miljø- og biovitskapelege universitet
Norwegian University of Life Sciences

Postboks 5003
NO-1432 Ås
Norway